ROLE OF FOCUSED ULTRASOUND IN CD40 MEDIATED ANTI-TUMOR IMMUNITY

By

MOHIT PRATAP SINGH

Bachelor of Veterinary Science and Animal Husbandry
Tamil Nadu Veterinary and Animal Sciences University
Chennai, Tamil Nadu, India
2010

Master of Veterinary Surgery and Radiology
Govind Ballabh Pant University of Agriculture and Technology
Pantnagar, Uttarakhand, India
2013

Submitted to the Faculty of the
Graduate College of the
Oklahoma State University
in partial fulfillment of
the requirements for
the Degree of
DOCTOR OF PHILOSOPHY
July, 2020

ROLE OF FOCUSED ULTRASOUND IN CD40

MEDIATED ANTI-TUMOR IMMUNITY

Dissertation Approved:

Ashish Ranjan

Dissertation Adviser

Jerry Malayer

Clinton Jones

Craig Miller

Daqing Piao

ACKNOWLEDGEMENTS

I would like to take this opportunity to thank and acknowledge everyone that provided support and encouragement during my PhD. I am grateful and thankful to my adviser, Dr. Ashish Ranjan, for dedicating his time and efforts to accomplish the work in this dissertation. Your suggestions and motivation helped me to develop as a critical thinker and an independent researcher. Thank you Dr. Ranjan for providing ample resources and diverse collaboration opportunities that enabled me to efficiently finish the works and learn from experts in the field. Sir, it has been a great honor and privilege to work with you.

My sincere thanks to the advisory committee members - Dr. Jerry Malayer, Dr. Clinton Jones, Dr. Craig Miller, and Dr. Daqing Piao for investing their time and efforts and providing expert advice to develop my knowledge and skills. I thank Dr. Jerry Ritchey for his insightful suggestions and support during my PhD. My special thanks to Dr. Shitao Li for giving suggestions and inputs to broaden my horizon in cancer immunotherapy research and being supportive throughout the process.

I am thankful to Dr. Pamela Lovern for guiding me from the day of my PhD application acceptance and providing wonderful suggestions during the seminar course that helped me to develop my presentation and communication skills. My thanks to Dr. Tom Oomens for taking time and discussing my progress in the research and giving suggestions during the seminar course. My heartfelt thanks to our collaborators, Dr. Carey Pope, Dr. Joshua Ramsey, Dr. Steven Fiering, Dr. Jack P. Hoopes, Dr. Chandan Guha, and Dr. Nicholas

Flynn for being very helpful and critical about our work and enabling us to progress in the diverse projects.

My sincere thanks to Dr. Jill Akkerman for training me to effectively teach and interact with students during gross and developmental anatomy course. Your clarity and organization were very helpful to balance my research and teaching responsibilities in an effortless manner. I am also thankful to Dr. Mark Payton and all other faculty who dedicated their efforts to teach me during the graduate coursework.

My thanks to Mr. Jacob Bass and Dr. Diane Hamilton from OMRF for training me for flow cytometry. My thanks to my past and current lab members, Josh, Selva, Willie, Aaron, Kalyani, Harshini, Mike, Cristina, Danny, and Kaustuv for being a part of my life during this journey. I thank Chris Pivinksi, Michelle Kuehn, Yurong Liang, and Amy for being kind and supportive to me throughout this journey. A very special thanks to all my friends for your timely support and for gifting me with a wonderful time in Stillwater.

I extend deep gratitude to my father, sisters, and Nandhini; without your sacrifice, love, and patience I would not be where I am. I dedicate this dissertation to my belated mother. I am deeply indebted for your love, sacrifice, and efforts in shaping my life.

Name: MOHIT PRATAP SINGH

Date of Degree: JULY, 2020

Title of Study: ROLE OF FOCUSED ULTRASOUND IN CD40 MEDIATED ANTI-TUMOR IMMUNITY

Major Field: VETERINARY BIOMEDICAL SCIENCES

Abstract: Advanced stage melanoma tumors are chemo- and radio-resistant, demonstrate poor antigenicity and defective antigen presentation mechanisms, and low tumor specific cytotoxic T cell population, resulting in poor survival rates in patients. Novel therapeutic approaches that can reprogram the tumor immune microenvironment and improve outcomes against refractory and aggressive melanoma is urgently needed. We hypothesized that focused ultrasound (FUS) and its combination with anti-CD40 agonistic antibody (CD40) will improve the melanoma therapy outcomes by activating the innate and adaptive immune cells in the tumors. Prior research has shown that FUS has an immunomodulatory effect in solid tumors, and CD40 is a known enhancer of antigen presenting cell (APC) function. To investigate our hypothesis, we exposed B16F10 murine melanoma to various FUS parameters (thermal and histotripsy [HT]) in the presence and absence of CD40 stimulation. We found that CD40 and FUS combination increased the anti-tumoral M1 macrophages and granzyme B+ cytotoxic T cell population in murine melanoma and suppressed both treated and untreated tumors. In particular, HT plus CD40 (HT40) caused a significant increase in the expression of immune checkpoints, namely CTLA4 and PD-L1, to aid the anti-CTLA4 and PD-L1 therapy (ICI), thereby prolonging the mice survival rates in HT40+ICI group compared to ICI therapy alone group. In conclusion, our data suggest that focused ultrasound and anti-CD40 agonistic antibody combination enhances the anti-tumor immunity and sensitization to checkpoint inhibitor therapy in advanced stages.

TABLE OF CONTENTS

Chapter Page

LIST OF TABLES

Table Page

LIST OF FIGURES

Figure Page

Figure Page

CHAPTER I

REVIEW OF LITERATURE

REPROGRAMMING MELANOMA MICROENVIRONMENT TO ACHIEVE IMMUNOTHERAPEUTIC SUCCESS

Abstract

Melanoma is an aggressive form of skin cancer that responds poorly to available treatments. Cancer evades immune clearance by inducing an immunosuppressive microenvironment, thereby limiting the efficacy of anti-cancer therapies based on immune recognition and response. Therapeutic interventions that can generate tumor specific systemic immunity are highly desirable to treat metastatic cancers. Novel therapies that can enhance tumor immune cell infiltration and activate tumor antigen presentation mechanisms can be highly beneficial to reprogram refractory malignancies into therapy responsive tumors. Here, we review how the tumor immune environment decides success of therapies and the potential role of upcoming novel technologies in linking innate immune players to adaptive immune players for a better therapeutic outcome.

Introduction

Skin is the largest organ of the body and is made up of different layers, namely epidermis, dermis, and subcutaneous adipose tissue [1]. Melanocytes are pigmented cells that are predominantly present in the basal layer of skin epidermis, producing melanin pigment that gives color to our skin, eyes, and hair [2,3]. Melanocytes protect skin from the harmful effects of UV radiation and are known to prevent occurrence of skin cancer [3]. However, the mutations of growth regulatory genes, autocrine production of growth factors and loss of adhesion receptors can impair the cell signaling in melanoma[4,5], causing an uncontrolled proliferation and melanoma formation [6]. Uncontrolled melanocyte proliferation from basal layer of epidermis may progress into other skin layers or metastasize to distant sites causing malignant melanoma [7]. When left untreated, malignant melanoma is the most fatal form of skin cancer [8] since it is refractory to most of the existing therapies [9]. In fact, the median survival rate of malignant melanoma in some cases can be as low as 6 months and less than 5% of malignant melanoma patient survive beyond 5 years [9]. U.S. cancer statistics data listed the overall incidence rate of melanoma as 21.8 per 100,000 from 2012 to 2016 [10]. The American Cancer Society estimated that 100,350 new cases of invasive melanoma will be diagnosed in 2020 in the US, impacting 60,190 men and 40,160 women [11], suggesting a need to urgently develop novel therapies to tackle this disease.

Current treatment options for melanoma

Chemotherapy

Different chemotherapy drug combinations have been evaluated in advanced melanoma patients, but the overall survival of patients show only a modest improvement with chemotherapy [12]. Dacarbazine is the drug of choice for metastatic melanoma. Dacarbazine achieves complete response in less than 5% of patients and only 2% to 6% of patients survived at 5 years post treatment [13]. Temozolomide, an active metabolite prodrug of dacarbazine has also been evaluated in advanced melanoma cases, but it showed minimal improvement in progression-free survival compared to dacarbazine [14]. A variation of

chemotherapy known as electro-chemotherapy, in which high intensity electric pulses were combined with cytotoxic drugs like cisplatin and bleomycin was attempted to facilitate drug delivery into the melanoma cells[15]. Electrochemotherapy was reported to be effective in treating cutaneous and subcutaneous melanoma nodules [16], but was not effective in tumors that metastasized to deep seated organs.

Photodynamic therapy (PDT)

Photodynamic therapy or PDT is a minimally invasive therapeutic procedure that uses a photosensitizer molecule, which gets activated upon exposure to light of a particular wavelength [17,18]. PDT generates reactive oxygen species (ROS) that causes an irreversible damage to tumor cells and blood vessels, resulting in inflammation and generation of anti-tumor immune response [19,20]. PDT as a monotherapy in melanoma shows only limited efficiency [21]. Dacarbazine and PDT combination therapy have been reported to be slightly more effective in metastatic melanoma [22].

Immunotherapy

Immunotherapies train the patient's own immune system to fight the cancer. Interleukin-2 (IL-2) was the first immunotherapy agent approved by FDA in 1998 for the treatment of metastatic melanoma. IL-2 achieved an overall response rate (patients with a complete or partial remission of cancer) of 16-60% in immune-sensitive patients [23]. The second immunotherapeutic adjuvant approved by the FDA was interferon-α (IFN-α) against resected high-risk melanoma. IFN-α showed an overall response rate (patients with a complete or partial remission of cancer) of 22% in metastatic melanoma patients, but only those patients with lower tumor load responded to the treatment [24]. The clinical responses to IL-2 and IFN-α therapy has significantly expanded an interest in immunotherapy research, leading to new developments in melanoma cancer research[23].

In 1987, James P. Allison identified an immune checkpoint molecule named cytotoxic T-lymphocyte antigen 4 (CTLA-4, an immune checkpoint) and demonstrated its involvement in T cell inactivation

and ability to prevent T cells from attacking tumor cells [25]. Dr. Allison proposed that CTLA-4 blocks the immune system to fight cancer. Subsequent developments of anti-CTLA-4 antibody to block the inhibitory effect of CTLA-4 molecule restored the T cell functional status and infiltration in to the tumors [26,27], and enhanced the 1 and 2 year survival rate by 46 and 24% in patients [23], leading to FDA approval in 2011 for advanced melanoma treatment [28]. In 1992, Tasuku Honjo independently discovered another immune checkpoint molecule on T cells, known as programmed cell death protein 1 (PD-1) [29]. PD-1 expressed on T cells binds to PDL-1 expressed on tumor cells to inactivate the T cells [30]. Tumor cells use the PDL-1/PD-1 axis to evade immune surveillance and anti-tumor response [31]. In CheckMate-066, a Phase III clinical study involving naïve patients with unresectable or metastaticBRAF WT melanoma, anti-PD-1 antibody (PD-1 inhibitor) achieved the objectivresponse rate (data included patients with a complete remission and those with a partial remission of cancer) of 40%in 63 out of 72 (88%) and 1-year survival rate of ~73% in the treated patients [32].

Another clinical study with anti-PD-1 antibody (Pembrolizumab) showed that melanoma patients demonstrated long term control with 78% of patients remaining progression free 2 years post treatment [33]. Additionally, the combination of anti-CTLA-4 antibody and anti-PD-1 antibody demonstrated better objective response rates (data included patients with a complete remission and those with a partial remission of cancer) compared to anti-PD-1 antibody and anti-CTLA-4 antibody alone, resulting in the objective response rates of 57.6%, 43.7%, and 19% respectively [34]. It may be noted that the efficacy of these immune checkpoint blockers is mostly limited to tumors with high mutation burden and is dependent on the expression of neoantigens on tumor cells [35,36]. In fact, a large proportion of patients (>50%) do not respond at all to checkpoint blockade [37-39]. Immune checkpoint inhibitors work well in patients with optimal baseline tumor specific T cell population, and poor antigen presentation by APCs to T cells can be one of the limiting factors for their efficacy [40,41]. A phase Ib clinical trial with the APC activator (CMP-001) in combination with anti-PD-1 supported this concept. A patient resistant to anti-PD-1 therapy demonstrated overall response rate

(patients with a complete or partial remission of cancer) of 22% when CMP-001, an APC activator, was added to the treatment regimen [42]. New therapies that increase the expression of tumor associated antigens and link innate immunity to adaptive immunity are needed to improve the efficacy of immune checkpoint inhibitors in non-responders.

Tumor immunogenicity decides patient survival

The ability of tumor cells to induce an adaptive immune response is known as the immunogenicity of the tumor [43,44]. Tumors develop from the body's own cells, making the immune system recognize them as "self" and tolerant to cytotoxic cells [45]. Transplantation experiments in mice have defined immunogenicity of different types of cancer as follows: a. Tumor cells that do not form tumor mass upon transplantation in naive syngeneic mice are considered highly immunogenic, b. Tumor cells that require development of immunity by prior immunization for rejection are known as intermediate immunogenic, and c. Tumor cells that are not rejected even after prior immunization and form tumor are known as non-immunogenic [46]. Possibly, all types of tumors have antigens that could be targeted by T cells, however, the expression of antigens is dependent on the cancer sub-type [47]. This differential antigen expression defines tumor immunogenicity [48]. Several dysregulated mechanisms such as mutations in major histocompatibility complex (MHC) expression and loss of DNA repair mechanism in immunogenic tumors, lead to antigenic mutation and expression of neoantigens on tumor cells, thus improving patient's response to immunotherapies [49,50].

There is a need to understand the nature of cancer tissue. For example, to develop successful therapy regimen for a cancer patient, it is of utmost importance to know the immunogenicity of the tumor [51,52]. In 1914, the first link between cancer and mutation was found by observing chromosomal abnormalities in cancer cells [53]. Mutations can result from cell replication errors or failure in repair of damaged DNA [53]. Damage to DNA can result from exogenous means like chemicals, ionizing radiation, ultraviolet (UV) light, and by endogenous factors such as reactive oxygen species, mitotic

errors or enzymes involved in gene editing or DNA repair [54]. Types of cancer that have high genetic mutation are readily detected by patient's immune system and have a better chance to respond to immunotherapies [55]. Melanoma and non-small cell lung carcinoma show higher mutational burdens than other tumors and are hence considered as the most responsive cancer types for immunotherapies, particularly to immune checkpoint inhibitors [56,57]. Previous reports have shown that lung adenocarcinoma patients with Kirsten rat sarcoma viral oncogene homolog (KRAS) mutations and concomitant TP53 mutations had upregulation of PD-L1 expression and responded well to PD-1 checkpoint inhibitors [58]. Similarly, melanoma patients who had high tumor mutation burden showed better overall survival after PDL-1 inhibitor therapy compared to patients with low mutation rates [57]. Tumor mutation load can result in generation of novel antigens known as neoantigens and as these neoantigens are non-self, they are mostly not subjected to immune system tolerance [59]. Expression of neoantigens on previously undetected tumor results in a robust adaptive anti-tumor immune response by the host [60]. These clinical findings clearly show that tumors with high mutation and antigen load respond well with immune based treatments.

Therapies aimed to increase the expression of antigens on tumor cells may hold promise to improve the survival of cancer patients. Preclinical murine solid tumor models namely CT26 colon cancer, renal cell carcinoma (RENCA) kidney cancer, and 4T1 breast cancer are highly immunogenic cancer models while B16F10 melanoma, MAD109 lung cancer, and LLC lung carcinoma are poorly immunogenic [61]. It was found that strongly immunogenic tumors like CT26, RENCA, and 4T1 had significant up-regulation of *CD45* (leukocyte), *CD11b*, and *CD11b* (myeloid cell), and (*CD3*, and *CD4*) T cell genes [61]. In contrast, poorly immunogenic tumors B16F10, LLC, and MAD109 showed downregulation of these genes, such differences in immunologic profile suggest that cancer cells have evolved to avoid immune system surveillance, due to loss of antigen expression, lower degree of antigen presentation, and eventually making themselves look like normal self-cells [61]. These findings also corroborated with lower frequency of co-stimulatory markers namely CD40, CD40L, OX40L,

and CD137L on tumor infiltrating leukocyte [14] in poorly immunogenic tumor models B16F10, LLC, and MAD109 than in immunogenic models [61]. To generate successful anti-tumor immunity efficient priming of APCsis also indispensable [62]. APCs should be in an activated state so that they can process tumor antigens and present them to T cells, the key player for tumor destruction [63]. These observations further our understanding to devise immunotherapy regimen that can provide exogenous stimulatory molecules to APCs in the form of agonist antibodies or fusion proteins to achieve better treatment outcomes in poorly immunogenic tumors.

Focused Ultrasound (FUS) - a non-invasive cancer treatment technology

Ultrasound has been used for diagnosing abnormalities in organs, observe fetal growth, and in the treatment of musculoskeletal conditions like ligament and muscle strains, inflammation of joints, arthritis etc. [64-67]. Focused ultrasound (FUS) is a proven, efficient, and non-invasive technology that has been extensively investigated for treatment of neuro-degenerative disorders, drug delivery, musculoskeletal abnormalities, and cancer [68]. In fact, FUS was used as early as in 1961 to treat breast cancer patients [69]. FUS as a therapeutic modality involves an interaction of acoustic waves with biological tissues for generation of thermal and non-thermal biological effects in the targeted treatment area without affecting the surrounding healthy tissue. This is because in FUS therapy, acoustic intensity is high only in the focal region and not in the intervening tissue, and thus it is associated with minimal side effects like discomfort, skin burns and collateral damage (i.e., hemorrhage). As sound waves are non-ionizing, multiple sessions of FUS therapy can be safely given to cancer patients. Thermal effects of FUS arise from the absorption of acoustic energy and subsequent vibration of molecules and macromolecules in the treated tissue, leading to generation of heat by friction [70]. The degree of heat generation and biological effects in exposed tissue depend on FUS parameters, beam focus, and tissue properties [71]. For example, application of FUS-hyperthermia to uniformly heat tumors to 42-45 °C for about an hour can effectively reduce tumor growth [72,73].

FUS based hyperthermia treatment increases the release of damage associated molecular patterns like calreticulin (CRT), ATP, and heat shock proteins (HSP) from dying tumor cells [74]. Released CRT and HSPs in the tumor microenvironment can act as an antigen source because of their inherent ability to chaperone intracellular tumor peptides and attract APCs [75]. Hyperthermia also increases adhesion molecules like vascular cell adhesion molecule 1 (VCAM-1) and intercellular adhesion molecule 1 (ICAM-1) in endothelial cells of tumor blood vessels [76]. The increase in expression of cell adhesion molecule is associated with improvement in translocation of APCs and lymphocytes from blood vessels into the tumor [77].. Studies have shown that FUS-heating improves antigen uptake and migration capacity of APCs and lymphocytes [78,79].

Efficient antigen uptake and immune cell migration to lymphoid organs and subsequent infiltration of T cells into tumors is critical for efficient anti-tumor therapy. FDA recently approved FUS therapy to treat prostate cancer patients [80,81]. In a clinical trial, a total of 181 prostate cancer patients underwent FUS therapy and the disease-free survival (DFS) rates were 84%, 80%, and 78% at 1, 3, and 5 years, respectively in all patients [82]. In another clinical trial in China, 48 women with breast cancer were randomized to control group (radical mastectomy was performed) and FUS group (extracorporeal FUS ablation of breast cancer followed by radical mastectomy). Pathologic and immunohistochemical analysis revealed that breast cancer tissue treated with FUS underwent complete coagulative necrosis and exhibited reduced ability to proliferate, invade, and metastasize [83]. In a preclinical B16F10 murine melanoma study, FUS treated mice delayed the tumor progression and frequency of lung metastasis compared to control mice [84].

In recent years, interest in using focused ultrasound to treat tumors by non-thermal mechanical effect is also increasing. Mechanical fragmentation of tumor tissue with FUS or histotripsy (HT) is achieved by treating tumor tissue by repeated microsecond to millisecond duration, high-intensity US pulses, and with low duty cycles [85]. When high intensity focused ultrasound pulses are applied for a short duration, small gas-filled or vaporized cavities or microbubbles are formed in the exposed area, a

phenomenon known as cavitation. Cavitation can be of two types: stable and inertial/unstable. In the case of stable cavitation, the bubble or cavity oscillates with the upcoming wave, as long as the bubble resonance frequency is smaller than that of the frequency of FUS wave [86]. Inertial cavitation happens when the resonance frequency of bubble or cavity becomes larger than the ultrasound frequency. This increase in frequency results in increase in size of cavity or bubble which is followed by collapse of bubble [86,87]. This bubble or cavity collapse creates an extremely large pressure shock wave resulting in fragmentation of treated tumor tissue [88].

HT technique for mechanical disintegration of tumor tissue liquefies tumor tissues, which then enhances physiological or immunologic responses [89,90]. HT has several important advantages over non-invasive thermal therapy: 1) Bubbles that are produced at the ultrasound focus are hyperechoic and visible as bright spots on ultrasound imaging which allows the operator to effectively monitor targeted volume; 2) Microbubble cloud is seen on an imaging monitor, thus providing real-time feedback to take prompt decision during therapy; 3) After HT treatment, the targeted lesion appears dark on imaging, giving operator information about successful disintegration of tumor tissue; and 4) HT technique without any thermal diffusion to surrounding healthy tissue can produce desired tumor fragmentation in a very precise and controlled manner [91-93]. HT damages tumor cells without thermal denaturation of proteins or antigens while the surrounding healthy areas are also protected from thermal diffusion [89]. HT based biological effect is different than the coagulation of tissue by thermal therapy, HT provides more precise control over targeted site with no thermal diffusion induced effects on surrounding tissue. In a rabbit model, kidneys were treated with histotripsy and after 1 to 60 days post treatment, kidneys were harvested for histological evaluation. Results suggested that the homogenized debris were resorbed completely with a little fibrotic tissue left behind as scar [94]. In canine studies, it was found that the application of HT on prostate gland liquefied the tissue and facilitated its drainage through urethra resulting in effective reduction of prostate size [95,96]. In a

subcutaneous hepatocellular carcinoma (HCC) model, tumors treated with HT exhibited delay in tumor growth and there was no sign of metastasis in lung and brain [97].

Recent European clinical trial results from HT therapy was published in February 2020. Eight patients between 46 to 87 years of age were enrolled in the clinical trial. These patients suffered from either primary or multifocal liver metastases after the development of breast cancer (1 patient), colorectal cancer (5 patients), hepatocellular carcinoma (1 patient), and gallbladder carcinoma (1 patient). Liver lesions ranging from 0.5 to 2.1 cm (average size was 1.3 cm) were chosen for the study. Researchers noted a reduction in the lesion which averaged 36.0% after first week, 53.6% one month, and 71.8% two months post HT therapy. Treatment was well tolerated by patients with no adverse event. Findings from renal cell carcinoma rat model suggested an increased plasma concentration of TNF, IL-6, high-mobility group box 1 (HMGB1), IL-10 cytokines with enhanced CD8+ T cells infiltration in tumors after histotripsy treatment [98]. In murine melanoma and hepatocellular carcinoma studies, it was observed that HT treated cohorts had significantly higher intratumoral infiltration of dendritic cells (DCs), natural killer cells (NK cells), B cells, CD4+ and CD8+ T cells. This increase in immune cell infiltration in HT treated mice correlated with a significant delay of tumor progression [99].

Despite these advancements and achievements in FUS based approaches, FUS alone has not been very successful in inhibiting tumor growth and improve survival in preclinical cancer models and clinical trials which may be due to the imbalance in efficient antigen processing and presentation by APCs and upregulation of immune suppressive factors in the tumor microenvironment. For example, in a 4T1 mammary tumor preclinical study, it was found that there was an increase in infiltration of immunosuppressive immune cells namely MDSCs and M2 macrophages after thermal ablation of tumors [100]. When an immune adjuvant namely CpG and immune checkpoint blockade, anti-PD-1, were added to their FUS treatment regimens, the authors observed an enhanced therapeutic efficacy and generation of robust anti-tumor immunity with FUS [101]. CpG is an activator of dendritic cell and anti-PD-1 checkpoint inhibitor presrves functional status of T cells by blocking immune checkpoint

PD-1 present on T cells. Based on these findings, we can speculate that addition of APC activators to FUS treatment regimen can be highly valuable in keeping tumor infiltrating APCs in an activated state to generate robust tumor specific cytotoxic T cell response.

Importance of tumor antigen presentation in generating potent anti-tumor immunity

For anti-tumor therapy to be effective, tumor associated antigens or neoantigens must be recognized and efficiently processed by APCs and eventually evoke T cell based anti-tumor response. Preclinical studies in different mouse cancer models have demonstrated the significance of effective tumor antigen processing and presentation process in the generation of anti-tumor immunity [102,103]. APCs ingest cancer cells expressing antigen and migrate to regional lymph nodes to present tumor specific antigen to naïve T cells and generate tumor specific immunity [104]. Tumor associated antigens presented by APCs are essential to prime tumor (antigen) specific T cells, which subsequently identify and kill tumor cells that express the target antigen [105]. APCs such as DCs, macrophages, and B cells act as a bridge between innate and adaptive anti-tumor immunity. Mature APCs after encountering tumor specific antigen migrate to secondary lymphoid organs for antigen presentation to naive T cells [106]. APCs break down ingested tumor antigens into peptides and express them on their surface as MHC-peptide complex. Naive T cells recognize and attach to MHC-peptide complex on the APCs through T cell receptor specific for the tumor antigen, this serve as first signal for T cell priming [107]. To effectively activate T cells, APCs must provide additional stimulation through co-stimulatory molecules on their surface [108]. Mature and activated APCs upregulate expression of CD80 and CD86 co-stimulatory molecules on their surface, which bind to CD28 on T cells to act as the second signal [109]. Immature and non-functional APCs express insufficient co-stimulatory molecules, resulting in generation of weak or non-functional T cells [109].

In addition to these two signals, production of specific cytokines after APC-T cell engagement drives differentiation of naive T cells towards CD4 T cells or CD8 T cells and serves as the third signal for T

cell activation [107]. Tumors acquire an important mechanism of immune escape by maintaining APCs in an immature stage and thus preventing these cells from generating anti-tumor T cell immunity [110]. Tumor cells secrete IL-10 cytokine that inhibits dendritic cell maturation and their secretion of IL-12, a T cell activating cytokine [111]. Several other studies have shown that tumor cells also secrete factors like VEGF and TGF-β which significantly inhibit maturation and function of DCs and enable them to escape T cell based immune response [112-114].

In a mouse melanoma study, it was found that intratumoral injection of CpG (a dendritic cell activator) resulted in enhanced infiltration of melanoma specific CD8 T cells into tumors and caused tumor suppression [115]. Combination of CpG and cryoablation in a B16F10 melanoma study resulted in a more effective tumor suppression than either of the treatments alone. The underlying mechanism behind superior efficacy of combination treatment was found to be synergy between antigen release after tumor ablation and DC maturation following CpG therapy, which together resulted in an efficient presentation of released tumor antigens and activation of T cells [116]. In line with these studies, when agonist anti-CD40 antibody, an APC activator, was combined with radiation therapy an improved therapeutic outcome was observed in preclinical pancreatic cancer models. This combination therapy enhanced T cell priming and there was a generation of CD8 T cell memory response against the tumor, resulting in long survival of mice [117]. Based on these studies, it is evident that the functional status of APCs is important for generation of tumor specific T cell immunity. Inclusion of APCs activator like CpG or agonistic CD40 antibody can enhance therapeutic outcomes of other therapies in poorly immunogenic tumors, where inefficient antigen processing and presentation is expected.

Role of CD40 signaling, cytokines (Interferon-γ, IL-2, IL-12, TGF-β2), and granzymes in anti-tumor immunity

CD40-CD40L signaling and antigen presentation

CD40 is a member of the tumor necrosis factor α (TNF-α) receptor family. It is a transmembrane glycoprotein with a molecular weight of 48 KDa [118,119], and is found in antigen presenting cells (APCs; e.g. DCs and macrophages), hematopoietic progenitor, epithelial and activated T cell [120,121]. CD40L (CD154) is the ligand of CD40 receptor. It is an integral membrane protein with a molecular weight of ~39 KDa, and is expressed on activated T cells, platelets, and B cells type II membranes [122-124]. The interaction of CD40L-CD40 invokes cell-mediated immunity via activation of APCs and efficient T-cell functions, and humoral immunity via B cells [125,126]. Specifically, CD40 enhances the maturation of DCs, upregulating costimulatory molecules that help the clonal expansion and differentiation of T cells [127].

Mechanistically, CD40-CD40L ligation induces the recruitment of tumor necrosis factor receptor–associated factors (TRAFs) adaptor proteins to CD40's cytoplasmic tail [128]. This binding activates the downstream signaling through activation of NF-κB inducing kinase (NIK), members of the mitogen-activated protein kinase (MAPK) family, and receptor interacting protein (RIP), leading to transcription of target genes and production of inflammatory mediators, prolongation of MHC/antigen complex presentation and improvement in DC survival [129-131]. In particular, activation of the NF-κB pathway via CD40 in mice and human can upregulate the level of antiapoptotic protein Bcl-XL and Bcl-2, which is vital for DC maturation and survival [132-134]. [135-137]. There are five members of NF-κB family in the mammalian system- NF-κB1 (p50), NF-κB2 (p52), c-Rel, RelA (p65), and RelB [138]. The canonical NF-κB pathway is comprised of active NF-κB dimers mainly NF-κB1/RelA, and the noncanonical pathway consists of NF-κB2/RelB [139]. The canonical NF-κB1 pathway induced IL-12 production from DCs leading to immediate inflammatory responses and differentiation of naïve T cells to Th1 phenotype [140,141]. The noncanonical NF-κB2 pathway regulates various chemokines such as CCL9 and CCL21 [142,143].

Interaction of CD40L present on activated CD4+ T helper cells with APCs [144], enhances the levels of MHC class II, CD80/CD86, and CD58, aiding the DC's antigen presentation efficiency by providing

a ‘second’ indispensable signal for T cell activation [145]. Besides providing the costimulatory signals to naïve T cells, mature DCs also secrete the proinflammatory cytokine IL-12, that drives differentiation of naïve CD4+ T cells towards Th1 phenotype [146,147]. In contrast, “immature” or “tolerogenic” DCs can present signal 1 (antigen peptide–MHC complex) but lack the costimulatory signals. This results in the differentiation of naïve CD4+ T cells to CD4+ regulatory T cells and dysfunction or anergy of antigen-specific cytotoxic CD8+ T cells [148]. Among various tumor types, melanoma in advanced stages can keep the DCs in an immature state by increasing the production of IL-10 and TGF-β, leading to T cell anergy [149,150]. T cell dysfunction or anergy is one of the biggest challenges faced by cancer immunotherapy. In normal conditions, CD40 ligand (CD40-L) present on helper T cell interacts with CD40 receptor on APCs and activates APCs. Agonistic CD40 antibody binds to the CD40 receptor present on dendritic cells and can substitute the need of CD40-L based stimulation of APCs by helper T cells [151]. The activation of DCs by CD40 stimulators such as agonistic CD40 antibody may therefore protect T cells from dysfunction. Additionally, CD40 stimulation can directly inhibit cancer growth in CD40+ tumors such as breast, bladder, ovarian, non-small cell lung, cervical, and squamous epithelial through apoptosis induction and/or blockade of cell cycle [152]. For instance, in one study, agonist CD40 antibody was shown to cause direct lymphoma and leukemia cell killing by antibody dependent cellular phagocytosis (ADCP) and antibody dependent cell mediated cytotoxicity (ADCC) [153,154]. Importantly, by enhancing the Fc receptor (FcγR) binding capacity of CD40 antibody through Fc end engineering, an 150 fold enhancement in ADCP and ADCC was observed in leukemia, multiple myeloma, and B-lymphoma cell lines [154].

Tumor cells evade recognition by cytotoxic T lymphocytes (CTL) by down-regulating MHCs and transporter associated with antigen processing (TAP), TAP is involved in transport of peptides from cytosol to endoplasmic reticulum, where then the transported peptides bind with nascent MHC molecules [155,156]. CD40 stimulations can prevent this immune escape mechanism, resulting in an enhanced TAP expression, MHC class I molecule expression, and processing of endogenous antigen

[157]. Further, the ligation of CD40 with endothelial cells drives proinflammatory cytokine production and expression of cell adhesion molecules such as ICAM-1, and VCAM-1, improving the migration of leukocytes and T cell homing [158].

CD40–CD40L engagement not only activates APCs, but is also crucial for the generation and survival of plasma and B memory cells [125]. CD40 stimulation on B cells promotes formation of germinal center, immunoglobulin isotype switching, and immunoglobulin somatic mutation to enhance antigen affinity of produced antibody, leading to efficient humoral immune response [159,160]. Like DCs, in macrophages, ligation of CD40 improves antigen presentation and effector function. Peritoneal macrophages activated with agonist CD40 antibody *in vivo* resulted in enhanced production of nitric oxide, tumor necrosis factor alpha (TNF-α), IL-12, IFNγ, and demonstrated cytostatic effect on B16 melanoma cells in vitro by apoptosis [161,162]. [163]. Additionally, CD40 stimulated macrophages were shown to achieve tumor cell killing, depleted tumor stroma and facilitated infiltration of immune cells into the pancreatic tumor [28].

CD40s can also directly or indirectly activate NK cells [164]. NK cells expressing CD40L can directly interact with CD40+ APCs, or indirectly following IL-12 production by the activated APCs [165]. IL-12 promotes proliferation of NK cells and enhances their effector function by inducing IFN-γ secretion [166]. Activated NK cells then exerts tumor cell killing by increasing the expression of TNF-related apoptosis-inducing ligand (TRAIL) [167]. TRAIL binds with death receptors DR4 and DR5, leading to target cell apoptosis [168]. Further, the activated NK cells can kill target cell by IL-12 dependent upregulation of perforin and granzyme B [169].

CD40 stimulation a novel approach towards anti-tumor immunity

In pancreatic tumor models like KPC and Panc02, where baseline T cell infiltration and presence of tumor associated or neoantigen is low, CD40 stimulation has been shown to achieve tumor regression and cure [117,170]. In murine tumors that had poor expression of tumor associated antigen the addition of

CD40 agonist antibody with chemotherapies (gemcitabine and paclitaxel) resulted in generation of anti-tumor immunity [171-174]. These studies demonstrated that APCs activation by CD40 antibody after tumor cell killing and release of antigens resulted in generation of tumor specific T cell immune response. Regression of tumors with combination of chemotherapy and CD40 was not observed in T cells depleted or BATF3 knockout (lacking antigen cross-presenting dendritic cells) mice, further validating the necessity of APCs and T cells cross-talk for the generation of anti-tumor immunity [170]. CD40 stimulation in mice has also been shown to activate macrophages which in turn lead to in the shrinkage of tumor stroma and eventually high immune cell infiltration followed by tumor regression [28]. In spite of encouraging therapeutic outcomes in pre-clinical study, anti-CD40 agonistic antibody achieved only moderate success in clinical trials as a monotherapy. .

CD40 antibody (Selicrelumab) produced partial responses in 27% of enrolled advanced melanoma patients (4 out of 15) while none of 14 non-melanoma solid tumors patients responded to single dose CD40 antibody monotherapy [175]. Other clinical trials with CD40 antibody as a single therapy agent also resulted in minimal anti-tumor response in spite of trying different routes of administration in the patients [176,177]. However, clinical outcomes were improved when CD40 antibody was used as a part of combination therapy. Based on clinical trials, CD40 antibody in combination with chemotherapy drugs namely cisplatin, carboplatin/paclitaxel, and gemcitabine achieved an overall response rate of 20-40% in solid tumor patients [173,178]. CD40 antibody in combination with anti-CTLA4 antibody (immune checkpoint inhibitor) was tested in 22 patients of metastatic melanoma. Clinicians observed complete remission of cancer in 2 patients while 9 out of 22 patients are long term survivor (more than 3 years) [179]. Combination of radiation and CD40 antibody in mouse pancreatic cancer models achieved tumor regression and better survival outcomes compared to either therapy alone [117]. Results from these clinical trials and pre-clinical studies support the notion that CD40 antibody therapy can be a potential candidate for evaluation with emerging non-invasive therapies like FUS or HT to achieve maximum therapeutic success.

Role of cytokines in cancer immunity

Cytokines are proteins with low molecular weight involved in cell to cell communication. Different types of immune cells and stromal cells such as macrophages, DCs, T cells, NK cells, endothelial cells, and fibroblasts produce cytokines [180]. These proteins interact with target cells having corresponding receptors by autocrine signaling (acting on the same cells that produce them), paracrine signaling (acting on the nearby cells), or in some cases by endocrine signaling (acting on distant cells) [181]. This interaction can regulate target cell survival, cell differentiation and proliferation, immune cell activation, or cell death (Fig. 1.1) [182]. Some of the important cytokines that are involved in cancer immunity are listed in Table 1.1. and discussed below.

Interferon-γ (IFN-γ)

Interferons (IFNs) are the cytokines with antiviral, antitumor and immunomodulatory properties [183]. These cytokines are named "interferons" since they protected the cells by interfering with the viral infection [184]. IFN are of three types. Type I IFN family is represented by IFN-α and IFN-β and type II IFN family is made up of IFN-γ. Type III IFN family comprising of four homologous proteins IFN-λ1 to 4 was recently reported [185]. Expression of type I and III IFNs is activated by pattern recognition receptors (PRRs) involved in host-pathogen interactions [186]. In contrast, Type II IFN responds to microorganisms and cancer cells [187,188].

IFN-γ is a homodimer with two 17 KDa polypeptide subunits [189,190]. The symmetry of IFN-γ allows it to bind simultaneously to two receptors, resulting in amplification of the underlying responses [186]. IFN-γ is secreted predominantly by activated CD4+ T helper type 1 (Th1) cells, CD8+ cytotoxic T cells, natural killer (NK) cells and to a lesser extent, by natural killer T cells (NKT), professional antigen-presenting cells (APCs) and B cells [191-195]. Expression of IFN- γ is induced by mitogens and cytokines like IL-12, IL-18, type I IFN, and IL-15 [196-199]. Autocrine secretion of IFN-γ by APCs contributes to sustained self and neighbor cell activation. This is needed for early control of pathogen

spread and in adaptive immunity. T lymphocytes are the main paracrine IFN-γ source [186,200,201]. The biological effects of IFN-γ happen through activation of intracellular molecular signaling, mainly by the JAK/STAT pathway [202]. Upregulation of the major histocompatibility complex (MHC) molecules is one of the first reported biological effects of IFNs [203,204]. IFNs are also involved in the upregulation of the MHC I and II antigen processing and presentation. In melanoma and multiple myeloma IFN-γ can result in upregulation of the MHC class II trans-activator (CIITA) leading to MHC II expression [205,206].

Th1-mediated immune response results in the production of IFN-γ which orchestrates activation of macrophages and NK cells. IFN-γ based upregulation of cell surface MHC I molecule mediates cell-based immunity through cytotoxic T cell activation against intracellular pathogens and tumor cells [186]. IFN-γ is crucial for the proliferation of cytotoxic T cell precursor and directly acts as a differentiation signal for cytotoxic CD8 T cell [207,208]. IFN-γ also promotes peptide-specific activation of CD4 T cells by upregulating cell surface MHC II on APCs [209,210]. IFN-γ promotes macrophages activation towards a pro-inflammatory phenotype leading to an increase in phagocytic ability [211]. IFN-γ induces tumor cell killing by various means such as nitric oxide production, activation of the NADPH-dependent phagocyte oxidase system, upregulation of lysosomal enzymes, and tryptophan depletion [212-214].

IFN-γ based activation of STAT1 regulates the expression of cyclin-dependent kinase inhibitor 1 (p21) in tumor cells, thereby inhibiting tumor cell proliferation [215,216]. IFN-γ can promote tumor cell apoptosis by upregulating expression of caspase-1, caspase-3, and caspase-8 and enhancing the secretion of FAS/FAS ligand [217-219]. IFN-γ induces tumoricidal effects through necroptosis, a form of regulated necrotic death that depends on the activity of the serine–threonine kinase known as RIP1 [220]. Interestingly, IFN-γ is also able to inhibit angiogenesis and survival of endothelial cells, leading to ischemia in the tumor stroma [221,222]. IFN-γ induces production of chemokines such as CXCL9, CXCL10, and CXCL11 that are involved in trafficking of T cell, NKT cell and NK cell into the tumors [223,224]. IFN-γ deficiency results in failure of T cells migration to tumor site [225]. IFN-γ induces

ifi202 and survivin genes that are involved in T cell survival, proliferation, and maturation in tumor-specific T cells [226].

IFN-γ can also lead to T cell suppression by increasing the population of myeloid derived suppressor cells (MDSCs) [227]. Nitric oxide produced by MDSCs decreases T and NK cells responsiveness to IFN- γ [228]. IFN-γ can also induce PD-L1 expression in cancer, myeloid, and stromal cells to inhibit effector tumor immunity [229]. It was demonstrated that for the induction of PD-L1 in tumors, the contact between tumor cells and CD8 T cells is crucial, suggesting the importance of paracrine IFN-γ exposure [230]. Anti-PD-1/anti-PD-L1 therapy may be effective in the cases where high levels of IFN-γ signaling is expected.

Interleukin-2 (IL-2)

IL-2 is a 15.5-kDa cytokine that is predominately secreted by antigen stimulated CD4+ T cells and CD8+ T cells, activated dendritic cells, and NK cells [231,232]. IL-2 stimulated cells express a high-affinity trimeric IL-2 receptor with the α-, β-, and γ-chains or a low-affinity dimeric receptor with β- and γ-chains [233,234]. Optimal activation of T cell with tumor antigen peptide-MHC-I complex and costimulatory ligands results in the production of IL-2 that in turn causes expression of IL-2Rα (CD25), IL-2Rβ (CD122), and IL-2Rγ (CD132), thereby forming the high affinity trimeric receptor for robust IL-2 signal transduction, resulting in clonal expansion of T cell and their differentiation into effector cells [235]. IL-2 stimulates cell growth of CD8+ T cells and their differentiation into memory and terminally differentiated lymphocytes occurs by multiple signaling cascades (e.g. STAT-5, Akt, and MAPK) [236] .

Following IL-2 stimulation, STAT-5 enhances Blimp-1 (a pro-differentiation transcription factor) to promote effector cell differentiation [237-239]. Activation of Akt by IL-2 regulates the expression of Bcl-6, leading to the control of Foxo family transcription factors activities and promotion of immune cell survival and proliferation [240]. IL-2-Akt activation also alters the expression of proteins involved in

trafficking of CD8 T cell such as CD62L, S1P1, and CCR7 and promotes their migration to peripheral sites of inflammation and infection [241,242]. In addition to STAT-5 and Akt signaling which mostly promote differentiation into effector T cell, IL-2 activates MAPK signaling that augments clonal expansion and activation of T cell [240]. IL-2 also promotes proliferation of T cell by upregulating cyclins and anti-apoptotic molecule Bcl-2 and downregulating p21 [243].

IL-2 produced from activated T cells can act in an autocrine or paracrine mode on cells expressing high affinity IL-2 receptor (IL-2R) [244]. Both helper T (Th) and nearby regulatory T cells (Tregs) upon IL-2 exposure upregulates the expression of L-2Rα (CD25) to form high affinity trimeric IL-2R [245,246]. IL-2 is not produced by Tregs but proliferation and function of Tregs is dependent on IL-2 secreted from Th cells [247,248]. Tregs act as a sink for IL-2 and compete with Th cells for IL-2. IL-2 can induce paracrine signaling in Treg cells leading to downstream activation of STAT5 and immunosuppression [249-251]. Thus, presence of high Treg cell population in cancer patients can deprive the effector T cells from IL-2 and severely affect their proliferation and expansion.

Redeker et al. showed that autocrine production of IL-2 promotes the expansion of antigen specific CD8+ T cells and this expansion of CD8+ T cells depended on the available dose of IL-2. The enhanced autocrine production of IL-2 by CD8+ T cells was able to delay tumor growth in mice [252]. Feau et al. demonstrated that autocrine production of IL-2 by CD8+ T cells is necessary for optimal secondary proliferation upon re-challenge with antigen. Interestingly, CD8+ T cells required their own autocrine IL-2 to generate optimal memory response even when adequate CD4+ T cell help was present to supply paracrine IL-2. CD4+ T cell help was required only to activate APCs via CD40-CD40L interactions and subsequent priming of CD8+ T cells to synthesize their own autocrine IL-2 [253]. Pro-inflammatory cytokines such as IL-12, IFN-γ, and IFN-α/β are believed to complement IL-2 in promoting clonal expansion of CD8+ effector T cells [254]. IL-2 based responses are highly desirable to achieve robust cytotoxic T cell based anti-tumor immunity.

Interleukin-12 (IL-12)

Interleukin-12 was originally described as a product of Epstein–Barr virus (EBV) transformed human B-cells that generated lymphokine-activated killer cells, activated NK cells, induced IFN-γ production and proliferation of T cell [255,256]. IL-12 is mainly produced by activated inflammatory cells such as monocytes, macrophages, DCs, neutrophils, and microglia [257-260]. During infection or presence of danger signals such as binding of LPS with toll like receptor on APCs induces production of IL-12. For instance, in macrophages IL-12 production can be induced through binding of TLR4 ligand such as LPS and TLR7/8 ligand such as R848 with their cognate receptors [261,262]. IL-12 receptor is expressed mainly by activated NK cells and T cells [263]. Other cell types, namely DCs and B cells express IL-12R [264,265]. Resting T cells have undetectable IL-12R but NK cells can express IL-12 at a low level [266].

IL-12 is a heterodimer made from 35 kDa light chain (p35 or IL-12α) and a 40 kDa heavy chain (p40 or IL-12β) [255]. IL-12 is a ligand of IL-12R receptor that is composed of two chains namely IL-12Rβ1 and IL-12Rβ2 [267]. Engagement of IL-12 with its receptor activates Janus kinase (JAK)–STAT (signal transducer and activator of transcription) pathway and in particular activation of STAT4 leads to specific cellular effects of IL-12 [268]. T cell activation upregulates the transcription and expression of both IL-12Rβ1 and IL-12Rβ2 chains of IL-12R. This upregulation, especially of the β2-chain is enhanced by IFN-γ, IFN-α, IL-12 itself, TNF and co-stimulation via CD28 [266].

Direct cell to cell contacts with other immune cells (via CD40L-CD40 interaction) or presence of cytokines like IL-1β and IFN-γ amplifies the production of IL-12 from DCs and monocytes [269-271]. The exact molecular event that triggers IL-12 production in solid tumors is uncertain, but CD40L–CD40 interaction may be the most likely mechanism involved in induction of IL-12 secretion [272]. Cytokines such as IL-10 and TGF-β produced in various cancers suppress production of IL-12 [273]. T-cell immunoglobulin and mucin domain-containing protein 3 (Tim-3) can also inhibit the production

of IL-12 by DCs [262]. IL-12 is a key player that links innate and adaptive immune response. Activated APCs produced IL-12 leads to activation and proliferation of T cells and NK cells, and enhances their effector function by inducing the transcription of cytokines and cytolytic factors such as perforin and granzyme B [274,275].

IL-12 promotes polarization of T cells into a Th1 effector cell phenotype [276,277]. Th1 polarization by IL-12 is achieved by inhibition of TGF-β. TGF-β induced T cell differentiation causes the production of Tregs and Th17 cells [278]. In addition, IL-12 programs T effector cells for the generation of effector T memory cells [279]. Direct effect of IL-12 on APCs has also been reported. The activation of IL-12R in APCs did not involve the canonical STAT pathway but it enhanced the ability of these cells to present poorly immunogenic tumor peptides [280]. IFN-γ secreted upon IL-12 stimulation alone or along with other synergizing cytokines such as IL-2 and IL-18 is the key mediator of IL-12 induced responses [196,281]. This secreted IFN-γ after IL-12 stimulation, in turn acts on APCs by positive feedback loop to initiate or increase IL-12 secretion [282]. In addition to IFN-γ release, IL-12 triggers the secretion of IL-2, TNF-α, and granulocyte-macrophage colony-stimulating factor (GM-CSF) [266]. IL-12 hampers tumor angiogenesis by IFN-γ dependent increase in the levels of CXCL9 and CXCL10 and decrease in vascular endothelial growth factor (VEGF) and metalloproteinase-9 production [283,284].

Transforming growth factor beta (TGF-β)

TGF-β is a major factor that controls development and physiology of both immune and hematopoietic cell [285]. The important role of TGF-β in the immune system regulation was demonstrated in mice that were deficient in TGF- β. It caused a multifocal and lethal inflammatory response along with disarrangement of various immune cell compartments including macrophages, dendritic cells, B cells, and T cells [286-288]. TGF-β is a cytokine that is conserved evolutionally and belongs to a large family of growth factors and morphogens [289]. In cancer, TGF-β supports evasion of

cancer cells from immune surveillance to promote malignant growth [290,291]. TGF-beta is produced by parenchymal and tumor infiltrating macrophages, dendritic cells, lymphocytes, and platelet cells [292]. Three isoforms of TGF-β identified in the mammals are TGF-β1, TGF-β2, and TGF-β3. TGF-β1 is the predominant isoform that controls the development, differentiation, function and homeostasis of different types of immune cells [293,294].

TGF-β is synthesized as an inactive molecule, containing a mature TGF-β's homodimer connected with latency-associated protein (LAP). This latent complex is either associated or released with latent-TGF-β-binding protein (LTBP). LTBP guides TGF-β to the extracellular matrix for activation [294,295]. To achieve its biological activity, mature TGF-β must be dissociated from LAP. This dissociation can happen through various mechanisms such as interaction with integrins, acidic pH based dissociation, or LAP proteolysis by matrix metalloproteinases [296]. Integrins play a very important role in TGF-β activation during both normal physiological and pathological conditions [285]. Integrin αvβ8 deletion on leukocytes resulted in age related autoimmunity and inflammatory bowel disease in mice, which suggested a crucial role of leukocyte's αvβ8 integrin in TGF-β activation and maintenance of T cell homeostasis and inflammation control [297].

Tregs present in tumor microenvironment can capture latent TGF-β by binding it to a transmembrane protein called glycoprotein A repetitions predominant (GARP) protein [298]. Integrin αvβ8 expressed on Tregs then mediates the activation and release of active TGF-β from the latent TGF-β/GARP complex [285]. Once released, active TGF-β binds to dimeric type 1 receptor (TGFbRI) and dimeric TGFb type 2 receptor (TGFbRII) to form a tetrameric receptor complex. This binding through its kinase activity initiates signaling pathways. TGFbRI activation leads to phosphorylation of SMAD2 and SMAD3 (mothers against decapentaplegic homologs 2 and 3)and these transcription factors then subsequently form a complex with the transcriptional intermediary factor 1 gamma (TIF1γ) or SMAD4 [299,300]. This complex translocates from cytoplasm into the nucleus and recruits transcription cofactors that modulate the expression of different target genes [301]. Additionally, TGF-β receptor complex can also

trigger SMAD-independent pathways such as phosphatidylinositol-3-kinase/AKT pathways, Rho-like GTPase signaling pathways, and various mitogen-activating protein kinases (MAPKs) pathways to regulate an array of functions in different types of cells and tissues [302].

TGF-β suppresses adaptive anti-tumor immune response by interfering with both differentiation and function of T cells. TGF- β inhibits differentiation of naïve T cells to Th1 phenotype. It was shown that mice lacking TGFBR2 on T cells had enhanced Th1 response [303], via TCR dependent activation of CD4+ and CD8+ T cells upon stimulation with antigen, and enhanced production of IFN-γ and granzyme-B [304,305]. TGF-β signaling impedes differentiation of T cells by silencing two master transcription factors of Th1 namely STAT4 and TBET. STAT4 blockade prevents (IFN)-γ production during the priming phase and TBET loss reduces production of IFN-γ during T cells re-stimulation after initial priming [306,307]. TGF-β affects T cell in early phase of activation by interfering with the Ca^{2+} influx-triggered T cell receptor stimulation (TCR) [308]. TGF-β also inhibits the proliferation of T cells by SMAD3, SMAD4, and cofactor TOB1 mediated silencing of IL-2 expression during the priming phase [309,310]. TGF-β controls various downstream regulators of cell cycle such as $p21^{Cip1}$, c-Myc, and $p27^{Kip1}$ and promote T cell apoptosis and cytostasis [311,312]. TGF-β activated SMADs along with transcription factor ATF1 suppress the promoters of genes involved in the lytic function of CD8+ T cells including granzyme B and IFN-γ, leading to direct inhibition of cytotoxic CD8+ T cells function [313]. TGF-β promotes the regulatory program on T cells and induce differentiation of naïve T cells or sub-optimally stimulated CD4+ T cells to the Tregs [314,315]. Transcriptomic datasets revealed correlation of FoxP3 expression with TGF-β levels in breast cancer and skin cutaneous melanoma [316]. Differentiation of naive CD4 + T cells to Tregs by TGF- β can be counteracted by pro-inflammatory cytokines rich environment that favors differentiation of T cells towards an effector phenotype [317,318].

In B16 melanoma tumors Tregs based inhibition of the cytolytic function of CD8+ T cells was observed and this immunosuppressive effect of TGF-β was reversed by TGF-β neutralizing antibodies [319]. TGF-β can inhibit antigen presenting abilities of dendritic cells by suppressing expression of

MHC-II genes or redirecting the differentiation of DCs toward an immunosuppressive immature myeloid cell phenotype [320]. This switching of DC phenotype is mediated by ID1 a transcriptional regulator of downstream TGF- β signaling [321]. Additionally, TGF-β affects the function of NK cells by silencing TBET and IFN-γ expression in these cells leading to inhibition of Th1 responses. TGF-β induced silencing of NK cell surface receptors namely NKp30 and NKG2D inhibit ability of these cytotoxic lymphocytes to recognize stressed and transformed cancer cells [322]. TGF-β also promotes phenotype switching of tumor associated macrophages towards pro-tumoral and immunosuppressive M2 phenotype [323]. All these effects of TGF- β promote growth of tumors by making a highly immunosuppressive tumor microenvironment.

Granzymes mediated killing of target cells by cytotoxic lymphocytes

NK cells and CTL identify and kill infected or transformed cells through two major pathways. CTL and NK cells use the granule exocytosis pathway to induce cell death in the target cell, once these cytotoxic cells come in contact with the target cell, cytotoxic secretory granules present in the CTL and NK cells traffic to the immunological synapse and a cargo of deadly proteins namely perforin and granzymes is released into the synaptic cleft [324].

Perforin granule protein forms pores on target cell and promotes delivery of granzymes into the cytosol of target cells, that on entry, cleave their substrates to induce efficient and rapid cell death [325]. The activity of perforin is highly pH and calcium ion (Ca^{2+}) dependent such that perforin is inactive under acidic condition of secretory granules (pH 5) and active in the neutral pH environment of the immunological synapse [326,327]. These properties of perforin make acidic secretory granule a safe storage platform for perforin inside cytotoxic lymphocytes. X-ray crystallography studies suggest that various perforin related proteins are homologous in their pore-forming domain (the membrane attack complex and perforin (MACPF) domain) to the bacterial cholesterol-dependent cytolysins (CDCs) [324]. Several clues about the function of perforin have been provided by this relationship. Initially, CDCs

bind and oligomerize on the membrane surface into a pre-pore of 20–50 monomers. After this pre-pore assembly, two α-helices (transmembrane helical region 1 (TMH1) and TMH2) in every monomer unwind and insert as a pair of amphipathic β-hairpins into the membrane. This forms a full pore with a large β-barrel of 80 to 200 strands [328,329]. Perforin induced pores result in the delivery of granzymes to cytosol of target cell.

Granzymes are serine proteases with two six-stranded β-barrels that regulates substrate specificity and in the middle present is a catalytic triad containing aspartic acid, histidine, and serine [330]. In humans there are five types of granzymes namely A, B, H, K, and M. Mice express granzymes from A to G, K, M, and N [331,332]. Granzyme A upon entering the target cell induces an inflammatory form of cell death known as pyroptosis. Pyroptosis is a caspase-1 dependent inflammatory form of cell death. During pyroptosis there is formation of pores in the target cell which results in ion imbalance leading to cell swelling and death. The cell undergoing pyroptosis spills its content and forms a depot of immunogenic molecules known as damage associated molecular patterns (DAMPs) leading to inflammation [333]. Caspase-1 activation during pyroptosis results in cleavage of pro-IL-1β and pro-IL-18 to active forms [334]. Release of IL-1β and IL-18 inflammatory cytokine during this form of cell death further enhances immune response [335].

Recent studies have shown that pore forming effector proteins known as gasdermins are actively involved in the process of pyroptosis. There are different types of gasdermins namely, GSDMA, GSDMB, GSDMC, GSDMD, GSDME, and DFNB5 [336]. Gasdermins have two domains connected by a flexible linker, a C-terminal repressor domain and cytotoxic N-terminal domain. Proteolytic cleavage separates cytotoxic N-terminal domain from C-terminal domain, this free cytotoxic domain then inserts itself into the cell membrane and forms cell death causing pores in the membrane [337]. Disruption of membrane integrity by pore formation results in failure of ion homeostasis which leads to cell death. Zhou et al. has shown that granzyme A can induce caspase-1 independent pyroptosis in the target cell by cleaving inter-domain linkage in gasdermin B (GSDMB), after cleavage of

GSDMB's cytotoxic domain, it forms a pore in the target cell membrane resulting in cell death. It was also found that presence of IFN-γ up-regulated GSDMB expression and promoted granzyme A based pyroptosis. Both NK and T lymphocytes can induce pyroptosis in the target cell by granzyme A [338]. Earlier studies had shown that granzyme A after entering the target cell is transported from the cytosol to the mitochondrial matrix, which results in cleavage of an electron transport chain complex I component [339,340]. This led to a defect in mitochondrial redox function, maintenance of membrane potential, and ATP generation. These changes in mitochondria generated superoxide that drove an endoplasmic reticulum associated oxidative stress response complex known as the SET complex, (containing nucleases) which then promoted granzyme A induced target cell nuclear damage and cell death [341].

Another important granzyme involved in control of infection and cancer is granzyme B. Both CTLs and NK cells express granzyme B. Effector immune cells lacking granzyme B are much slower in killing target cells than the wild type cell. This suggests the important role of this serine protease in executing destruction of infected or oncogenic cells [342,343]. Granzyme B after entering into target cell induces cell death by directly or indirectly activating cell's intrinsic cell death proteases known as caspases [344]. Direct proteolysis of pro-caspase-3 and -7 into active caspases-3, and -7 by granzyme B results in caspase based degradation of numerous cellular protein substrates, promoting efficient and fast apoptosis [345,346]. Granzyme B is also able to directly cleave inhibitor of caspase activated DNAase (ICAD), promoting DNA hydrolysis. Studies have shown that granzyme B can cleave various proteins involved in protection against cell death such as MCL-1, DNA repair (DNA-PKcs), and Lamin B that are involved in the maintenance of nuclear integrity [344]. Additionally, granzyme B can also activate caspases through the cytochrome c/Apaf-1 pathway in which granzyme B mediated activation of the BH3-only protein Bid opens up BAX/BAK channel in the outer membrane of mitochondria [347]. This results in release of cytochrome c from the mitochondrial intermembrane space into the cell cytosol. Cytochrome c then binds and activates apoptosome, a caspase-activating

platform. Activation of the apoptosome in turn promotes downstream activation of caspases leading to cell death [348,349].

Granzyme H is highly expressed in NK cells and plays a crucial role in NK cell mediated immune response [350,351]. Studies have shown that granzyme H induces cell death by both caspase dependent and caspase independent manner [350,352]. Hou et al. found that granzyme H induced apoptosis in target cell by activating caspase-3 and Bid protein which resulted in release of cytochrome c from mitochondria into the cell cytoplasm and mitochrondrial damage. Cytochrome c release in the cytoplasm leads to activation of downstream apoptotic caspases and cell death. Granzyme H cleaves inhibitor of caspase activated DNAase (ICAD) directly, thus promoting fragmentation of DNA. The cell death induced by granzyme H is typically characterized by caspase activation, externalization of phophatidylserine, DNA fragmentation, condensation of nucleus, and cytochrome c release [352]. Fellow et al. demonstrated that granzyme H induced damage to mitochondria was due to its proteolytic activity and did not accompany with caspase activation. Mitochondrial depolarization resulted in production of reactive oxygen species (ROS) and cell death in target cell. In addition, condensation of chromatin and DNA degradation were also noticed while the induction of cell death was not mediated by Bid cleavage, cytochrome c release, activation of downstream caspases, or inactivation of ICAD [350].

Granzymes K and A are tryptases and closely linked on the same chromosome in both humans and mice [353,354]. Granzyme K is expressed in NK cells and CTLs [355]. Zhao et al. showed that granzyme K can directly cleave Bid to generate its active form and result in cell death by mitochondrial damage. This active form of Bid resulted in disruption of the outer mitochondrial membrane and escape of cytochrome c and endonuclease G in cytosol. The collapse of mitochondrial inner membrane potential was accompanied with rapid generation of ROS and cell death. It has also been shown that granzyme K can hydrolyze SET (nucleosome assembly protein), promote single stranded DNA nicks,

and inhibit repair mechanisms in target cell. These changes induce rapid cell death that is independent of caspase activation [354].

Granzyme M is highly expressed in NK cells and plays a critical role in NK cell mediated target cell killing [356]. Lu et al. showed that granzyme M directly cleaves ICAD to unleash the nuclease activity of CAD for inducing DNA fragmentation in the target cell. In addition, granzyme M also prevents cellular DNA repair by cleaving the DNA damage sensor enzyme poly(ADP-ribose) polymerase and forces cell to apoptosis [357]. Bovenschen et al. found that granzyme M can cleave the linker of actin-plasma membrane known as ezrin and also α-tubulin, the microtubule component. These cleavage events were independent of caspases involvement and granzyme M caused disorganization of microtubules affecting cell cytoskeleton [358]. NK cells and lymphokine activated killer (LAK) cells in mice express another granzyme known as granzyme F [359]. Shi et al. demonstrated that granzyme F can induce mitochondrial swelling and depolarization leading to ROS generation. Cell death caused by granzyme F death did not involve cleavage of Bid or caspase activation but was characterized by condensation of nucleus, mitochondrial damage and cytochrome c release, phosphatidylserine externalization, and nicking of single-stranded DNA [360].

Nanoparticles - a new era in therapeutics

In the last two decades, nanoparticle (NP) based therapeutics are successfully used in the treatment of cancer, infectious diseases, and pain management [361,362]. These nano-therapeutics are able to deliver cargo drugs precisely to the target site, enhance solubility of drugs, extend drug half-life, and also reduce drug immunogenicity [363,364]. First generation of NPs were made of lipids and polymers commonly known as liposomes and polymeric NPs [365]. Liposomes are spherical vesicular structure surrounded by a bilayer that can encapsulate both hydrophobic and hydrophilic agents and protect these agents (proteins, nucleotides, small molecule drugs, radionucleotides or imaging agents) during circulation in the body [366]. Encapsulation of agents in the liposomes protects them from early

degradation, inactivation, and dilution in blood after administration [367]. In 1980s, the first studies to evaluate the clinical potential of liposomes were conducted and it was found that liposomes improved therapeutic index of drugs namely amphotericin and doxorubicin [368,369]. NPs can also be functionalized, for example, with ligands for cell surface receptors, to promote targeting to specific cells and tissues. In addition, they can be coated with polymers to prolong circulation half-life [370].

Liposome formulations modified pharmacokinetics and biodistribution of encapsulated drugs and enhanced their delivery to diseased tissue in comparison to free drug [371]. This resulted in reduction of free drug toxicity *in vivo*. Doxil, a FDA approved liposomal formulation, showed significantly reduced cardiotoxicity compared to free doxorubicin (chemotherapy drug) [372,373]. In spite of these advantages, therapeutic efficacy of liposomal formulations is greatly affected by their rapid elimination from circulation [374]. To increase stability and circulation time of liposomes they were sterically stabilized by coating with a hydrophilic polymer know polyethylene glycol (PEG). This modification resulted in a modest improvement of liposome circulation time both in mice and humans [375-377]. To further improve the stability of nanoparticles, resilient materials like polymers were introduced in the field of nanotherapy.

Polymeric nanoparticles can be made from either natural polymers like chitosan, dextran etc. or biodegradable synthetic polymers like polylactic-co-glycolic acid (PLGA) and poly l-lysine (PLL)-LL. Thick and tough membrane of polymeric nanoparticles provides them better stability both *in vitro* and *in vivo* and addition of PEG further enhance their biological stability in circulation by protecting them from recognition by immune cells [378]. The advantages of higher stability of polymer nanoparticles than liposomes can be harnessed to obtain better control over drug delivery. These developments are encouraging but still nanoparticle based formulation achieve <10% of delivery to target site *in vivo* [379]. Once injected intravenously, proteins adsorb onto nanoparticles and form a protein corona on them, this leads to their recognition by immune cells mainly macrophages and rapidly get cleared [380]. Since, reticulo-endothelial system has very high population of macrophages it

clears off injected flagged nanotherapeutics within minutes of injection [381]. PEGylation can help in improving circulation life of nanoparticles to some extent, but it is not enough for clinical translation of NPs [382]. Preclinical studies done with polymeric nanoparticles showed that ~95% of particles were eliminated from the circulation in <30 minutes after injection [383,384]. To avoid rapid clearance of NPs from the circulation, new approaches which can make them less detectable by macrophages and RES can be highly beneficial for their clinical translation [385,386].

Red blood cell (RBC) an old carrier with new role

Erythrocytes or RBCs are natural carriers of oxygen and involved in oxygen transportation to various tissues and are key to sustain life. RBCs are biconcave discs of about 7 µm in diameter, have a surface area of about 160 μm^2, and life span of 100-120 days [387]. There are ~$5x10^6$ RBCs in 1 µl of blood and the total number of RBCs in a human being is ~$30x10^{12}$, and thus are the most abundant cells in the blood [385]. All these properties make them an ideal candidate to serve as a drug delivery platform. The life cycle of a blood parasite known as Mycoplasma *hemofelis*, a parasite that attaches itself to RBC, shows that the organism circulates for several weeks, completely undetected by immune cells [384]. This key observation paved the way for several investigations that were focused on the feasibility of attaching drugs or nanoparticles to RBCs and improve their circulation life. In early efforts, various agents like steroid, antibiotics, DNA, and proteins were encapsulated into RBC by hypotonic modification or electric insertion resulting in a loading efficiency of 10-70% of the agent [388-390]. Modification of RBC by osmotic swelling during hypotonic drug loading or electrical drug insertion caused unintentional changes in RBC namely cytoskeletal dysfunction (loss in stability and plasticity) and damage to the membrane resulting in phosphotidylserine exposure (a signal of cell damage and attracts phagocytes like macrophages) [391,392]. To improve drug delivery by RBCs, an alternate approach of coupling therapeutics on RBC surface has been immensely investigated in the last decade. RBC membrane has large surface area and provides opportunity to anchor multiple copies of therapeutics or proteins on them [385]. Coupling of drugs to the surface of RBCs theoretically

avoids damages caused by osmotic or electrical encapsulation procedures and therefore achieves drug loading on RBCs without compromising their biocompatibility [385,393]. Surface coupling greatly resolves diffusional issues of encapsulated drug inside cell, as drug coupled outside can interact easily to their substrate [394]. In a preclinical study, rat RBCs were tagged with tissue plasminogen activator (tPA) *ex vivo* and reinfused and circulation kinetics of RBC-tPA was compared with free tPA. RBC coupled tPA remained in circulation for about 2 hours whereas free tPA was eliminated from circulation within a few minutes after injection [395]. This study encouraged researchers to further explore *ex vivo* coupling procedure for nanoparticles. Polystyrene polymeric nanoparticles were adsorbed on the surface of harvested rat RBCs *ex vivo* and nanoparticle-RBC complexes were reinfused into the rats. 95% of the injected free polymeric nanoparticles were cleared from circulation within <30 minutes whereas 10% of the injected RBC coupled nanoparticles remained in circulation for 2 hours [384]. In a similar study with mice, harvested RBCs were modified *ex vivo* by coupling polymeric nanoparticles on their surface. These modified RBC-nanoparticle complexes when reinfused in mice remained in circulation for about 24 hours [396]. *Ex vivo* RBC manipulation procedures require availability of compatible blood donor, technical skills, and there is possibility of transferring blood-borne infection to the patients, thereby limiting smooth translation of this approach to clinics [385]. Nanoparticle based drug delivery system that can target anchor sites (e.g. glycophorin A receptors) present on RBC surface can allow safe and easy coupling of therapeutics on the circulating RBCs [397]. Nanotherapeutics decorated with RBC targeting ligands (e.g. Ter119 antibody) may resolve the limitations of *ex vivo* RBC modification and greatly enhance the clinical translation of RBC based drug delivery.

Abbreviations

ADCC	Antibody dependent cell mediated cytotoxicity
APC	Antigen presenting cell
CAD	Caspase activated DNAase
CTL	Cytotoxic T lymphocyte
DC	Dendritic cell
FUS	Focused ultrasound
ICAD	Inhibitor of caspase activated DNAase
ICAM	Intercellular adhesion molecule
MAPK	Mitogen-activated protein kinase
MHC	Major histocompatibility complex
MDSC	Myeloid derived suppressor cells
NK cell	Natural Killer cell
TRAIL	TNF-related apoptosis-inducing ligand
Th cell	Helper T cell
Treg	Regulatory T cell
STAT	Signal transducer and activator of transcription proteins
VCAM	Vascular cell adhesion molecule

Table 1.1. Cytokines and granzymes in cancer immunity

Cytokine/granzyme	Signaling pathway/target	Primary source	Target cell
IFN-γ	JAK-STAT	Activated CD4+ Th1 and CD8+ T cells, NK cells, NKT cells, APCs	T cells, NK cells, macrophages
IL-2	STAT-5, Akt, and MAPK	Antigen stimulated CD4+ and CD8+T cells, activated DCs and NK cells	T cells
IL-12	JAK-STAT	Activated monocytes, macrophages, DCs	T cells, NK cells
TGF-β	SMAD, JNK, and MAPK	Macrophages, DCs, T cells	T cells, NK cells, DCs
Granzyme A	Gasdermin B, mitochondrial electron transport chain	CTLs, NK cells	Cancer cell
Granzyme B	Caspase-3, -7, -8 ICAD, Bid	CTLs, NK cells	Cancer cell
Granzyme H	Caspase-3, Bid, ICAD, mitochondrial depolarization	NK cells	Cancer cell
Granzyme K	Bid, mitochondrial depolarization, nucleosome assembly protein SET	CTLs, NK cells	Cancer cell
Granzyme M	ICAD, poly (ADP-ribosome) polymerase, cell cytoskeleton	NK cells	Cancer cell
Granzyme F	Mitochondrial and nuclear damage	NK cells, lymphokine activated killer cells	Cancer cell

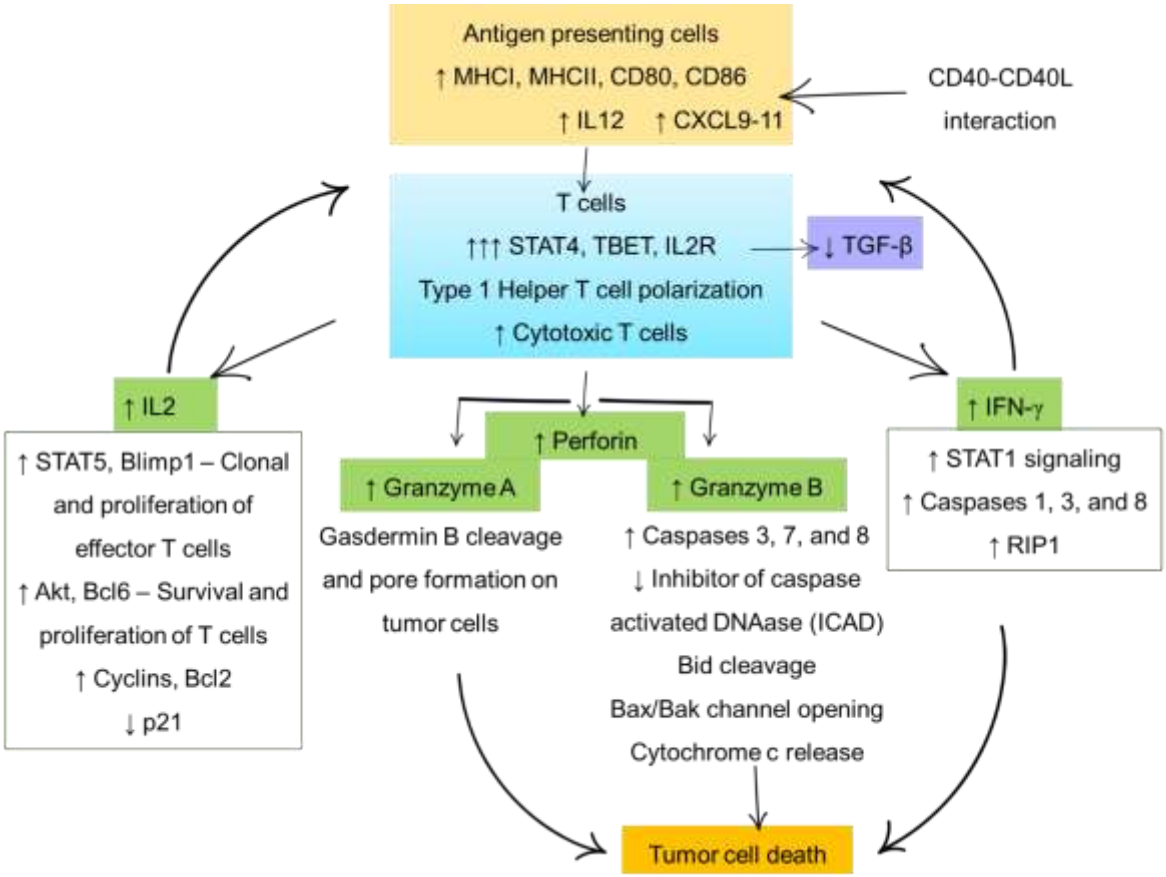

Fig. 1.1. Summary of CD40-CD40L interactions between APCs and T cells and the resultant antitumor immunity.

CENTRAL HYPOTHESIS

In-situ vaccination with CD40 agonist antibody (CD40) and local focused ultrasound (FUS) will improve anti-tumor immune response and immune checkpoint inhibitor (ICI) efficacy against advance stage melanoma

Aim 1: Investigate the role of FUS+CD-40 (FUS40) in preservation of immune cell function, and anti-tumor immunity in murine melanoma

- Evaluate the local and systemic anti-tumor effects of FUS40
- Determine the role of FUS40 in the preservation of T-cell function
- Assess the generation of melanoma-specific systemic immunity with FUS40

Aim 2: Determine the ability of FUS induced histotripsy (HT) with CD40 to improve checkpoint inhibitor therapy of advanced stage melanoma tumors

- Determine the immune mechanisms of HT+CD40 (HT40) in melanoma tumors
- Determine the role of HT40 priming in ICI therapy
- Evaluate abscopal effect of HT40 ± ICI in murine melanoma

CHAPTER II

IN-SITU VACCINATION USING FOCUSED ULTRASOUND HEATING AND ANTI-CD-40 AGONISTIC ANTIBODY ENHANCES T-CELL MEDIATED LOCAL AND ABSCOPAL EFFECTS IN MURINE MELANOMA

Abstract

The success of melanoma immunotherapy is dependent on the presence of activated and functional T-cells in tumors. The objective of this study was to investigate the impact of local-focused ultrasound (FUS) heating (~42–45°C) and in-situ anti-CD-40 agonistic antibody in enhancing T-cell function for melanoma immunotherapy. We compared the following groups of mice with bilateral flank B16 F10 melanoma: 1) Control, 2) FUS, 3) CD-40, and 4) CD-40+FUS (FUS40). FUS heating was applied for ~15min in right flank tumor, and intratumoral injections of CD-40 were performed sequentially within 4h. A total of 3 FUS and 4 anti-CD-40 treatments were administered unilaterally 3 days apart. Mice were sacrificed 30 days post-inoculation, and the treated tumor and spleen tissues were profiled for T-cell function and macrophage polarization. Compared to all other groups, histology and flow cytometry showed that FUS40 increased the population of tumor-specific CD-4+ and CD-8+ T cells rich in Granzyme B+, interleukin-2 (IL-2) and IFN-γ production and poor in PD-1 expression. In addition, FUS40 promoted the infiltration of tumor-suppressing M1 phenotype macrophages in the treated mice. The resultant immune-enhancing effects of FUS40 suppressed B16 melanoma growth at the treated site by 2-3-folds compared to control, FUS, and CD-40, and also achieved significant

abscopal effects in untreated tumors relative to CD40 alone. Additionally, the local FUS40 prevented adverse liver toxicities in the treated mice. Our study suggests that combined FUS and CD-40 can enhance T-cell and macrophage functions to aid effective melanoma immunotherapy.

Introduction

Metastatic melanoma is a highly metastatic and often lethal cancer, and incidence rates continue to rise steadily [398]. Most melanoma patients with metastatic disease are resistant to chemo- and radiotherapy and median survival rates are typically <4years. Immunotherapy using antibodies that block CTLA-4, PD-1, and PD-L1 to activate anti-tumor immunity has improved outcomes in a subset of patients [399,400]. This is a highly promising strategy, and depending on the tumor microenvironment, expression of target proteins, and cancer types can generate a response rate of 10-50% [401]. Despite profound clinical benefits for some, a large proportion (>50%) of melanoma patients do not respond to the immunotherapy. This is attributed to a lack of a baseline T-cell infiltration, and presence of dysfunctional T-cells characterized by an enhancement of PD-1 inhibitory functions and reduced Interleukin-2 (IL-2), Granzyme B and IFN-γ cytokine production [402]. Thus, new approaches are needed to prevent immune cell dysfunctions and T-cell exhaustion for effective immunotherapy. Towards this goal, this study investigated the role of locally applied focused ultrasound (FUS) heating (~42–45°C) and in-situ (intratumoral) injection of anti-CD-40 agonistic antibody in augmenting T-cell and macrophage functions for local and systemic immunity against murine melanoma. In-situ vaccination compared to systemic therapies utilize all relevant antigens, whether tumor-associated or neoantigens to generate robust antitumor response, therebyl eliminating the need to identify and isolate the tumor antigens for adaptive immunity [403,404].

CD-40 is a member of the tumor necrosis factor receptor family and is highly expressed in antigen presenting cells (APCs) including macrophages, monocytes, dendritic cells, and B cells [118,405]. Under normal conditions, T-helper cells expressing CD-40 ligand (CD-40L, CD154) can interact with APCs via CD-40, resulting in enhanced antigen-presentation and release of proinflammatory cytokines [406-410]. Some studies have also shown that the systemic administration of CD-40 agonists lowers the intratumoral PD-1 expression in T-cells, and aid the phenotypic

conversion of macrophages from M2 to M1 [411-413]. Currently, several clinical trials are investigating the role of anti-CD40 in various tumor types (NCT02376699, NCT03389802, NCT03123783, NCT03597282 NCT03165994, NCT02706353) [177,179]. FUS-induced local heating and associated stress can modify the tumor cells and microenvironment, causing antigen release, expression of heat-shock proteins, upregulation of pro-phagocytic signals such as calreticulin (CRT), and overall stimulate tumor immunity. Unlike ionizing radiation, which damages collateral tissues and induces oncogenic proteins, FUS generates protein coagulation and non-lethal thermal stress in less aggressively treated tumors [414,415]. Although radiation combined CD40 studies are starting to emerge [117,416], not much is currently known about how anti-CD40 synergises with FUS heating. Here, murine melanoma treated locally with CD-40 and FUS were profiled for the polarization status of macrophages and T-cell phenotypes. Data suggest that the combined CD-40 and FUS can prevent T-cell dysfunction and exhaustion, and improve macrophage polarization dynamics, suggesting the value of the proposed combinatorial modality in melanoma immunotherapy.

Materials

B16F10 murine melanoma cells were provided by Dr. Mary Jo Turk at Geisel School of Medicine at Dartmouth (Hanover, NH). B16F10 cells were cultured in DMEM supplemented with 10% fetal bovine serum (FBS) and 1% streptomycin/penicillin. Anti-CD-40 agonist antibody (FGK45) was purchased from BioXCell (West Lebanon, NH, USA). Fluorochrome-conjugated monoclonal antibodies (mAbs) for flow cytometry were purchased from BioLegend (San Diego, CA) and are listed here: APC anti-CD-4 (GK1.5), PE anti-CD3 (145-2C11), BB515 anti-MHCII (2G9), APC-Cy7 anti-IFN-γ (XMG1.2), APC-Cy7 anti-CD11c (1A8), FITC anti-CD-45.2 (104), PE anti-Granzyme B (QA16A02), APC anti-CD206 (C068C2), PE anti-CD11b (M1/70), and Pe-Cy7 anti-IL-2 (JES6-5H4) and anti-CD16/CD32 (Clone 93). Alexa Fluor 700 or Pe-Cy7 anti-CD-45 (30-F11), BV480 anti-F4/80 (T45-2342), V500 anti-CD3 (500A2), BV786 anti-CD-4, APC-H7

anti-CD-8a (53-6.7), BV650 anti-IFN-γ (XMG1.2), and Alexa Fluor 488 anti-Foxp3 (MF23) were purchased from BD Biosciences (San Jose, CA2).

Methods

Mouse melanoma model generation and study design

All animal-related procedures were approved and carried out under the guidelines of the Oklahoma State University Animal Care and Use Committee. We compared the following groups (n=6): 1) Control, 2) FUS, 3) CD-40, and 4) FUS+CD-40 (FUS40). 0.5×10^6 B16F10 cells in 50 μL of PBS was injected subcutaneously (sc) in the right flank regions of C57/BL6 mice. 4 days later, the mice were injected with 0.125×10^6 cells in the left flank region by sc route. Mice tumor volumes were measured daily by serial caliper measurements using the formula (length × width^2)/2, where length was the largest dimension and width was the smallest dimension perpendicular to the length. Unilateral treatment of the right flank tumor was initiated at a volume of 20-40 mm^3. FUS heating (42-45ºC) was applied for ~15min, and intratumoral injections of CD-40 antibody (50μg/session) was performed sequentially within 4h after FUS heating (Fig. 2.1). A total of 3 FUS and 3 anti-CD-40 treatments 3 days apart was performed. Additionally, on day 20 post inoculation, CD-40 alone was administered in the mice. Mice were sacrificed when the tumors reached >1cm in any dimension or 30 days post-inoculation. The right flank tumors and the spleen from the euthanized mice were excised, weighed, and processed for flow cytometry and histopathological studies. For flow cytometry, two-thirds of the harvested tumor was processed immediately. Specifically for flow studies, tumor samples (n=5/group) and spleen (n=4-5/group) were randomly selected and processed for immune cell profiling. For histopathological analysis, the remaining one-third of the tumor tissue was fixed in 10% neutral buffered formalin. Blood samples (n=6) were also collected by intracardiac route for biochemical analysis of liver function.

FUS set-up and treatment methodology

All FUS tumor treatment was performed using an Alpinion transducer with a 1.5 MHz central frequency, 45 mm radius, and 64 mm aperture diameter with a central opening of 40 mm in diameter. For FUS exposure, the center of the tumor was aligned at a fixed focal depth for efficient coverage (voxel size: 5 x 5 x 12 mm), and the alpinion VIFU-2000 software was used to define target boundary and slice distance in x, y, and z directions for automatic rastering of the transducer for 15 min. As the tumor grew, the focal point was rastered to cover the entire tumor. FUS treatment parameters used were as follows: 5 Hz frequency, 50% duty cycle, and 6 W acoustic power. The combination of these parameters achieved a mean target temperature of 42–45°C at the focus (measured by inserting a fiber optic temperature sensor; Qualitrol, Quebec, Canada) inside the tumor (Fig. 2.S3).

Immunophenotyping of melanoma tumors with flow cytometry

Single-cell suspensions obtained from the mechanical disruption of the tumors (n=5 mice/group) followed by enzymatic digestion with 200 U/mL collagenase IV (Life Technologies, NY, USA) were filtered through a 70-μm cell strainer (Corning Inc, Corning, NY). Cell suspensions were stained using the fixable viability stain 575V (BD Biosciences) according to the manufacturer's instructions to exclude dead cells and anti-CD16/CD32 antibody to block FcγIII/II receptor-mediated unspecific binding (93). The following panel of the indicated fluorochrome-conjugated anti-mouse antibodies were used to stain cells for 30 min in dark on ice: CD-45+ (Tumor infiltrating leukocytes; TILs), CD3+, CD-4+ (CD-4+ T or helper Th cells), CD3+, CD-8+ (CD-8+ T cells), CD11b+, F4/80+ (macrophages), CD11b+, F4/80+, MHCII high (MHCII high M1 macrophages), and CD11b+, F4/80+ MHCII lo/neg, CD206+ (M2 macrophages). For detecting IL-2, IFN-γ, Granzyme-B, and Foxp3 positive Treg cells, cells were washed after surface marker staining, fixed and permeabilized with transcription factor buffer set (BD Biosciences, San Jose,

CA) and incubated with Pe-Cy7 anti-IL-2, BV650 or APC-Cy7 anti-IFN-γ, PE anti-Granzyme-B or Alexa Fluor 488 anti-Foxp3 antibody for 30 min in the dark on ice. Stained cells were run in an LSRII analyzer (BD Biosciences) within 24h. Compensations were performed with single-stained UltraComp eBeads or cells (Fig. 2.S5). Datasets were analyzed using FlowJo software v.10.2 (Treestar Inc, Ashland, OR, USA). For all channels, positive and negative cells were gated on the basis of fluorescence minus one control.

Characterization of the T-cell activity and melanoma-specific systemic immunity

Single cell suspension of splenocytes (n=4-5) were stimulated *ex-vivo* with melanoma-specific differentiation antigen tyrosinase-related protein 2 (TRP-2) peptide for 10-12h to evaluate generation of TRP-2 melanoma antigen-specific immunity [417,418]. Briefly, 1-2x10^6 splenocytes were incubated with 2.5 μg TRP-2 peptide for 10-12h in the presence of Brefeldin A (eBioscience, 1000X solution) at 37°C and 5% CO2. Treated cells were washed with PBS and stained with CD-45, CD3, CD-4, CD-8, IL-2 and IFN-γ antibodies for flow cytometry. The number of T-effector (Teff) responding to TRP-2 stimulation was calculated as CD-45+ CD3+ CD-4+ or CD-8+ T cells that were positive for IFN-γ or IL-2. Data were expressed as the percentage of the total splenocytes.

Histopathological analysis of treated tumors

The control, FUS, CD-40, and FUS/CD-40 tumor tissues (n=5) were fixed in 10% neutral buffered formalin, processed, and embedded in paraffin as previously described [419]. Histopathological examination was made on sections (4 μm) stained with hematoxylin and eosin (HE). The tumor sections were screened qualitatively for immune infiltration using an Olympus BX50 microscope with Olympus DP26 digital photography by a veterinary pathologist blinded to treatment groups. These findings were also validated by quantitative flow cytometry assessment of tumor infiltrating leukocytes in the tumor samples (n=5).

Hepatotoxicity assessment of serum samples from the treated mice

Serum samples (n=6/group) from mice that reached study endpoints were analyzed by Dr. Charles Wiedmeyer from Comparative Clinical Pathology Services (Columbia, MO) for the liver function test. Specifically, Alanine aminotransferase (ALT), Aspartate aminotransferase (AST) and albumin to globulin ratio were evaluated to assess liver function.

Statistical analyses

Statistical analyses were performed using GraphPad Prism 8.0 software (GraphPad Software Inc, La Jolla, CA, USA). Data are presented as mean ± SEM unless otherwise indicated. For analysis of 3 or more groups, a one-way ANOVA test was performed followed by Fisher's LSD without multiple comparisons correction. Analysis of differences between 2 normally distributed test groups was performed using an unpaired t-test assuming unequal variance. P values less than 0.05 were considered significant.

Results

FUS40 enhanced survival and delayed tumor growth rates in treated and untreated sites

The treated and untreated flank tumor volumes in mice were monitored over 30 days post-inoculation (pi). Both control and FUS treated tumors showed a progressive increase in the tumor volumes in the treated site and reached sacrifice end-points (>1cm in any dimension or >15% loss in the body weight) by day 21 pi. In contrast, CD-40 and FUS40 achieved significant growth delay at the treated site. That said, FUS40 most effective amongst all the treatment groups (~2-3-fold> tumor supression compared to control, FUS, and CD-40; Fig. 2.2A). FUS40 also decreased tumor weight to a significantly greater extent by visual and statistical measures compared to all other groups (Fig. 2.2B & 2C). We next compared abscopal effects in the contralateral untreated site. As control and FUS mice reached sacrifice endpoint early in the trial, they were not included

for the enumeration of systemic immune-effects. Data showed that FUS40 induced superior suppression of untreated tumor volumes over 30 days compared to CD40 alone (Fig. 2.2D). Furthermore, two out of six FUS40 treated mice demonstrated systemic immunity against tumor challenge. In contrast, CD-40 treated mice demonstrated a 100% tumor take at the untreated side (Fig. 2.2E).

FUS40 promoted the recruitment of tumor infiltrating leukocytes (TILs) and Granzyme B+ PD-1- CD-8+cells in treated tumors

Analysis of tumor sections by H&E staining revealed prominent multifocal regions of coagulative necrosis in treated tumors compared to untreated control (Fig. 2.3A). FUS40-treated tumors exhibited significantly higher levels of perivascular infiltration of lymphocytes within the tumor mass and the presence of CD-45 expressing leukocyte in histology and flow cytometry among all the groups (Fig. 2.3A-C). To further characterize the functional status of the infiltrated immune cells, the CD8 T-cells were probed for Granzyme B+ and PD-1+ expression by flow cytometry. We found that FUS40 promoted an activated Granzyme B+ PD-1-CD-8+ T-cells phenotype and these were 2-fold higher than other groups (Fig. 2.3D). In contrast, the control, FUS, and CD-40 tumors were primarily composed of PD-1+ Granzyme B- or non-activated PD-1- Granzyme B- phenotypes, indicating that the functional status of CD-8+ was likely preserved by FUS40 therapy.

FUS40 enhanced the melanoma-specific production of IL-2 and IFN-γ from T-cells in the spleen

Dysfunctional and exhausted T-cells are not efficient in producing cytokines such as IL-2, TNF-α, and IFN-γ, or Granzyme B. Thus, to gain an understanding of the functional status of T-cells, the splenocytes were stimulated with the melanoma-specific TRP-2 peptide and assessed for the

production of IL-2 and IFN-γ. A 2-fold higher expression of the cytokines was noted in the CD-4+ and CD-8+T cells for FUS40 compared to CD-40, FUS, and control treatments (Fig. 2.4A-C).

FUS and CD-40 promoted the M1 macrophage phenotype in the tumors and spleen without significantly altering T-reg populations

Tumor-associated macrophages (TAMs) are known to release cytokines and chemokines that generally suppress cytotoxic effects of CD-8+ T cell [420,421]. These suppressive cells are often referred to as M2 macrophages or MDSC. One potential mechanism of immunotherapy is reducing the prevalence of immunosuppressive macrophages and increasing immunostimulatory macrophages MHCII high expressing M1 phenotype cells can activate and restore T cell effector activity [422,423]. We analyzed the tumors and spleen for M1 and M2 macrophage populations. FUS40 resulted in a ~1.3-2- fold enhancement of M1 phenotype compared to other groups in spleen and tumors (Fig. 2.5A-B). The increase in M1 phenotype did not accompany an increase of M2 macrophages in the tumor. Additionally, the M2 macrophage was significantly decreased (~2-2.5 fold) in the spleen with FUS40 compared to FUS and CD-40 alone (Fig. 2.5B). Furthermore, the population of Tregs that infiltrate tumors in response to chemokines secreted by TAMs was found to be unchanged between various treatments (supplementary data) [424].

In-situ FUS40 treatment did not impair liver functions

Systemic anti-CD-40 agonist administration is known to cause immune-mediated hepatotoxicity [425]. To assess whether intratumoral CD-40 impacted the liver functions, the ALT, AST, and albumin/globulin ratio in the treated mice sera were assessed. Both monotherapies (CD-40 or FUS) and combined FUS40 did not significantly alter the serum levels of liver enzymes and protein compared to untreated mice (Fig. 2.6).

Discussion

The success of melanoma immunotherapy is highly dependent on the type of tumor microenvironment [426]. The objective of this study was to test whether combined FUS40 can modify key immune-suppressive pathways and stimulate immune effector pathways in melanoma tumors to promote local and systemic immunity. FUS-induced local heating and stress are known to modify the tumor microenvironment to enhance vascular permeability and infiltration of immune cells [414,427-436]. We hypothesized that FUS enhanced immune infiltration combined with intratumoral agonistic anti-CD-40 antibody would enrich the populations of functional T-cells and macrophages, allowing superior protection against metastatic disease.

For evaluation of therapeutic and systemic immune effects, mice with bilateral tumors were exposed to FUS, CD-40 and combined FUS and CD-40 (FUS40) on the right flank tumor (Fig. 2.1). Monotherapy with FUS failed to improve survival rates compared to control. In contrast, CD-40 and FUS40 prolonged survival and suppressed the tumor growth rates at the treated sites (Fig. 2A-C). Also, amongst all the groups, FUS40 was most potent at inducing tumor growth delay and abscopal effect at the untreated site compared to CD40 alone, highlighting that the nonablative FUS dose can synergize with in-situ immune therapies (Fig. 2.2D and supplementary data). To determine if the induction of abscopal effects was mediated by the infiltration of cytotoxic T-cells, the treated tumor and spleen tissues were characterized for the production of IL-2, IFN-γ, and Granzyme B and the surface expressions of PD-1 [421,437]. Production of cytokines such as IL-2 from CD-4+ and CD-8+ T cells regulate the differentiation of T cells to Th1 cells, induce perforin, granzyme B, and IFN-γ production, and prevent T-cell exhaustion [234,438]. Results indicated that the splenocytes from the FUS and CD-40 treated mice that were stimulated with melanoma-specific TRP-2 antigen did not alter the IL-2 and IFN-γ productions from the CD4+ and CD8+T cells. In contrast, the FUS40 treated mice achieved a 2-3 fold higher production of the cytokines as well as the expansion of the T-cells. To gain further understanding of the

activation mechanisms, we next characterized the surface expression of PD-1 checkpoint protein and production of Granzyme B from the T-cells present in the treated tumor. Granzyme B is the key to T-cell tumor lysis [439]. However, a higher expression of PD-1 expression can reduce Granzyme B effect and drive T-cells to an exhausted stage [440]. We found that FUS40 consistently increased the proportion of Granzyme B+ PD-1- CD-8+ T-cells in the treated tumors (Fig. 2.3) compared to the control, FUS and CD-40 treated mice. In contrast, CD-40, FUS, and control mice tumors showed the presence of more dysfunctional PD-1+ Granzyme B- and non-activated PD-1- Granzyme B T cells. Collectively, these data suggested that adding FUS heating prior to CD-40 tumor treatments protected the T-cells from PD-1 mediated exhaustion, and expanded the population of activated and effector T cells populations rich in IL-2 and IFN-γ; features crucial for systemic immunity and abscopal effects.

The presence of activated innate cells (e.g. macrophages) and Treg can also influence immunotherapy outcomes in patients [441-443]. In particular, tumor-associated macrophages (TAMs) of M1 origin suppress T-cell exhaustion [444,445]. In contrast, M2 macrophages suppress antigen presentation and adaptive immune responses [446]. To dissect the TAM profiles, the M1 and M2 populations in the tumor and spleen tissues were assessed. We noted a significant enhancement of macrophage population of MHCII high M1 phenotype for the FUS40 mice compared to FUS, CD-40, and untreated control. Also, a significant reduction in the population of CD206+ M2 macrophages (~2-fold; Fig. 2.5) in the spleen tissues for FUS40 relative to other treatments was observed. Importantly, the increase of M1 macrophages in the FUS40 tumor was not associated with significant changes in the Treg populations (supplementary data). Tregs infiltrate tumors in response to chemokines secreted in the tumor microenvironments by TAMs (e.g., IL10, a cytokine produced by tumor macrophages) and can inhibit cancer cell cytotoxicity [447-449]. Our data suggest that FUS40 induce the polarization of macrophages without altering the Tregs.

Finally, the systemic administration of anti-CD-40 can damage hepatocytes and impair liver function [425]. A damaged liver is characterized by the release of ALT and AST enzymes from the hepatocytes and decreased albumin producing capacities. We tested if in-situ administration of anti-CD-40 antibody mitigates the adverse liver toxicity outcomes. Data suggested that the serum ALT and AST, and albumin levels were not impacted by CD-40 or FUS, or with FUS40 relative to control (Fig. 2.6). Thus, the proposed in-situ CD-40 approaches modulated tumor immunity without triggering liver toxicities.

Our study has some limitations. We didn't investigate the FUS40 therapeutic effects in a second tumor model. We believe that investigating the local and abscopal effect in tumors that are relatively more immunogenic (e.g. colon) compared to melanoma with FUS40 can shed new lights on the merits of the proposed combinatorial approach for clinical translational. Notably, a recent study in murine Panc02 pancreatic model showed that local CD-40 and radiation (5 Gy) induced infiltrations of T-cells (~20-fold higher) and improved anti-tumor immunity compared to representative controls [117]. Similarly, another study showed that anti-CD40 antibody and 5 Gy total body irradiation (TBI) increased T-cell–mediated survival by 100 days in murine B-cell lymphoma[416]. Additionally, a recent phase 1 clinical trials with anti-CD-40 and anti-CTLA-4 therapy in malignant melanoma caused the activation of cytotoxic immune cells and achieved an objective response rate of 27.3%[179]. These promising findings highlight the important role of anti-CD40 in augmenting therapeutic outcomes in the combinatorial regimen, and a need to conduct additional studies in various tumor types with FUS. The second limitation is that we didn't notice dramatic differences in tumor growth retardation between anti-CD40 alone and FUS40. We speculate that this is likely due to an insufficient CD40 treatment dosage/frequency or the release of tumor antigens with heating, and the development of adaptive resistance in tumors. Future studies with modulated anti-CD40 dosages, heating conditions, and combinations with other immunotherapies (e.g. checkpoints) can be performed to achieve superior outcomes. Finally, the

differences in the immune-activation mechanisms between FUS and tumor irradiation were not compared in our model system. Hypo-fractionated irradiation is known to induce immunogenic death of cancer cells. For example, local irradiation of B16gp melanoma tumors with a single dose of 10 Gy achieved significant retardation of tumor growth by increasing the infiltration of $CD45^+$ leukocytes (2-2.5-folds),enhancement of specific cytotoxic $CD8^+$ T cells, and macrophages [450]. Although promising, the enhanced immune responses with radiation is often inconsistent, and contrastingly some studies also show an increase in the immunosuppressive TGFβ cytokine production, and impaired effector T-cell function[451,452]. Importantly, prior studies conducted in 3LL Lewis lung carcinoma heated to to 42–43 °C for 1h achieved infiltration of DC and T cells in the tumor while also decreasing the regulatory T cells [453] and myeloid-derived suppressor cells (MDSC) [454]. Similarly, B16 primary tumors heated to 43°C for 30 min activated the dendritic and $CD8^+$ T cells in the tumor-draining lymph node (~1.35-fold) to result in local and systemic tumor growth inhibitions [455]. Furthermore, local heating has been shown to release heat shock protein from cancer cells to enhance sensitization to chemo-, radio- and immune-therapies[456-458]. These promising studies and our current data shows that FUS heating and CD40 can play a crucial role in mitigating the inconsistent immune responses from radiation.

In conclusion, our *in vivo* data show that FUS40 enhanced the proportion of IL-2, IFN-γ, and Granzyme B rich CD-4+ and CD-8+ T cells and population of M1 macrophages to suppress B16 tumor growth at the treated and untreated site, more so than CD-40 or FUS treatment alone. Studies are currently underway to characterize the role of FUS parameters (hyperthermia vs ablative) and CD-40 treatment sequences to aid the development of a pharmacologic phase 1 clinical trial.

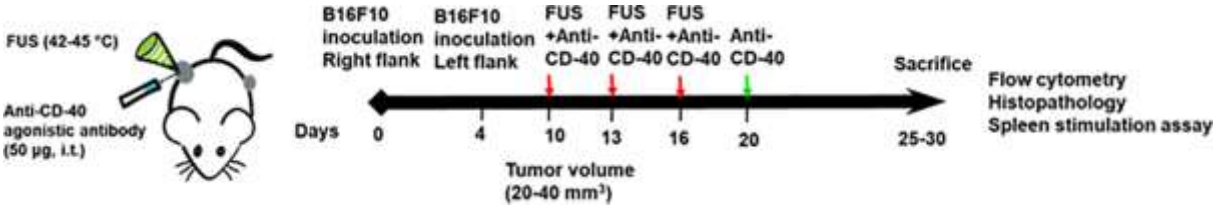

Fig. 2.1. Experimental design to assess the efficacy of FUS and CD-40 combination against melanoma tumors. 0.5×10^6 B16F10 cells were injected subcutaneously (sc) in the right flank regions of C57/BL6 mice. 4 days later, the mice were injected with 0.125×10^6 cells in the left flank region by sc route. Unilateral treatment of the right flank tumor was initiated at a volume of 20-40 mm^3. FUS heating (42-45ºC) was applied for ~15min, and intratumoral injection of anti-CD-40 agonistic antibody (50 µg) was performed sequentially within 4h of FUS heating. Red arrows indicate the three treatments with FUS and CD-40. Green arrow indicates the fourth anti-CD-40 dose. Mice were sacrificed when tumors reached >1cm in any dimension or reached 30 days post-inoculation. The harvested treated tumor and spleen were analyzed for the population and type of immune cell.

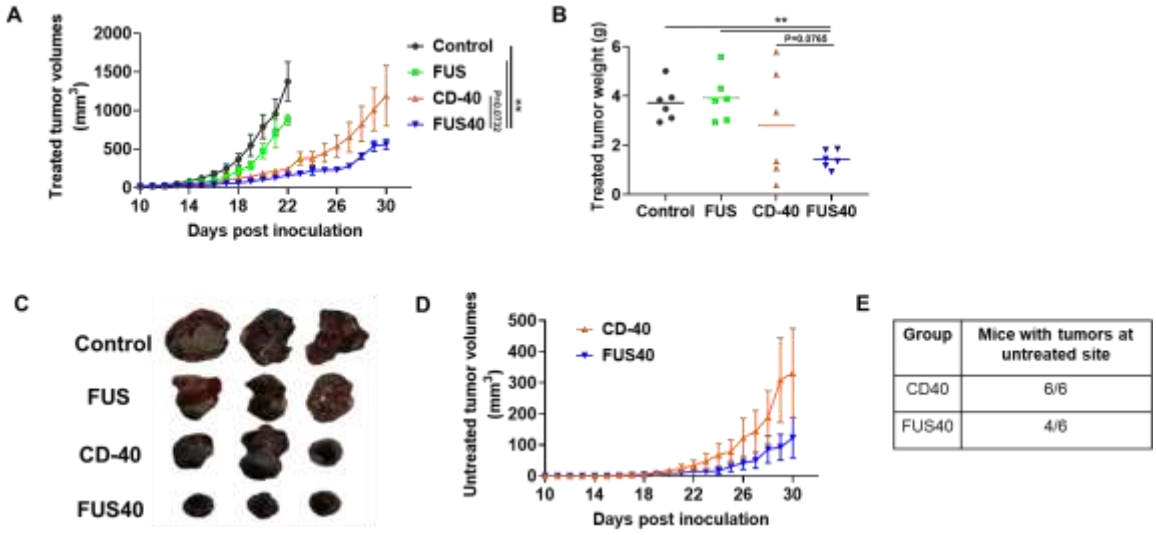

Group	Mice with tumors at untreated site
CD40	6/6
FUS40	4/6

Fig. 2.2. Local FUS therapy and in situ anti-CD-40 agonistic antibody suppressed the tumor growth of local and distant untreated site in B16F10 melanoma model. (A) Mean volumes of the treated tumors are shown till 30 days. Control and FUS reached sacrifice end points by day 21. CD-40 and FUS40 significantly decreased tumor volumes compared to FUS and untreated tumors; (B) Tumor weights at the time of sacrifice showed a significant reduction in the overall weight for FUS40 compared to other groups. (C) Representative images of the treated tumor. (D) Mean volumes of the distant untreated tumors are shown till 30 days. (E) Number of mice that were tumor free at the distant untreated site. Results are shown as mean ± SEM. One-way ANOVA followed by Fisher's LSD without multiple comparisons correction. * $p < 0.05$, ** $p<0.01$.

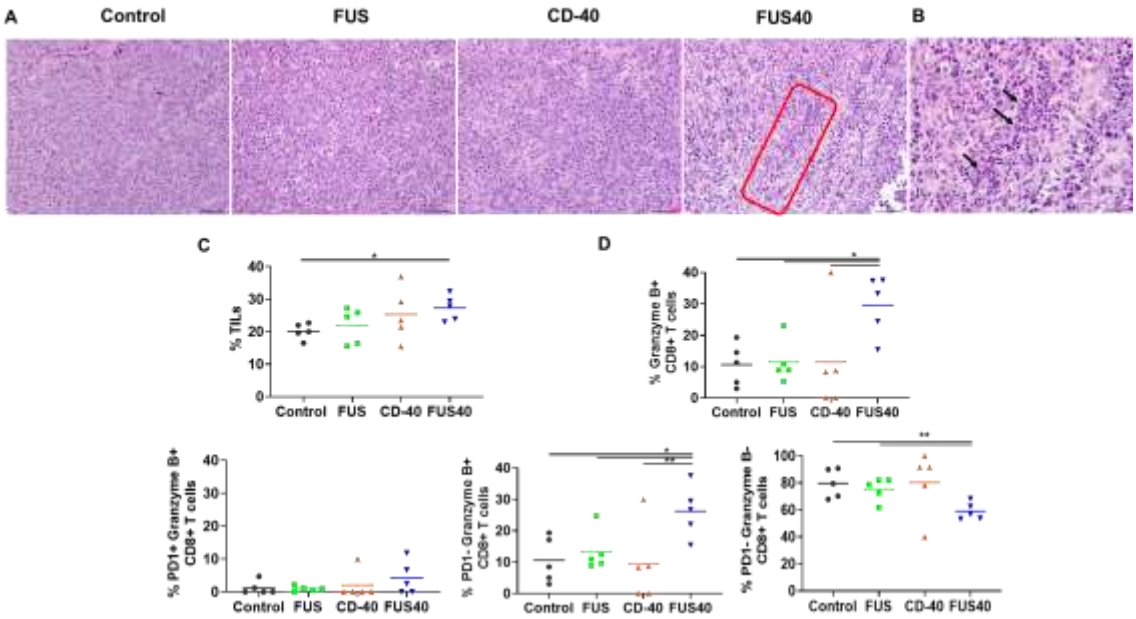

Fig. 2.3. FUS40 enhanced the recruitment of leukocytes and prevented T-cell dysfunction. (A) Compared to other groups, FUS40-treated tumors exhibited relatively higher perivascular infiltration of lymphocytes (red box) within the tumor mass upon qualitative imaging by a veterinary pathologist blinded for the groups; n=5, Hematoxylin:Eosin stain, Bar = 50µm. (B) Enlarged view of FUS40 tumor sections (red box) showing perivascular infiltration of lymphocytes (black arrows). Bar = 20µm. (C) Flow cytometry showed that the frequency of tumor infiltrating leukocytes in FUS40 tumors was significantly greater than the control tumors ($p<0.04$). (D) Percentage of Granzyme-B+ CD3+ CD8+ T cells was significantly higher for FUS40 (2-3-fold) compared to all other groups. FUS40 preserved activated CD8+ T cell from functional exhaustion by inhibiting PD-1 expression and enhancing Granzyme B production. For all channels, positive and negative cells were gated on the basis of fluorescence minus one control. Results are shown as mean ± SEM. * $p < 0.05$, Data were analyzed using a one-way ANOVA followed by Fisher's LSD without multiple comparisons correction.

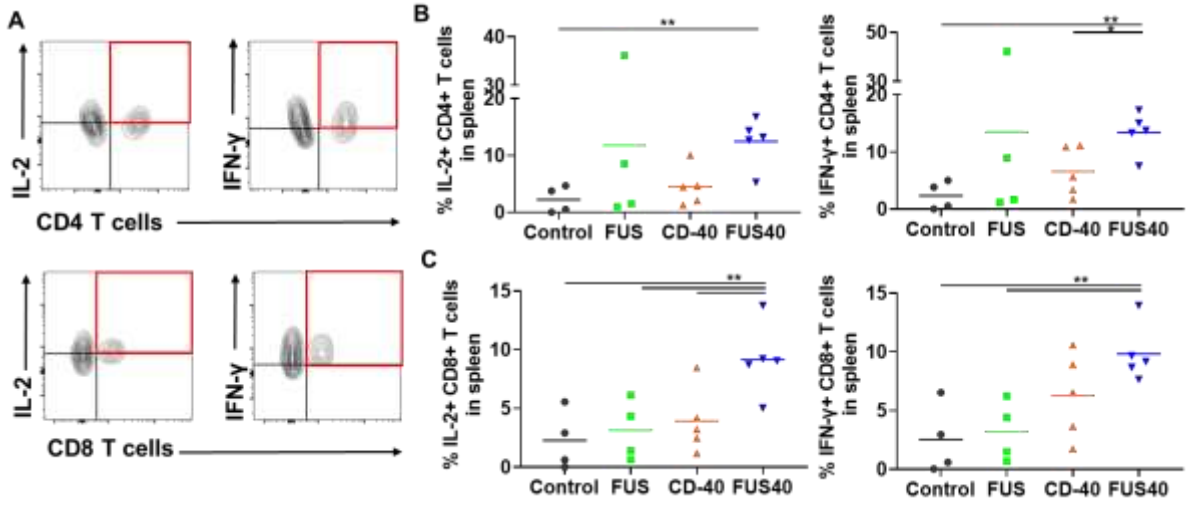

Fig. 2.4. FUS40 revived the production of effector cytokines from melanoma specific CD4+ and CD8+ T cells in spleen. B16F10 melanoma bearing mice treated sequentially with FUS and anti-CD-40 agonistic antibody were sacrificed and spleen was evaluated for TRP-2 specific immunity in an *ex vivo* stimulation assay. (A) Flow cytometry contour plots representing the gating strategy for CD4+ and CD8+ T cells producing IL-2 and IFN-γ. (B) IL-2 and IFN-γ secreting CD4+ T cells in splenocytes after *ex vivo* TRP-2 stimulation were significantly increased by the FUS40 compared to control. Differences were analyzed by an unpaired t test assuming unequal variance. (C) The highest frequency of CD8+ T cells producing IL-2 and IFN-γ was observed in FUS40. * $p < 0.05$, ** $p < 0.01$, one-way ANOVA followed by Fisher's LSD without multiple comparisons correction.

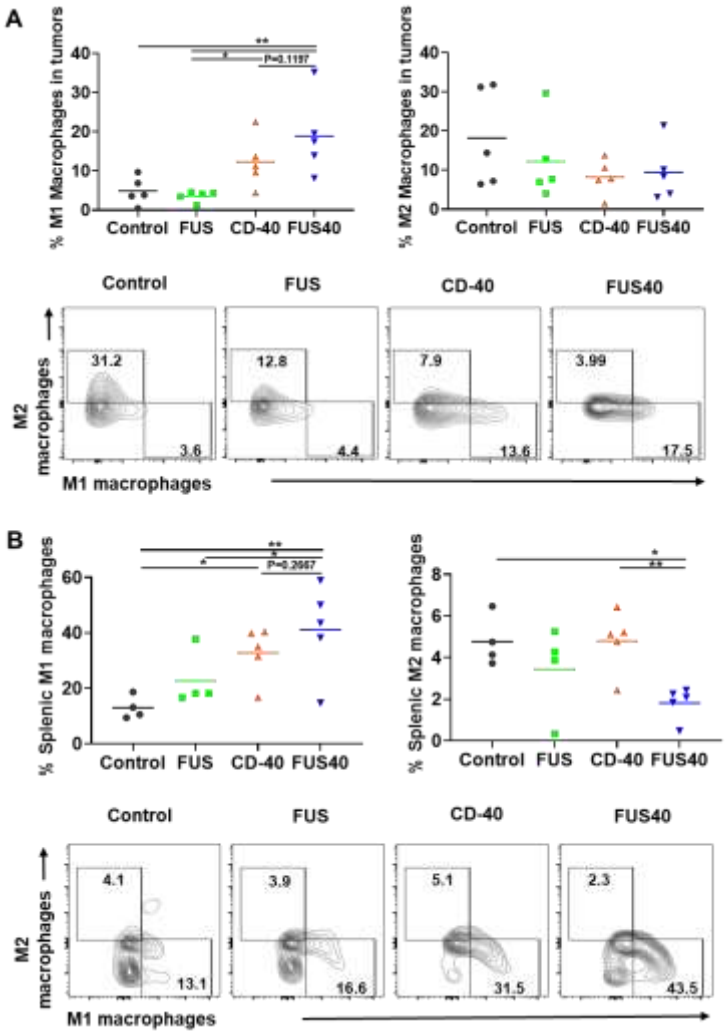

Fig. 2.5. FUS40 promoted M1 macrophage polarization in the tumor and the spleen. (A) Frequency of M1 macrophages in the tumor was increased by 4-fold for FUS40 compared to FUS and control, whereas M2 macrophages in treated tumors remained unaltered compared to controls. CD11b+ F4/80+ MHCII high (M1 macrophages) and CD11b+ F4/80+ MHCII lo/neg CD206+ (M2 macrophages). (B) An increased percentage of M1 macrophages was observed in the spleens from CD-40 and FUS40 cohorts. FUS40 reduced the frequency of M2 macrophages in the spleen compared to other groups. Data are shown as mean ± SEM. Statistics were determined by ANOVA followed by Fisher's LSD without multiple comparisons correction. * $p < 0.05$, ** $p < 0.01$.

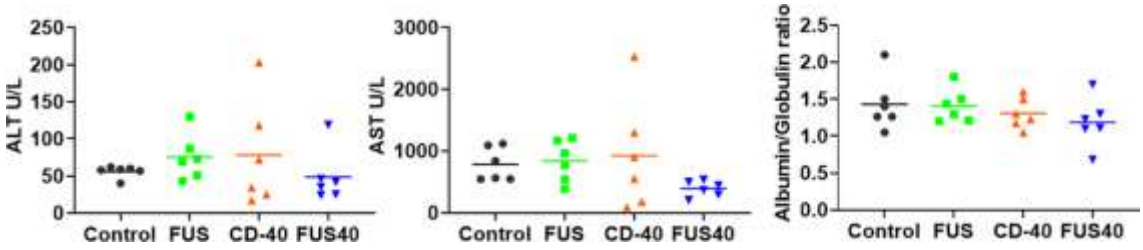

Fig. 2.6. Local FUS40 and CD-40 therapy did not cause liver toxicity in B16F10 melanoma bearing mice. Levels of ALT, AST, and Albumin to Globulin ratio in the serum of mice were determined at the time of sacrifice 25-30 days post tumor inoculation. Data were analyzed by ANOVA followed by Fisher's LSD without multiple comparisons correction (n=6).

Supplementary data

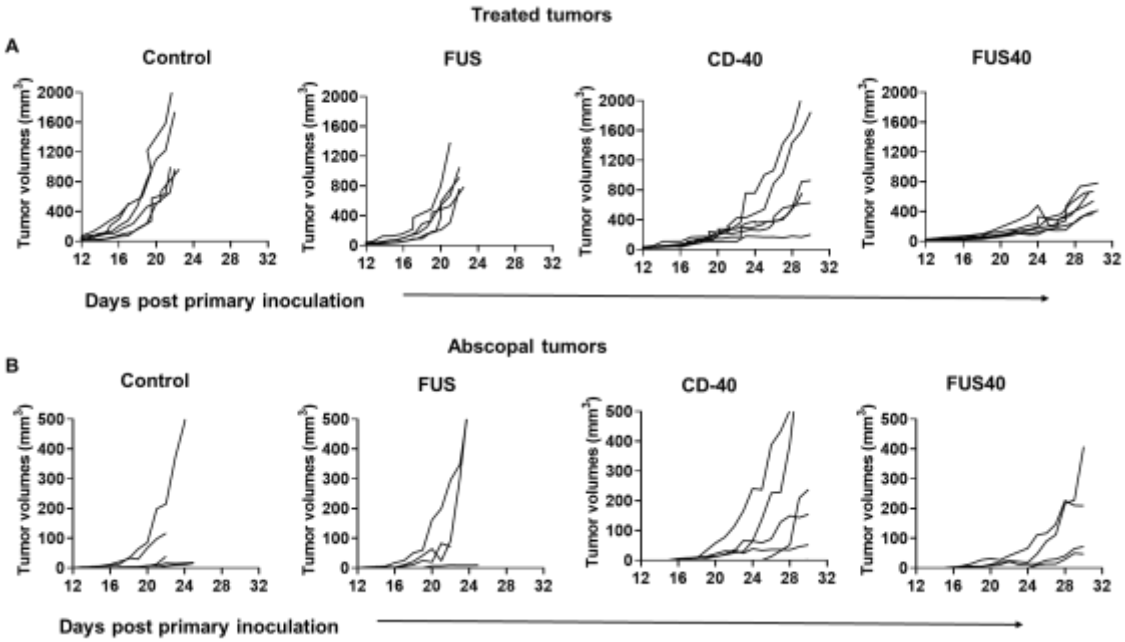

Fig. 2.S1. (A) Tumor volumes at the primary treated site from different groups (n=6 per group). (B) Individual tumor growth curves at contralateral untreated tumor site.

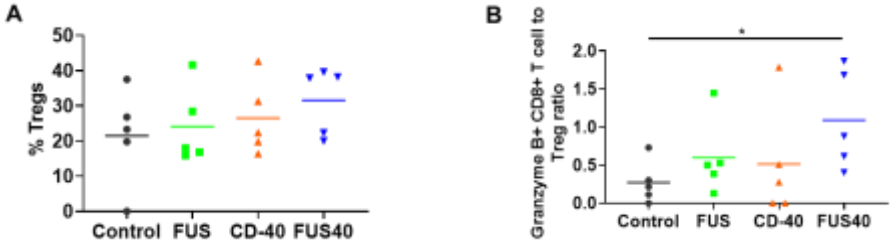

Fig. 2.S2. FUS40 therapy improved the functional cytotoxic Teff to Treg ratio in tumors. (A) Frequency of Foxp3+ CD3+ CD4+ Tregs was unaltered between the groups. (B) FUS40 exhibited higher Granzyme-B+ cytotoxic Teff cells to Tregs ratio than control. Data are shown as

mean ± SEM, * $p < 0.05$, ** $p < 0.01$, one-way ANOVA followed by Fisher's LSD without multiple comparisons correction.

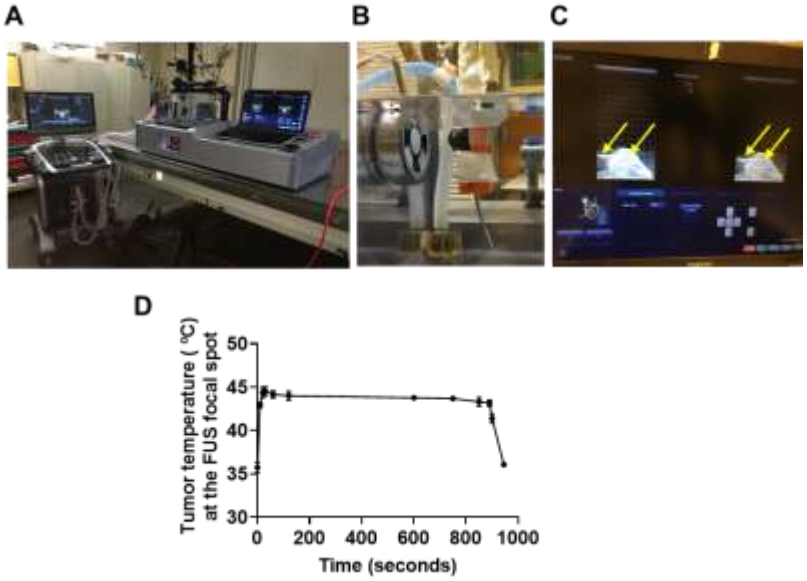

.**Fig. 2.S3.** (A) FUS system for mice tumor treatment; (B) Tumor regions of the anesthetized mice were aligned with the therapeutic transducer; (C) Tumor temperature during FUS therapy was measured by inserting a fiber optic temperature sensor into the solid core (indicated by yellow arrows); (D) Mean tumor temperature (n=3) measured during FUS treatment. Data are expressed as mean ± SEM.

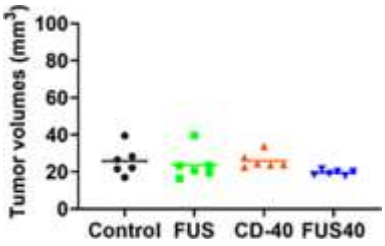

Fig. 2.S4. Mean initial treatment volumes in the treatment groups.

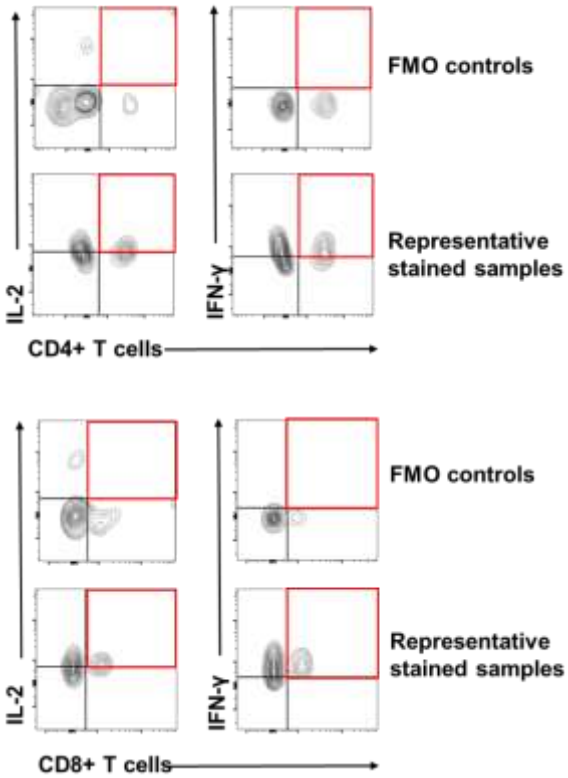

Fig. 2.S5. Flow cytometry contour plots showing the gating strategy for CD4+ and CD8+ T cells producing IL-2 and IFN-γ based on FMO controls. \

CHAPTER III

LOCAL IN-SITU HISTOTRIPSY AND CD40 STIMULATION IMPROVE THE CHECKPOINT BLOCKADE THERAPY OF MURINE MELANOMA

Abstract

Advanced stage cancers with a suppressive tumor microenvironment (TME) are often refractory to immune checkpoint inhibitor (ICI) therapy. Recent studies have shown that focused ultrasound (FUS) TME-modulation can synergize ICI therapy, but enhancing survival outcomes in poorly immunogenic tumors remains challenging. Here, we investigated the role of FUS histotripsy (HT) and in-situ anti-CD40 agonist antibody (HT+CD40: HT40) in ICI refractory murine melanoma. Unilateral and bilateral large (~330-400 mm^3) and poorly immunogenic B16F10 melanoma tumors were established in the flank regions of mice. Tumors were exposed to single local HT followed by an in-situ administration of anti-CD40 agonistic antibody. Inflammatory signatures post treatment were assessed using pan-cancer immune profiling and flow cytometry. The ability of HT40 ± ICI to enhance local and systemic effects was determined by immunological characterization of the harvested tissues, and by tumor growth delay of local and distant untreated tumors 4-6 weeks post treatment. Immune profiling revealed that HT40 upregulated a variety of inflammatory markers in the tumors. Immunologically, HT40 treated tumors showed an increased population of granzyme B+ expressing functional CD8+ T cells (~4-fold) as well as an increased M1 to M2 macrophage ratio (~2–3-fold) and CD8+ T: regulatory T cell ratio (~5-fold) compared to the untreated control. Systemically, the proliferation rates of the melanoma-specific memory T

cell population were significantly enhanced by HT40 treatment. Finally, the combination of HT40 and ICI therapy (anti-CTLA-4 and anti-PD-L1) caused superior inhibition of distant untreated tumors, and prolonged survival rates compared to the control. Data suggest that HT40 reprograms immunologically cold tumors and sensitizes them to ICI therapy. This approach may be clinically useful for treating advanced stage melanoma cancers.

Introduction

Immune Immune checkpoint inhibitors (ICIs) targeting CTLA-4, PD-1, and PD-L1 proteins have revolutionized the treatment of melanoma and other tumor types in patients [38,459-461]. Although promising, the immunosuppressive tumor microenvironment (TME) can influence ICI outcomes in a large proportion of treated patients [462-467]. This occurs due to masking of tumor antigens and proliferation of suppressive immune cells (e.g., regulatory T cells and M2 macrophages), which directly influence the functions of cytotoxic T cells [468-472]. Thus, there is a critical need to develop novel means for efficient activation of innate and adaptive immunity in the TME for superior ICI outcomes [62,473-476]. Herein, we evaluated the role of anti-CD40 agonistic antibody combined with focused ultrasound (FUS)-induced local histotripsy (HT) in TME activation and ICI therapy of melanoma tumors.

Focused ultrasound (FUS) is a non-invasive treatment modality that utilizes sonic energy to treat at an unlimited depth from the body surface. We and others have shown that FUS thermal therapy has an immunomodulatory effect in melanoma tumors [477-479]. Recently, mechanical FUS was also shown to cause immune-modulations [99]. In particular FUS induced mechanical tissue fractionation (aka histotripsy or HT) achieved with microsecond-length ultrasound pulses was shown to be particularly efficient in enhancement of tumor inflammation [99,480-482], and anti-tumor immune effects [483,484]. HT generates negligible heat, and thereby protects the tumor antigens from denaturation, which enhances immune cell infiltration by chemotaxis [485,486]. The activation of infiltrated antigen-presenting cells (APCs) and their subsequent migration to lymphoid tissues improve tumor antigen presentation to naïve T cells, thus causing antigen-specific tumor destruction [99,108,487].

Although the feasibility of HT in murine models has increasingly been reported [488], its ability to reprogram advanced stage poorly immunogenic tumors (e.g., B16F10) that lack major histocompatibility complex (MHC) and co-stimulatory molecules is not known. In general,

"immunologically cold" tumors such as B16F10 exhibit minimal APC functions, failure to accumulate cytotoxic infiltrating lymphocytes, dominant expression of PDL1 on tumor cells, and poor response to ICIs in advanced stages, thereby evading antitumor immunity [489,490]. To overcome this barrier, we combined HT with an in situ anti-CD40 agonist antibody. Agonist anti-CD40 antibody attaches to the CD40 receptor on APCs, enhancing CD40 signaling as well as expression of CD80, IL-12, and CCR7. These cause efficient APC activity and T cell-based cytotoxic responses [28,491-493]. Based on this premise, we posited that anti-CD40 agonist antibody will prevent B16F10 tumors from undergoing anergy or exhaustion and resistance to ICI. To investigate our hypothesis, we established late stage ICI refractory B16F10 melanoma and assessed the gene signatures involved in APC infiltration and T cell homing. Additionally, we assessed the types of immune cells in the treated and systemic organs. Our data suggested that HT40 sensitized poorly immunogenic B16F10 melanoma to ICI therapy and improved the survival outcomes in melanoma bearing mice.

Materials

B16F10 murine melanoma cells were provided by Dr. Mary Jo Turk at the Geisel School of Medicine at Dartmouth College (Hanover, NH, USA). They were cultured in DMEM supplemented with 10% fetal bovine serum and 1% streptomycin/penicillin. Agonist anti-CD40 antibody (FGK45), anti-PDL-1 antibody (10F.9G2), and anti-CTLA-4 antibody (9H10) were purchased from BioXCell (West Lebanon, NH, USA). Fluorochrome-conjugated monoclonal antibodies (mAbs) purchased from BioLegend (San Diego, CA, USA) and BD Biosciences (San Jose, CA, USA) for flow cytometry were as follows: FITC, APC-Cy7 or PE-Cy7 anti-CD45.2 (104 and 30-F11), APC-Cy7 anti-CD11c (1A8), APC or BV786 anti-CD4 (GK1.5 and RM4-5), PE, PERCP, or BV510 anti-CD3 (145-2C11), BB515 anti-MHCII (2G9), PE anti-Granzyme B (QA16A02), APC anti-CD206 (C068C2), AF700 anti-IFN-γ (XMG1.2), BB700 anti-CD11b (M1/70), PE-Cy7 anti-IL-2 (JES6-5H4), APC anti-CD44 (IM7), AF488 anti-CD62L (MEL-14), BV711 anti-F4/80 (T45-2342), PE-Cy7 anti-CD8a (53-6.7), and Alexa Fluor 488 anti-Foxp3

(MF23). Quick-RNA Miniprep Kits were purchased from Zymo Research (Tustin, CA, USA). The nCounter PanCancer Immune Profiling Panel was purchased from NanoString Technologies, Inc. (Seattle, WA).

Methods

Mouse melanoma study design and ICI treatments

All the animal related procedures were approved by the Oklahoma State University Animal Care and Use Committee. For tumor inoculation, B16F10 cells at 80– 90% confluency were harvested, washed, and diluted with sterile cold PBS. Male C57/BL-6 mice (n=5/group, 6-8 weeks old), were subcutaneously implanted with 0.5×10^6 cells (50µL) in the right flank for flow cytometry and gene expression assessment. To measure the abscopal effect and survival, mice (n=5) were injected subcutaneously in the right flank on day 0 with 0.5×10^6 cells and in the left flank on day 4 with 0.125×10^6 cells [477,494]. Tumor volume of mice was measured every day using a serial caliper (General Tools Fraction™, New York, NY, USA); volumes were calculated using the formula (length × width^2)/2, where length was the largest dimension and width was the smallest dimension perpendicular to the length. Treatments were initiated once the mice tumor volumes reached 330–400 mm^3. We compared the following groups: 1) Untreated Control, 2) HT, 3) CD40, and 4) HT40, each with and without the combination of anti-CTLA-4 and anti-PDL-1. HT treatment of tumors covered 40–50% of the tumor volume. For group 4, anti-CD40 agonist antibody at a dose of 50 µg was injected by intratumoral injection within 2 h of HT. Anti-CTLA-4 (100 µg/dose) and anti-PD-1(200 µg/dose) were injected intraperitoneally following HT, CD40, or HT40 treatment, and two subsequent ICI dose were given every third day. Mice were sacrificed for survival studies when the tumors reached ~2 cm in any dimension. For pan-cancer immune profiling and flow cytometry, mice tumors (n=3-5) and spleens (n=3-5) from surviving mice were harvested 1wk post treatment. For flow cytometry, harvested tissues were processed

on the same day. For gene expression analysis, tumor tissues were snap-frozen in liquid nitrogen and stored at −80 °C until further use.

HT set-up and tumor exposures

We utilized the Alpinion FUS transducer with a 1.5 MHz central frequency, 45 mm radius, and 64 mm aperture diameter with a central opening of 40 mm in diameter for HT exposures. For ultrasound exposure, the tumor was aligned at a fixed focal depth to cover voxel size of 1 x 1 x 10 mm. VIFU-2000 software was used to define the target boundary and slice distance in x, y, and z directions for automatic rastering of the transducer during treatment. The focal points were rastered to cover 40-50 % of the tumor. HT parameters were used in the boiling ranges (1 Hz PRF, 1 % duty cycle, 450 W acoustic power) and were adapted from prior publications that used a similar device [488,495]. Each focal spot was treated for 10 sec. Mice were given sub-cutaneous injections of buprenorphine (0.1 mg/kg) for 3 days post HT treatment.

Histopathological analysis

Prior to survival and immunological studies, HT was confirmed by histopathology. HT exposed tumor tissues (n=3) were fixed in 10% neutral buffered formalin, processed, and embedded in paraffin as previously described [419]. Histopathological examination was made on sections (4 μm) stained with hematoxylin and eosin (H&E). The tumor sections were analyzed by a veterinary pathologist.

Pan-cancer immune profiling of tumors

Total RNA extracted from snap-frozen tumors (n = 3/treatment group) using the Quick-RNA Miniprep Kit (Zymo Research) was profiled using the nCounter® PanCancer Immune Profiling Panel (NanoString Technologies, Inc., Seattle, WA, USA). This panel contains 770 genes involved in the cancer immune response. Gene expression profiling was performed using the following steps: (i) Hybridization: 25 ng of total RNA were hybridized with the mouse

PanCancer immune profiling code set having 770 unique pairs of 35–50 base pair biotin-labeled capture probes and reporter probes with internal reference controls. Hybridization was performed overnight at 65 °C. (ii) Washing: Excess probes were removed with magnetic bead purification on the nCounter® Prep Station (software v4.0.11.2). Unbound probes were washed away, the tripartite structure was bound to the streptavidin-coated cartridge by the biotin capture probe, aligned by an electric current (negative to positive), and immobilized. Degradation of fluorophore and photobleaching were prevented by adding SlowFade. Read counts from the raw data output were assessed for differential gene expression and cell type scoring after normalization using NanoString nSolver (version 3.0) [496]. Briefly, Log_2 counts were represented as z-scores in heat map to indicate alterations in gene expression and immune cell profile for each sample. Additionally, the relative differences in gene signatures between treated and control tumors were represented as volcano plots (log_2 fold change vs log_{10} P-value).

Immune profiling of melanoma tumors by flow cytometry

Tumors were mechanically disrupted and digested with 200 U/mL collagenase IV (Life Technologies, NY, USA) followed by filtration through a 70 μm cell strainer (Corning Inc., Corning, NY, USA) to obtain a single cell suspension. Fixable Viability Stain 575V (BD Biosciences) was used to stain cell suspensions to exclude dead cells from analysis as per the manufacturer's instructions. To block FcγIII/II receptor-mediated unspecific binding, anti-CD16/CD32 antibody was used. Cells were stained with indicated anti-mouse fluorochrome-conjugated antibody combinations for 30 min on ice in the dark using the following panel: CD45+ (tumor infiltrating leukocytes; TILs), CD11b+, F4/80+ (macrophages), CD11b+, F4/80+, MHCIIhi (M1 macrophages), CD11b+, F4/80+ MHCII lo/neg, CD206+ (M2 macrophages), CD11b+ CD11c+, F4/80−, MHCII+ (dendritic cells), CD3+, CD4+ (CD4+ T or helper Th cells), CD3+, CD4+, CD44hi CD62lo (CD4+ T effector/memory cells), and CD3+, CD8+ (CD8+ T cells). To detect IFN-γ, IL-2, Granzyme-B, and Foxp3 positive T cells, cells were washed after

surface marker staining, fixed and permeabilized with a transcription factor buffer set (BD Biosciences), and incubated with Pe-Cy7 anti-IL-2, BV650 or APC-Cy7 anti-IFN-γ, PE anti-Granzyme-B, or Alexa Fluor 488 anti-Foxp3 antibody for 30 min in the dark on ice. Stained cells were run in an LSRII flow cytometer (BD Biosciences) within 24 h. Compensations were performed with single-stained UltraComp eBeads or cells. FlowJo software v.10.2 (Treestar Inc., Ashland, OR, USA) was used for data analysis. For all channels, positive and negative cells were gated based on a fluorescence minus one control.

Evaluation of the melanoma-specific systemic T cell response

Single cell suspension of splenocytes were stimulated *ex-vivo* with the melanoma-specific differentiation antigen tyrosinase-related protein 2 (TRP-2) peptide for 8 h to determine generation of TRP-2 melanoma antigen specific immunity in mice [417,418]. Briefly, 1–2 x 10^6 splenocytes were incubated at 37°C and 5% CO2 with 2.5 µg of TRP-2 peptide for 8 h in the presence of Brefeldin A (eBioscience, San Diego, CA; 1000X solution). Treated cells were washed with PBS and stained with CD45, CD3, CD4, CD8, IFN-γ and IL-2 antibodies for flow cytometry analysis. The number of T effector cells responding to TRP-2 stimulation was calculated as CD45+ CD3+ CD4+ or CD8+ T cells that were positive for IFN-γ or IL-2, and results were expressed as percentage of total splenocytes.

Tumor regression and survival rate evaluations in murine melanoma

Tumor regression in the treated and untreated sites were determined by computing the difference in the tumor volumes for the various groups relative to untreated control. For survival studies, tumor bearing mice were followed for 40 days post inoculations, and the median survival for each treatment group was assessed by the Kaplan-Meier survival curve.

Statistical analyses

Statistical analyses were performed using GraphPad Prism 8.4.2 software (GraphPad Software Inc, La Jolla, CA, USA). The differences between the treatments compared to the untreated control were analyzed by multiple t-tests without multiple comparisons correction. The nanostring data were represented as mean of $\log_2$ fold change relative to control. All other data were presented as mean ± standard error of the mean (SEM) unless otherwise indicated. For analysis of three or more groups, one-way analysis of variance was performed followed by Tukey's multiple comparison tests. The overall P value for Kaplan-Meier analysis was calculated using the log-rank test. Analysis of differences between two normally distributed test groups was performed using an unpaired t-test assuming unequal variance and multiple t-tests. $P < 0.05$ was considered to be statistically significant.

Results

Local HT achieved precise fractionation of the treated regions

H&E showed that HT created a core of fractionated tumor tissue covering 40-50% of the total volume and this was surrounded by intact tumor tissue (Fig. 2A). There was a clear transition zone between the HT-treated and non-treated tumor regions such that viable tumor tissue was negligible in the area treated with HT. These were also verified by real-time US imaging during HT treatment in those regions, whereby hyperechoic regions during each pulse at the focal point followed by hypoechoic contrast at the end of the pulse was noted (Fig. 2 B-D).

HT40 induced inflammation and checkpoint expression in established melanoma

HT40 was performed in established B16F10 melanoma tumors (Fig. 3A). Screening of immune related genes in the tumor microenvironment using nanostring technique suggested an increased expression of inflammatory genes associated with phagocytosis, cell adhesion, cytokine, and antigen processing and presentation for HT, CD40 and HT40 compared to the control, but this profile was most significant and dominant in HT40-treated tumors (Supplementary Fig. S1). HT

alone increased immune infiltration markers (1.26 log_2 fold for ICAM-2 and 0.71 log_2 fold for VCAM-1), and APC chemo attractants (CCL8: ~2.6- and CSF1R: ~1.78-log_2 fold) compared to control (Fig. 3B; also see Fig. S2 volcano plots for quantitative changes in gene expression). CD40 and HT40 upregulated the expressions of the genes associated with CD45, T cells, and NK cell activations (Fig. 3C). Also, HT40 tumors enhanced dendritic, Th1, CD8+ T, cytotoxic, and NK $CD56^{dim}$ cell markers. For example, HT40 increased the CXCL9 (~4.23 log_2 fold), TLR-8 and TLR-9 (~2 log_2 fold), and ~ IL12-α and STAT1 (~1 log_2 fold) (Fig. 3C). Further, it upregulated the T cell activation genes (IFNβ1, IFNL2, granzyme α, granzyme β, IL1b, IL2, ICOSL, ICOS, TBET, CD69, CD44, CD160, and 4-1BB) and downregulated TGFβ2 (Fig. 4A). Consistent with T cell activation, the checkpoint marker genes (CTLA4, PDL1, PD1, TIM3, and LAG3) were enhanced with CD40 and HT40 treatment (Fig. 4B). In particular, immune activation markers such as TIGIT, IDO1, STAT1, and EOMES were significantly expressed in HT40-treated tumors relative to controls (Fig. 4B). Finally, to test, whether the gene expression results correlated with flow cytometry findings, we isolated the CD45+ and CD45- cells harvested from the tumors and assessed the PDL1 expressions. A 1.3–1.5-fold enhanced expression of PDL1 in TILs for CD40 and HT40 treated tumors were noted, demonstrating strong associations between assays (Fig. 4C).

Local treatment suppressed tumor progression and enhanced melanoma immunogenicity

HT treatment alone slightly inhibited the tumor growth rate 1-wk post treatment, but its combination with anti-CD40 antibody reduced tumor growth by > 70% compared to the control. This reduction was 30-50% greater than that of respective monotherapies (Fig. 5A). The reduction in tumor volumes accompanied a significant reduction in tumor weights for the HT40 cohort compared to the other groups (Fig. 5B). Local and systemic evaluation of the immune responses of harvested tumors revealed an increase (~1.2-2-fold) in the populations of CD45+ TILs and CD3+ T cells in the HT-treated group compared to the untreated control. The TIL

increase was not accompanied by a significant increase in CD8+ subtypes in HT-treated tumors. In contrast, HT40 enhanced the CD3+ CD8+ T cell population by 2–3-fold relative to HT post treatment (Fig. 5C-E). The populations of effector CD8+ T cells exhibited an increased level of IFN-γ and granzyme B expression, suggesting an activated cytotoxic phenotype (Fig. 6A and B). We also found that the T cell activation was not accompanied by a concurrent increase in the Foxp3+ CD4+ Tregs. Overall, we found a 2.5 to 5-fold increase in the granzyme B+ CD8+ T cell to Treg ratio in CD40 and HT40-treated tumors compared to the untreated control, which reflects enhanced mobilization of cytotoxic cells in the treated tumor (Fig. 6C).

HT40 promoted melanoma specific immunological memory

A significant increase in CD44+ CD62lo CD4+ T cells, which represent the CD4+ effector-memory T cell population, was observed for the HT- and HT40-treated tumors (1.5–2-fold). Additionally, an increased population of M1 macrophages along with a concurrent decrease of M2 macrophages was noted for HT40-treated tumors. CD40 alone did not increase CD4+ effector cells, but it did enhance the populations of M1 macrophages, which suggests APC activation (Fig. 7A-C). HT, CD40, and HT40 also increased M1 macrophages and reduced the M2 phenotype in the spleen tissues, with HT40 having the greatest effect (Fig. 7D and E). To assess antigen specificity, splenocytes stimulated *ex vivo* with TRP-2 were assessed for IL2 production. A significant (1.3–1.7-fold) increase in TRP-2 specific IL2+ CD4+ T cells in the spleen of HT40-treated mice compared to the control was noted, and this number was relatively higher compared to that of the other therapies (Fig. 7F). Thus, we posited that the HT40 induced a potent melanoma memory response.

HT40 therapy sensitized melanoma tumors to checkpoint blockade

For assessing ICI effect in a bilateral melanoma model, HT40 treatment of the right flank tumor was followed by intraperitoneal injection of ICI (n=5, Fig. 8A). ICI by themselves were

ineffective in inducing tumor growth suppression and survival rates compared to the control, suggesting that B16F10 melanoma was refractory to the checkpoint blockade therapy in the selected size-range (Fig. 8B and Fig. 9). Also, HT or CD40 alone did not enhance checkpoint blockade efficacy compared to ICI alone (Fig. 9). In contrast, HT40 significantly reduced tumor rates compared to HT or CD40 alone. Additionally, when primed with HT40, ICI therapy was most effective in delaying tumor growth rates, and in enhancing survival responses compared to all other combination treatments (Fig. 8B and Fig.9). We next probed whether the enhanced survival with HT40+ICI was because of superior anti-tumor effects. We found that 40% (2 out 5) of HT40+ICI mice showed abscopal tumor suppression and survived the entire treatment period (40 days, Fig. 8B&9). In contrast, other treatments were relatively less effective, and mice reached the sacrifice end points before the end of study.

Discussion

The objective of this study was to understand the ability of HT40 to reprogram the immunologically cold melanoma tumor such that it becomes more receptive to ICI therapy. HT has been utilized to debulk tumor tissue, release damage associated molecular patterns (DAMPs), and improve immune sensitization in various tumor models [98,99,482,486]. We and others have also shown that local anti-CD40 agonistic antibody therapy activates APCs and improves the functional status of TILs [117,477,497]. This is likely via enhanced antigen presentation by APCs through improved CD40L binding with CD40 receptor on APCs, and by the upregulation of costimulatory molecules such as MHC class II, CD80, CD86, and CD58 on the cell membrane [125]. However, whether the combination of HT and anti-CD40 antibody can be effective in anti-tumor immunity induction in immunologically cold tumors was not known prior to this study.

To investigate the potential of the HT and CD40 combination, we utilized an ICI refractory and poorly immunogenic B16F10 model. B16F10 tumors downregulates the MHC class I and co-

stimulatory molecules such as *CD80, CD86, OX40L, GITRL, CD40, CD137L,* and exhibit low levels of IL2 and IFN-γ levels in the tumors [489]. Its self-antigen *(*TRP-2) also shows poor affinity to T cell receptors, thereby making it an excellent poorly immunogenic model for immunotherapy studies [498,499]. High intensity, low duty cycle, and short ultrasound HT pulses were used to fractionate ~40–50% of the tumor mass (Fig. 2A&B). Pan-cancer immune profiling suggested that the selected HT parameters elevated the expression of chemo-attractants (CCL8 and CSF1R) and cell adhesion molecules (ICAM and VCAM). These markers are essential for cell-cell interaction and leukocyte migration into tumors (Fig. 3) [500-502]. HT treatment also lowered the immunosuppressive cytokine TGFβ2 in tumors, and the addition of CD40 caused upregulation of several immune-activation markers, including CXCL9. Chemokines such as CCL3-5, CCL8, CCL11-12, CXCL9 and CXCL10 produced from mature APCs play a crucial role in recruiting CD8+ T cells, CD4+ helper T cells, and natural killer cells into TME [501,503]. CXCL9 also positions tumor infiltrating T cells in APC rich regions to remove T cell anergy [504]. CXCL9 is constitutively produced from myeloid cells following stimulation of IFN secreting T cells [504,505]. IFN-γ can induce additional production of this chemokines via STAT1 signaling to enhance CD8+ T cells recruitment into tumors [506-508]. Our tumor immune analysis suggested that HT40 treatment induced an influx of CD8+ IFN-γ expressing T cells (Fig.5&6), indicating a CXCL9 mediated amplification of cytotoxic T cell-based antitumor immunity [509,510]. In addition, increased accumulation of M1 macrophages and granzyme B+ activated CD8+ T cells without alteration of Tregs was noted in tumors treated with HT40 (Fig.7). Also, the population of TRP-2 specific CD4+ T cells and CD44hi CD62lo CD4+ T cells that help with the memory T cell response was enhanced. Surprisingly, HT also increased PD-L1, CTLA4, and other immune checkpoints within the tumor microenvironment (Fig. 3). These phenotypic alterations are typically an adaptive mechanism to suppress T cell function [511]. However, enhanced expression of checkpoint proteins can also be a positive prognostic marker of ICI outcomes in melanoma patients [512-514]. To investigate whether this was true in our model system, ICIs were added to the HT40 regimen, and

this resulted in improved efficacy and mice survival rates (Fig. 8 and 9). Thus, we believe that HT40 may have significant clinical value, especially when combined with ICIs or other immune activators such as TLR and chemokine/cytokine agonists.

Our study had some limitations. First, HT40 therapy improved survival but did not eliminate the melanoma. We do not know the reasons for this outcome, but the response of melanoma to HT40 may depend on the degree of mechanical damage, dosing, sequence, and schedule of the HT and CD40 therapies. Studies are currently underway to further investigate these mechanisms. These include first enhancing CD40 stimulation in smaller tumors, followed by HT40 treatment of larger tumors to provide sufficient priming. Alternatively, combining other FUS parameters (e.g., mild hyperthermia + HT) with CD40 stimulation might be more insightful. Second, although the addition of HT40 to ICI improved the response of refractory melanoma, local recurrence and emergence of distant metastasis may still be possible [515]. Future re-challenge studies and histopathological evaluations of lung tissues may shed more light on such mechanisms. Third, only a single B16F10 model was investigated. Future studies employing multiple models would elucidate the differences in clinical efficacies of various therapies. Lastly, mechanical fractionation of tumors using HT can induce metastasis. This aspect was not studied, although recent studies from other groups suggest that it is highly unlikely [482,484].

In summary, HT40 therapy augmented innate and adaptive immunity in the B16F10 model. An inflamed TME with an active interaction of CXCL9-cytotoxic T cell axis was the likely mechanism responsible for sensitization to ICI and improved survival rates of mice. Combining HT40 with ICIs may enhance outcomes in advanced stage cancer patients.

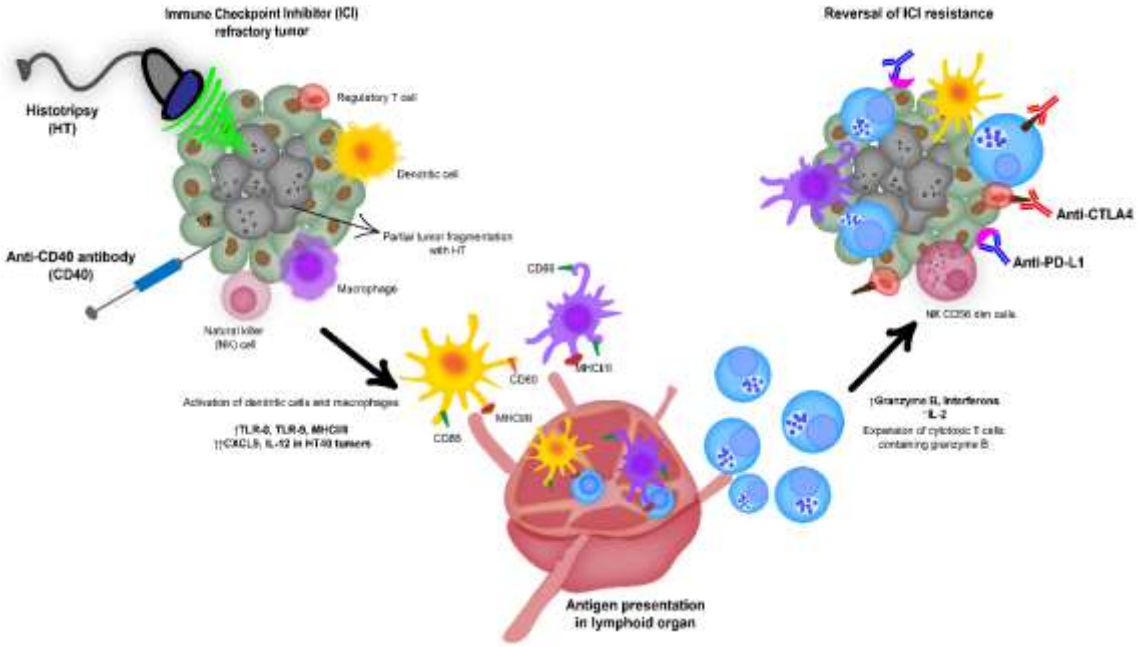

Fig. 3.1. Schematic representation of HT40 induced reprogramming B16F10 tumor microenvironment and subsequent sensitization of the tumors to ICIs therapy.

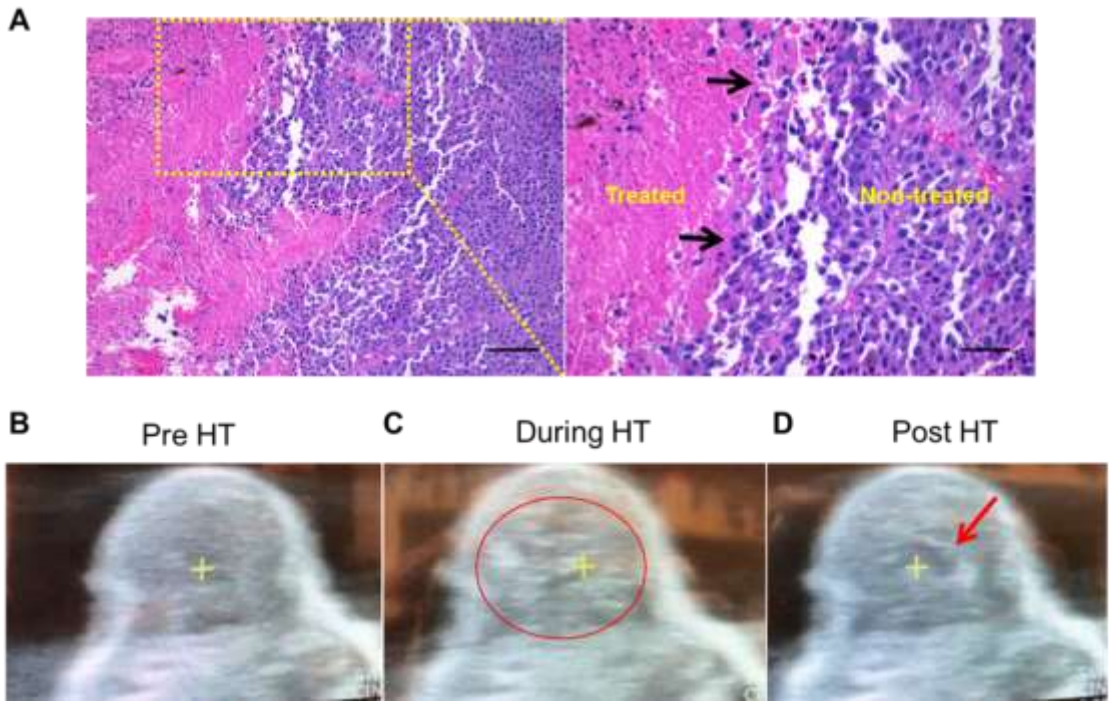

Fig. 3.2. Local HT achieved precise melanoma fractionation. (A) The H&E stained tumor sections showing sharp transition zone (black arrows) between histotripsy treated and non-treated tumor region (n=3). Left image: 20x, scale bar 200μm; Right image: 40x, scale bar 100μm. (B-D) Ultrasound images collected during HT therapy of melanoma tumors. (B) Pre-treatment image. (C) Hyperechoic regions during each pulse (indicated by the red circle). (D) Hypoechoic contrast at the end of the pulse that was visible adjacent to the focal point (indicated by red arrow).

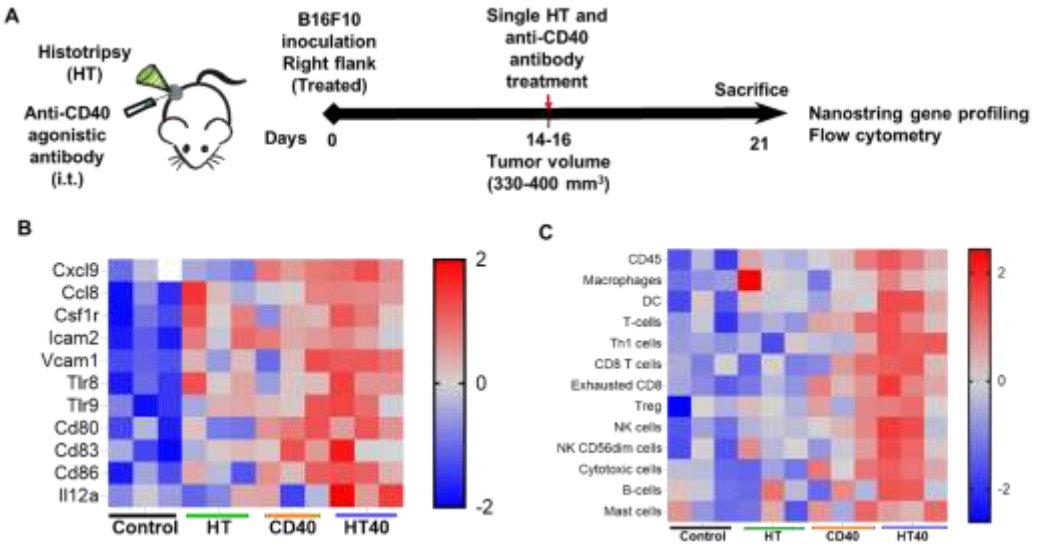

Fig. 3.3. HT40 therapy increased pro-inflammatory immune markers in tumors. (A) C57BL/6J mice were implanted subcutaneously in the right flank with 0.5 million B16F10 cells and treated once with HT, CD40 or HT40 (n=4-5 per group). Tumors were harvested 7 days post treatments. Total RNA (n = 3/group) was isolated, and immune profiling was performed using the NanoString PanCancer Immune panel. (B) Gene markers of cell adhesion molecules, chemokines, innate sensors, and activation status of APCs was higher for HT40 tumors relative to the corresponding controls. (C) Total tumor infiltrating leucocytes, dendritic cells, Th1 cells, cytotoxic cells and activated NK cell expression markers were significantly higher with HT40 therapy compared to the control, CD40, an HT40 tumors. Statistical analysis was performed using multiple t-tests without correction for multiple comparisons. $p < 0.05$ is considered significant.

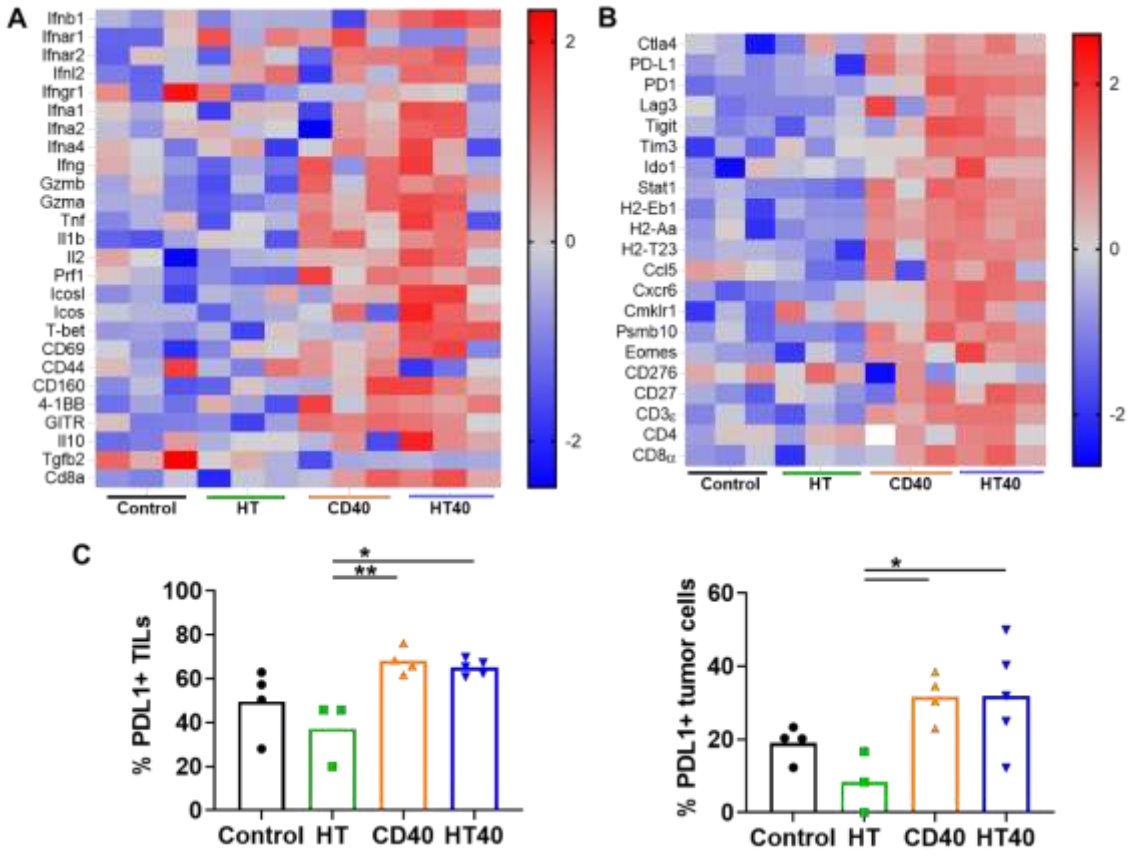

Fig. 3.4. HT40 and CD40 therapy enhanced T-cell activation and checkpoint expressions in the melanoma tumors. (A) Enhanced expression of T-cell activation genes in the treated tumors compared to the control. (B) The checkpoint marker genes (e.g. CTLA4, PDL1, PD1, TIM3, and LAG3) were enhanced with CD40 and HT40 treatment. (C) PD-L1+ CD45+ (tumor infiltrating leukocytes; TILs) and PD-L1+ CD45- (tumor cells) cells assessed using flow cytometry (n=3-5). Gene expression statistical analysis was performed using multiple t-tests without correction for multiple comparisons. For flow cytometry, data were presented as mean ± SEM and the statistical differences between groups were measured by ANOVA followed by Tukey's multiple comparisons. * $p < 0.05$, ** $p < 0.01$.

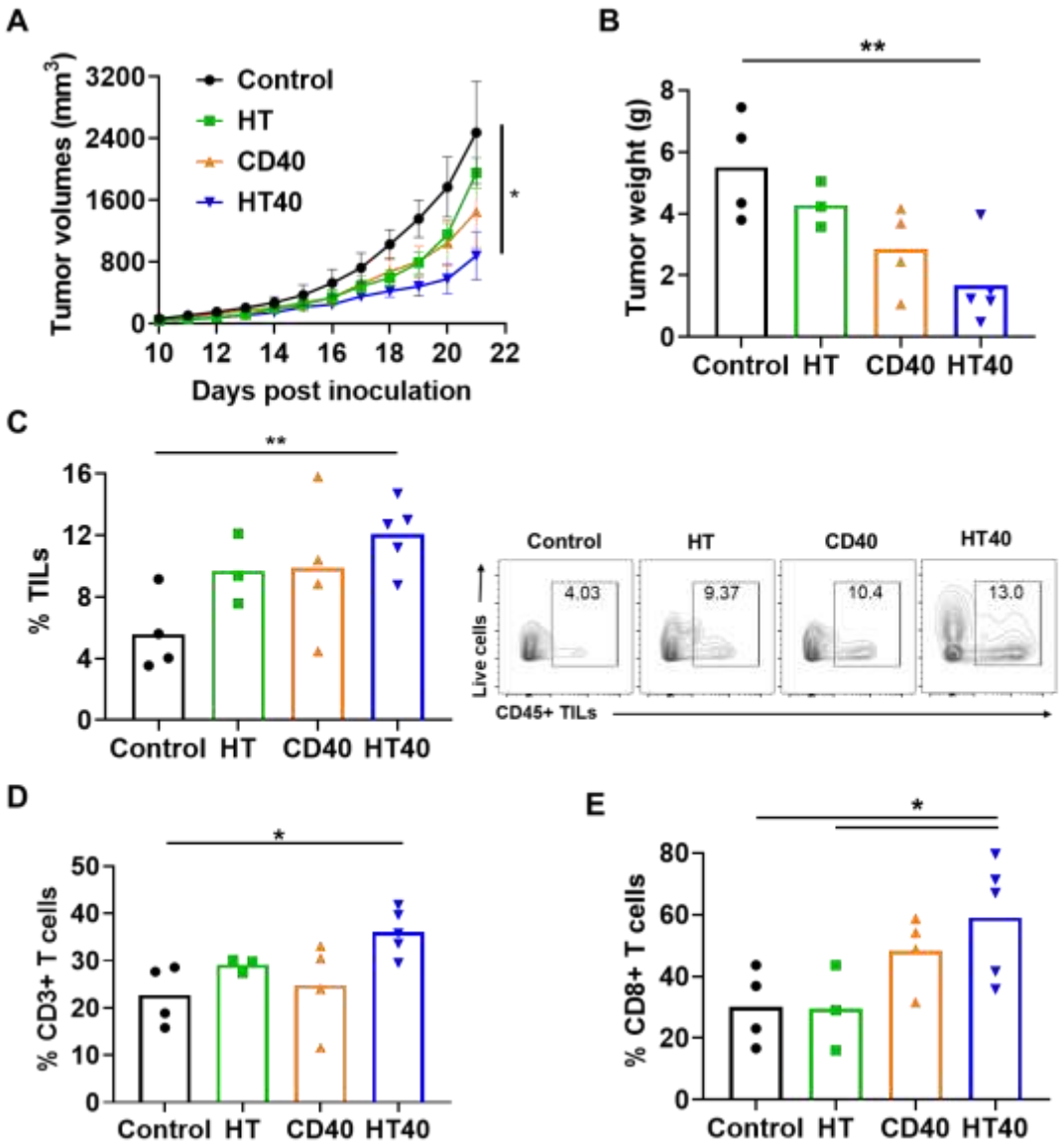

Fig. 3.5. Local HT40 suppressed tumor progression and improved the infiltration of T lymphocytes. (A) Mean volumes of the treated tumors plotted till 21 days post tumor inoculation. HT40 induced significant growth inhibitions compared to the respective controls. (B) Tumor weights at the time of harvest. HT40 mice showed significant reductions in mean weight compared to other groups. (C) HT, CD40, and HT40 enhanced the populations of tumor infiltrating

leucocytes (TILs) compared to control in the harvested tumors of surviving mice. Overall, HT40 demonstrated the highest infiltration rates compared to the other groups. (D) HT40 induced a higher percentage of CD3+ T cell population than the control. (E) Frequency of CD8+ T cells in HT40 group was 2-folds higher compared to the HT and control group. Results are shown as mean ± SEM, n=3-5 per group. One-way ANOVA followed by Tukey's multiple comparison was used for data analysis. * $p < 0.05$, ** $p<0.01$.

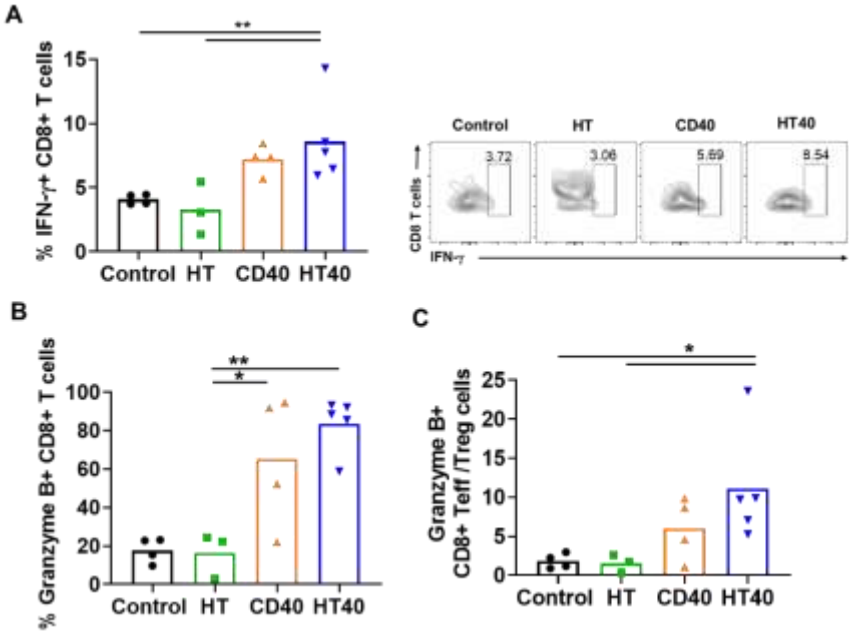

Fig. 3.6. HT40 augmented the T cell functions in tumors. (A and B) HT40 promoted IFNg (~2-fold) and Granzyme B (~4-fold) secretion from CD8+ T cells in tumors. (C) Ratio of cytotoxic CD8+ T cells and immunosuppressive regulatory T (Treg) cells in tumors increased by 2.5 and 5-fold with CD40 and HT40 compared to the untreated controls, respectively. Data are shown as mean ± SEM, n=3-5 per group, * $p < 0.05$, ** $p < 0.01$. Data were analyzed by One-way ANOVA followed by Tukey's multiple comparisons; changes between control and treatments in Fig. 5C were analyzed using an unpaired t test assuming unequal variance.

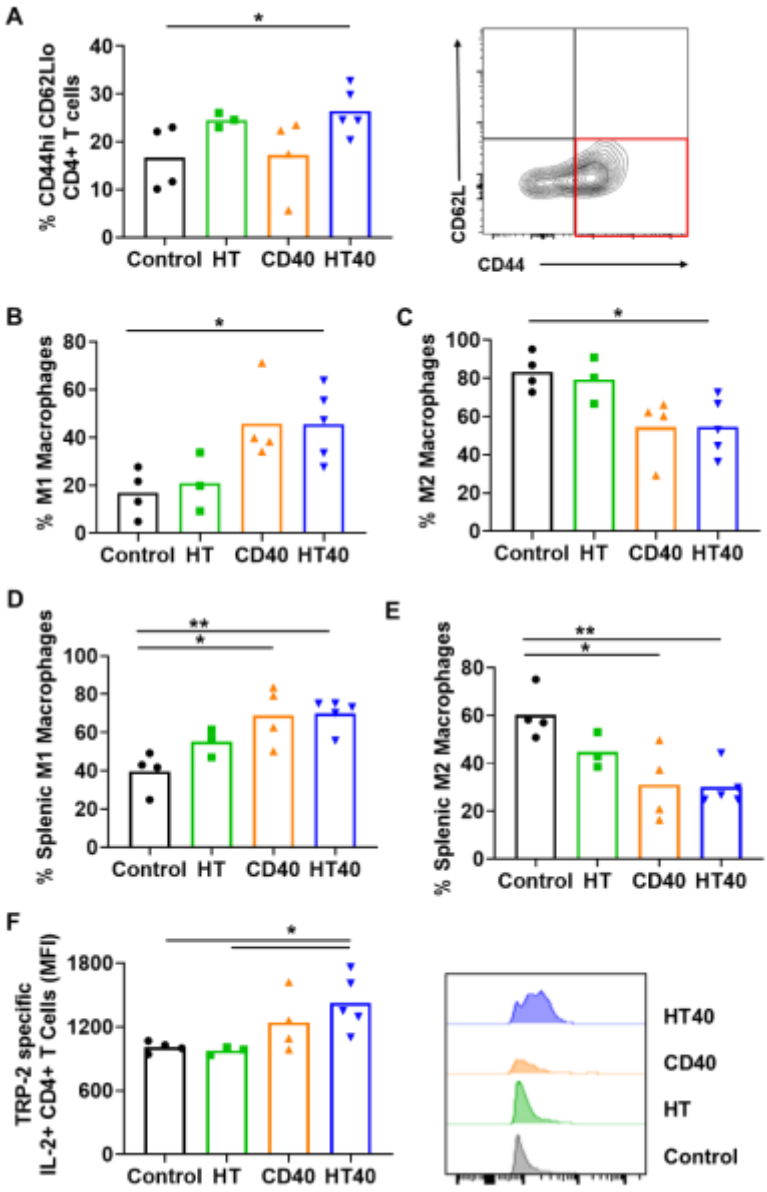

Fig. 3.7. HT40 increased melanoma specific antitumor immunity. (A) A significant increase in CD44hi CD62lo CD4+ effector T memory cells (percentage out of total leukocytes) in HT and HT40 treated tumors was noted. (B and C) CD40 and HT40 enhanced the percent of M1 macrophages by 2-fold and decreased M2 macrophages by 1.5-fold compared to controls. (D and E) HT, CD40 and HT40 increased M1 macrophages (~1.3-1.7-fold) and decreased M2

macrophages (~1.5-2-fold) in splenic tissues compared to the control. (F) IL-2 production from CD4+ T cells was significantly improved by CD40 and HT40 treatments compared to untreated controls. Amongst all the treatments, HT40 showed the most dominant effect upon TRP-2 stimulation *ex-vivo*. Data are shown as mean ± SEM, n=3-5 per group. Data were analyzed by ANOVA followed by Tukey's multiple comparisons. * $p < 0.05$, ** $p < 0.01$.

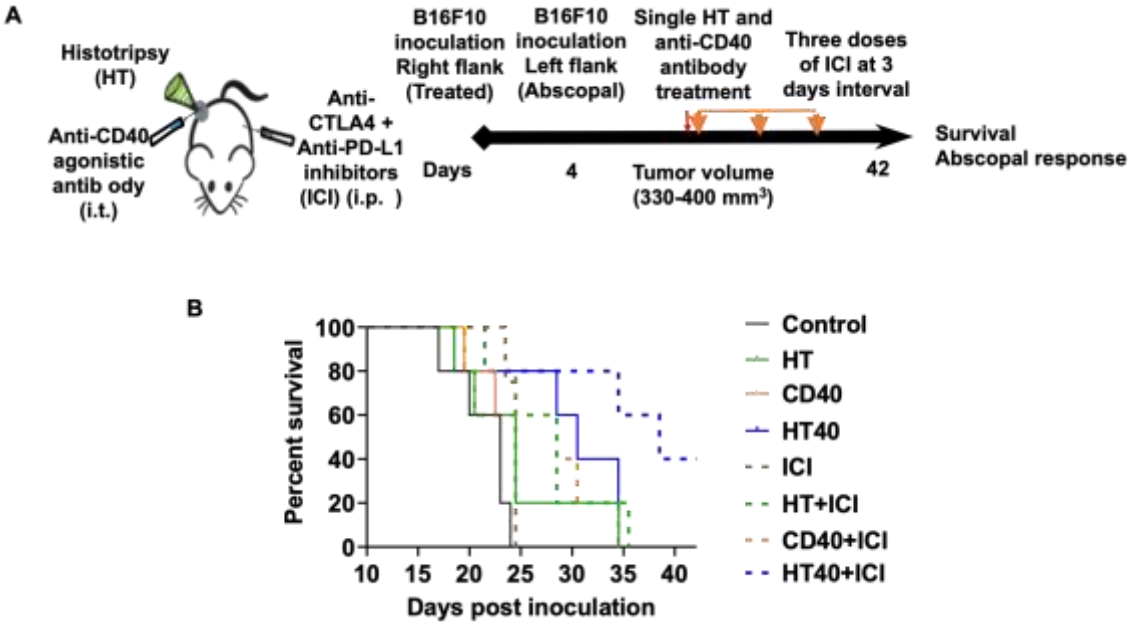

Fig. 3.8. HT40 priming enhanced the therapeutic effects in ICI refractory melanoma. (A) HT40 priming of tumor (unilateral) was followed by ICI therapy in mice bearing B16F10 melanoma in the left and right flank regions. (B) HT40 priming improved dual immune checkpoint blockade outcomes. Differences in the median survival (n=5) were determined by the Kaplan–Meier method and the log-rank test was used to determine P value. $p < 0.05$: HT40+ICI vs CD40+ICI; $p < 0.1$: HT40+ICI vs HT+ICI, HT40.

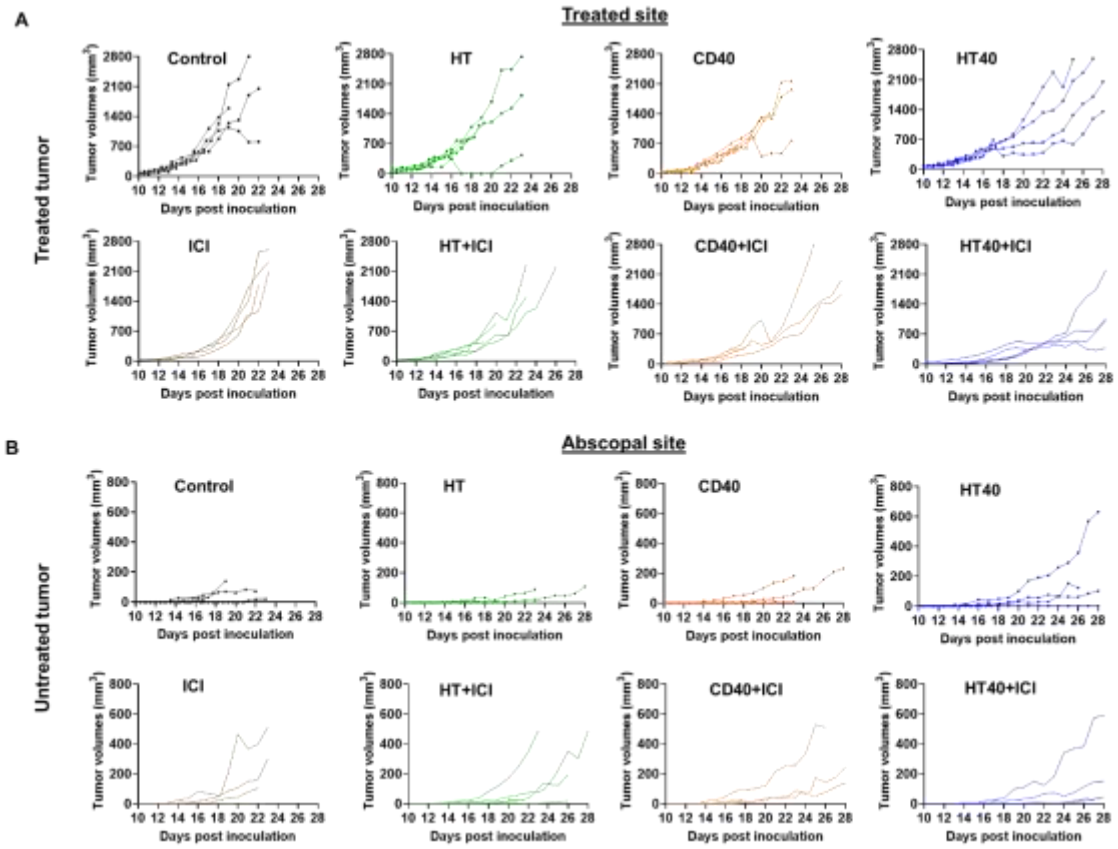

Fig. 3.9. Tumor growth rates in mice bearing melanoma in left and right flank regions. (A) HT40 and HT40+ICI delayed growth of treated tumors compared to HT and CD40 alone. (B) Tumor growth rates at distant untreated sites were relatively slower with HT40+ICI and HT40 compared to other treatments. Data shown till day 28 post inoculation. Data were analyzed by ANOVA followed by Tukey's multiple comparisons; * $p < 0.05$, ** $p < 0.01$.

Supplementary data

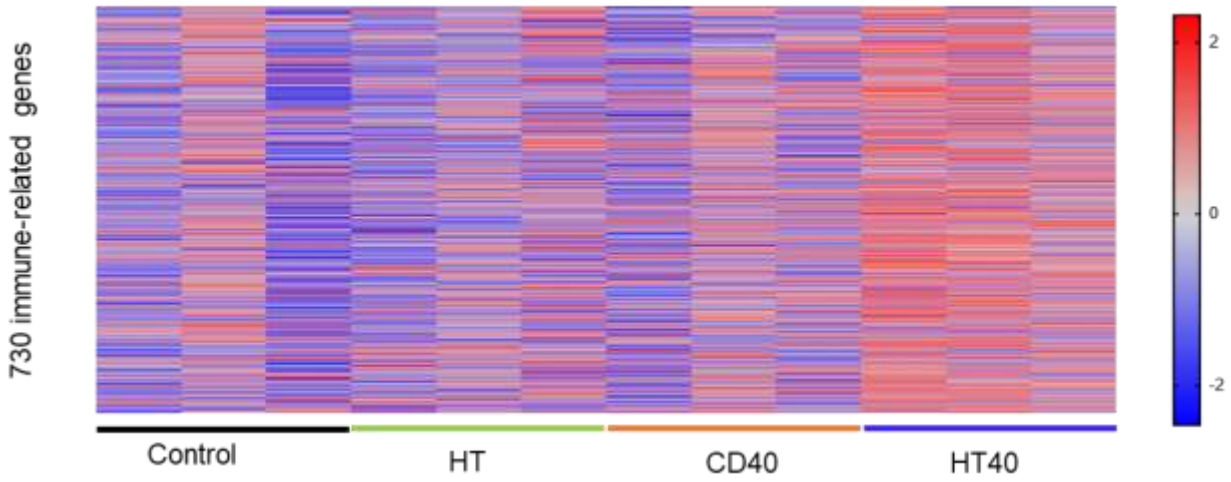

Fig. 3.S1. Pan cancer immune profiling by nanostring analysis assessed 730-immuno regulatory genes in the treated tumors (n = 3).

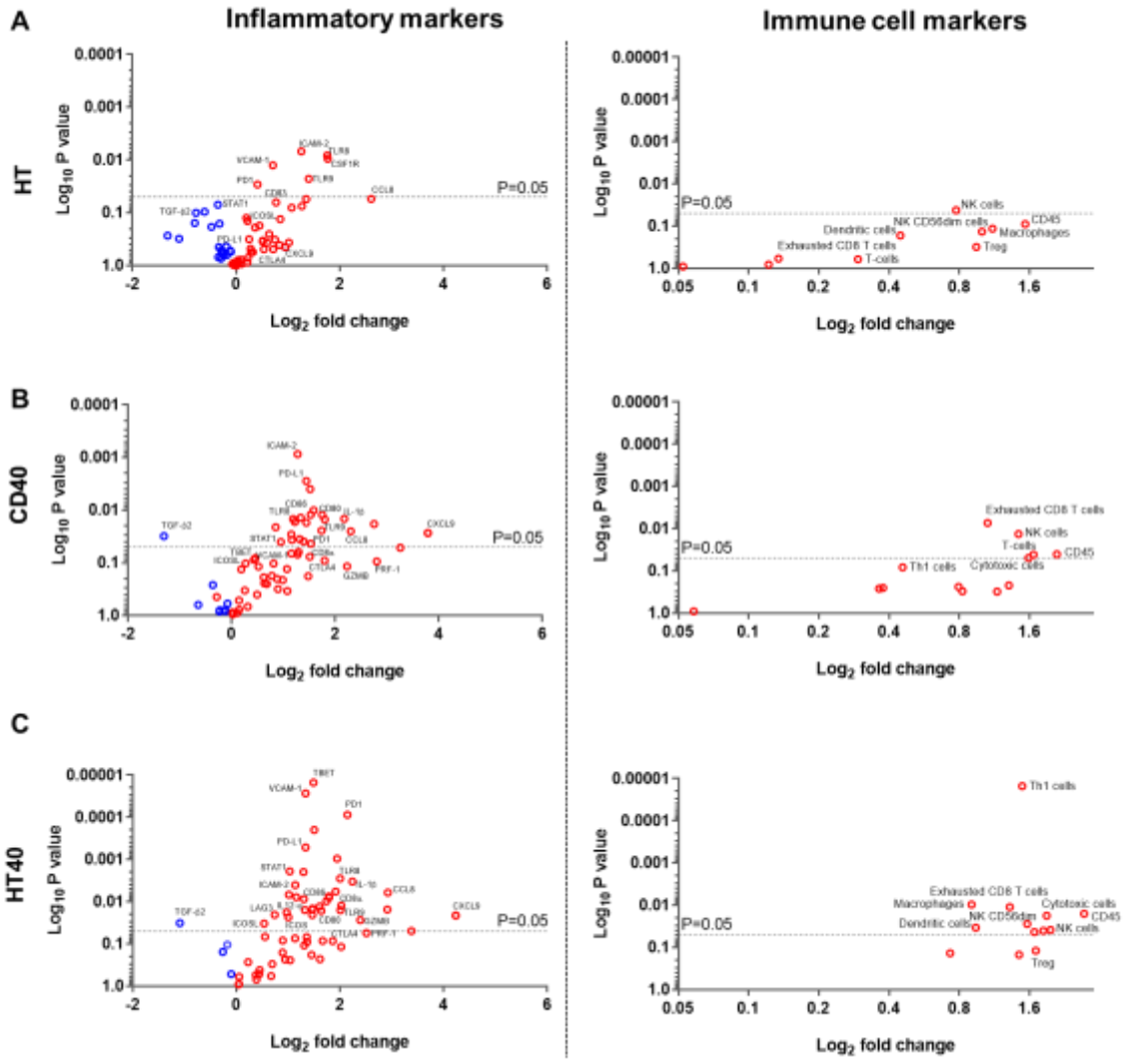

Fig. 3.S2. Quantitative assessment of inflammatory and immune cell markers. (A-C) Significantly higher expressions of cell adhesion molecules, chemokines, innate sensors, activation status of APCs, natural killer cells (NK), and T cells was noted in HT40 tumors relative to control. The volcano plots represent log2 fold change in gene expression compared to control. Statistical analysis was performed using multiple t-tests without multiple comparisons correction. $p < 0.05$ is considered significant.

CHAPTER IV

REPROGRAMMING THE RAPID CLEARANCE OF THROMBOLYTIC AGENTS BY AN ON-DEMAND ANCHORING OF NANOPARTICLES TO CIRCULATORY ERYTHROCYTES

Abstract

Rapid clearance of thrombolytics from blood following intravenous injection is a major clinical challenge in cardiovascular medicine. To overcome this barrier, nanoparticle (NP) based drug delivery systems have been reported. Although superior than conventional therapy, a large proportion of the injected NP is still cleared by the reticuloendothelial system. Previously, we and others showed that *ex vivo* attachment of bioscavengers, thrombolytics, and nanoparticles (NPs) to glycophorin A receptors on red blood cells (RBCs) improved the blood half-life. This is promising, but *ex-vivo* approaches are cumbersome and challenging to translate clinically. Here, we developed a novel Ter119-polymeric NP encapsulating a model thrombolytic agent for on-demand targeting of GPA receptors *in vivo*. Upon intravenous injection, the Ter119-NPs achieved remarkable RBC labeling efficiencies (>95%) and their blood residence time markedly increased from minutes to several days without any morphological, hematological, and histological complications. In addition, the RBC labeling of NPs prevented its lysis by reticuloendothelial and the activations of innate and adaptive system. Our data suggests that real-time targeting of therapeutics to RBC with NPs can be an innovative means to improve outcomes and reduce complications in chronic diseases.

Introduction

Thromboembolic diseases (e.g. myocardial infarction, deep-vein thrombosis) are frequently treated with thrombolytic agents (e.g. altepase, tissue plasminogen activator (tPA etc.) [516-518]. Although a commonly used treatment modality, thrombolytics typically demonstrate rapid clearance (<15-20 minutes) from the body following intravenous injection, thereby requiring large dosages and increasing the risk of intracranial hemorrhages [519,520]. To overcome this limitation, nanoparticle (NP)-encapsulation of thrombolytics have been attempted, and these have shown to prolong circulatory half-life compared to conventional therapy[521,522]. Despite this, the *in vivo* effectiveness of NP-based therapies can be impacted by the rapid reticuloendothelial clearance, thereby pointing towards a need for discovering innovative methodologies for efficient reprograming of the thrombolytic pharmacokinetics [523-525]. Towards this goal, in this study, we investigated the feasibility of direct labeling of the red blood cell (RBC) membranes with intravenously administered NPs for improving the pharmacokinetics and biodistribution of thrombolytic agents [379,526,527].

RBCs have a large surface area and are involved in clot formation [2,528], so the premise of labeling their membranes with NP-encapsulated thrombolytics can be clinically relevant for preventing clot formation. Previous studies employing the *ex-vivo* coating of drugs and NPs with RBC membranes have shown to enhance the drug half-life, but the limitations imposed by the donor availability, damages to the cell membranes, and lack of necessary infrastructures prevented the large-scale translation of this approach for human use [379,527,529-531]. We propose that these treatment barriers can be overcome by decorating the NPs with RBC-specific targeting ligands for selective targeting of the circulating erythrocytes, and this will allow prolonged blood residence time of thrombolytic agents and reduce toxic outcomes. To meet our objectives, herein, we targeted the transmembrane glycophorin A [532] docking sites on the RBC membrane since it represents approximately 2% of the total RBC membrane proteins[533]. GPAs can be targeted by

ligands such as dodecapeptide acid peptide (ERY1) that are derived from phage proteins, and single chain variable fragment (scFv) of the Ter119 antibody [534-536]. Importantly, we have shown that ERY1 can localize NPs on to the RBC membrane in vitro, however, its feasibility for *in vivo* therapy is yet to be demonstrated [537]. In this study, we innovated further by designing a novel polymer-based Ter119-NP encapsulating tPA, as a model drug. We compared the *in vivo* RBC labeling efficiency and improvement in circulation time for Ter119-NP, ERY1-NPs and tPA alone in a mice model. Our mice data suggested that targeting the circulating RBCs using intravenously injected Ter119-NPs prolonged the circulatory retention of tPAs from minute to days compared to unbound-tPA or ERY1-NPs. Furthermore, the direct labeling RBC with NPs did not impact the hematological or histological parameters, indicating a high translational value of our described approach.

Materials

Tissue plasminogen activator (Alteplase; tPA) was purchased from Genentech (South San Francisco, CA). Polyethylene glycol (2kDa mPEG-NHS and 5kDa Maleimide-PEG-NHS) was purchased from Creative PEGWorks (Winston Salem, NC). Poly-l-lysine (15-30kDa) and fluorescein isothiocyanate (FITC) was purchased from Sigma Aldrich (St. Louis, MO). ERY1 peptide with C-terminal cysteine linker (WMVLPWLPGTLDGGSGCR) was custom synthesized by EZBiolab (Caramel, IN). Ter119 antibody was purchased from eBioscience (San Diego, CA). Glutaraldehyde, AlexaFluor 790 antibody labeling kit, acrylamide/bisacrylamide, and other gel electrophoresis materials were purchased from Fisher (Hampton, NH). The fluorochrome-conjugated monoclonal antibodies (mAbs) were purchased from BioLegend (San Diego, CA): FITC anti-CD45.2 (104), PE anti-CD3 (145-2C11), APC anti-CD4 GK1.5), and APC-Cy7 anti-IFN-γ (XMG1.2) and PERCP anti-CD8a (53-6.7).

Methods

PLL-g-PEG-Maleimide Synthesis

PLL-g-PEG-Maleimide was synthesized using methods previously described [537]. A 50/50 (w/w) mixture of 40 mg of mPEG-NHS (2kDa) and Mal-PEG-NHS (5 kDa) was added to 15 mg of PLL dissolved in 200 µl of PBS. The mixture was allowed to react for two hours before the PLL-g-PEG mixture was washed with PBS containing 50% ethanol in a 10 kDa Pierce centrifugal concentrator. The copolymer was then air-dried and stored at -20°C until use. The grafting ratio was determined using H1 NMR with a Bruker INOVA 400 spectroscope. The PEG : PLL grafting ratio was determined by integrating the peaks corresponding to the PEG linkage to PLL ε-amino groups at 3.2 ppm and the PLL α-carbon at 4.2 ppm, as has been previously described [538]. The ratio of the two peak areas was used to calculate the grafting ratio.

Synthesis of NPs

Encapsulation of tPA into nanoparticles was performed using an approach previously described [1]. PLL-g-PEG-Mal in PBS (14 mg/ml, 50 µl) was added dropwise to tPA (2 mg/ml, 50 µl) while gently vortexing. After incubating one hour, PLL-g-PEG/tPA was cross-linked with glutaraldehyde (0.06%) for three hours to produce non-liganded NPs (Bare NPs). To produce ERY1-NPs, 125 µg of ERY1 peptide dissolved in DMSO was added to Bare NPs immediately after glutaraldehyde cross-linking and allowed to incubate 30 minutes. To produce Ter119-NPs, Ter119 antibody (100 µg) was treated with dithiothreitol (DTT) (20 mM), according to previous methods, for 30 minutes at 37°C [539]. The reduced antibody was added to the Bare NPs after cross-linking and allowed to incubate for 30 minutes to produce Ter119-NPs (Fig. 4.1A). For pharmacokinetic studies, the tPA, Bare NPs, ERY1-NPs, and Ter119-NPs were labeled with FITC (4 mM) overnight at 4°C to facilitate free tPA or NP detection using flow cytometry and spectrophotometry. For biodistribution and *in vivo* imaging experiments, tPA and all tPA-NP (Bare NP, ERY1-NP, Ter119-NP) groups were labeled with AlexaFluor 790 using the

manufacturer's suggested protocol for standard protein labeling. After labeling, unconjugated FITC, AlexaFluor 790 and ligands were removed by washing with 300 kDa Pall centrifugal concentrators.

Physicochemical characterization of NPs

SDS-PAGE was used to characterize tPA association with the PLL-g-PEG copolymer. Standard acrylamide/bisacrylamide SDS-PAGE gels (8%) were prepared to perform the assay. A control sample of free tPA (5 µg) as well as tPA NPs (5 µg) were loaded onto SDS-PAGE gels and the gels were run at 200 V on a Bio-Rad Mini-PROTEAN Tetra Cell electrophoresis system [540]. Approximately 45 minutes after beginning the run, SDS-PAGE gels were removed and stained with Coomassie G-250 to visualize protein migration.

Dynamic light scattering (DLS) was used to characterize the size of Bare-NPs, ERY1-NPs, and Ter119-NPs. A 50 µl aliquot of each type of NP was loaded into a cuvette and the size was measured at 90° using a Brookhaven Instrument Corporation ZetaPALS ζ-potential analyzer. The mean of triplicate measurements, with each measurement consisting of five runs (each lasting one minute), was used to determine the NP size.

Characterization of *in vivo* RBC targeting and binding of NPs by flow cytometry and confocal microscopy

We compared the RBC binding efficiency of FITC labeled NPs by infusing tPA loaded Ter119-NPs or ERY1-NPs in Balb/C mice. FITC labeled Bare NPs containing tPA and FITC-tPA served as representative control. A single NP or free tPA injection at a dose of 90 µg of tPA/mouse was performed intravenously. To estimate RBC targeting and binding efficiency of NPs, whole blood (30-50 µL) was collected by facial vein phlebotomy at 1, 3, 6, 24, 48, 72, 96, 120, 144, and 168h (n=3 per time point) for 7 days post injection. The fluorescence signal of FITC labelled NPs and free tPA on isolated RBCs was measured using FACS Calibur (BD Biosciences, NJ) with an

excitation/emission of 488/530 nm. Datasets were analyzed using FlowJo software v.10.2 (Treestar Inc, OR). The relative density of injected FITC-NPs attached to RBCs at different time points were represented as histograms showing median fluorescence intensity (MFI) of the cells.

To confirm cellular attachment of NPs, the isolated RBCs were examined under confocal microscope (n=3/time point). All imaging was performed with constant acquisition and display parameters using an inverted microscope (Olympus IX81-ZDC2) equipped with a color CCD camera, cooled monochrome CCD camera, motorized scanning stage, and mosaic stitching software (Metamorph) with a 10x objective. The FITC channel (480/520 nm) was used for gating to quantify the percentage of cells positive for FITC signal after excitation with a mercury lamp-based monochromator.

Quantitative estimation of tPA-NPs in blood by spectrophotometry

To evaluate NP half-life, a single intravenous injection of FITC labeled tPA and tPA-NPs was performed in Balb/c mice at a dose of 90 µg of tPA/mouse. Blood samples were collected at specified time points for 5 days (n=3 per time point). Diluted samples were analyzed for FITC fluorescence at 490/525 nm using a SpectraMax M2e spectrophotometer. DPBS was used as blank control. Time-dependent *in vivo* concentration of tPA-NPs was represented as the percentage of injected dose (%ID). %ID in circulation at a given time (t) was calculated using the equation below

$$\%\ Injected\ Dose\ (ID) = \frac{(I_t - Blank)}{(I_0 - Blank)} \times 100$$

where I_0 represents the initial fluorescence intensity at 0 h, and I_t is its intensity at time (t).

The data from %ID in circulation were exported to GraphPad Prism 7.0 software (GraphPad Software Inc, La Jolla, CA, USA) and area under the curve (AUC) from time 0h through 5 days

post injection was calculated by trapezoid rule using the software and compared between the treatments.

Investigation of biodistribution and clearance kinetics of RBC targeted NPs in mice by *in-vivo* and *ex-vivo* imaging

The tPA or tPA-NPs were labeled with Alexa Fluor 790 near infrared (NIR) fluorescent probe and injected at a dose of 90 µg tPA/mouse via tail vein. Injected tPA or tPA-NPs were tracked longitudinally (n=3/time point) using an *in vivo* imaging system (Bruker *In-vivo* Xtreme II, MA, USA). Longitudinal *in vivo* imaging was controlled by image acquisition and analysis software (Bruker molecular imaging (MI) software). Mice were sacrificed on day 7 post-treatment and organs of interest (heart, lungs, liver, kidneys, spleen, and lymph nodes) were harvested for *ex-vivo* imaging. Quantitative *ex-vivo* image analysis (n=3) was done based on the region of interest [75] using the MI software. Fluorescence images from the *ex-vivo* harvested organs were overlaid on respective x-ray images and represented as merged images for enhanced visualization of the organ boundaries.

Assessment of the systemic effect of functionalized NPs on hematological and biochemical parameters

Mice were sacrificed 7 days post intravenous injection of tPA and tPA-NPs. Whole blood and serum samples were analyzed by Dr. Charles Wiedmeyer from Comparative Clinical Pathology Services (Columbia, MO). Hematological parameters such as Red Blood Cells (RBC) count, White Blood Cells (WBCs) count, Differential count, Hemoglobin (Hb), Hematocrit (HCT), Mean Corpuscular Volume (MCV), Mean Corpuscular Hemoglobin [541], Mean Corpuscular Hemoglobin Concentration (MCHC), RBC Distribution Width [403] and Platelets were determined (n=3). Total protein, albumin, albumin/globulin ratio, alanine transaminase (ALT), and aspartate transaminase (AST) were evaluated in mice sera to assess liver function (n=3).

Determination of immunotoxicity of RBCs bound NPs by splenocyte stimulation assay

Single cell suspensions were prepared from the spleen (n=3-5) and lymph nodes (LN) (n=3) harvested from treated mice [477]. Briefly, splenocytes and LN cells were incubated with 5 µg/ml (tPA, Bare NPs, ERY1-NPs, Ter119-NPs) for 6-8 hours in the presence of Brefeldin A. The stimulated cells were stained with antibodies for 30 min in the dark on ice to assess activated $CD45^+$ $CD3^+$ helper CD4+ or cytotoxic CD8+ T cell subsets. For detecting intracellular IFN-γ, cells were fixed and permeabilized prior to staining with APC Cy7 anti-IFN-γ antibody. Stained cells were run in a LSRII analyzer within 24 h. Datasets were analyzed using FlowJo software v.10.2 (Treestar Inc, Ashland, OR, USA).

Histopathological evaluation of major organs

Liver, spleen, kidney, lung, and brain tissues from mice (n=3) were fixed in 10% neutral buffered formalin, processed, and embedded in paraffin as previously described [419]. Histopathological examination was made on sections (4 µm) stained with hematoxylin and eosin. The tissues sections were screened for any pathological changes using an Olympus BX50 microscope with Olympus DP26 digital photography by a veterinary pathologist blinded to treatment groups.

Statistical analyses

Statistical analyses were performed using GraphPad Prism 7.0 software (GraphPad Software Inc, La Jolla, CA, USA). Data are presented as mean ± SEM unless otherwise indicated. Treatment groups were compared for differences in fluorescence intensity using analysis of variance [539] followed by Tukey's multiple comparison post-hoc test. *P* values less than 0.05 were considered significant.

Results

Characterization of tPA-NPs

The encapsulation of tPA into NPs occurred through the electrostatic self-assembly of tPA with PLL-g-PEG, which were then cross-linked to provide stability. SDS-PAGE was used to identify cross-linking conditions that would result in stable NP complexes. Compared to non-complexed tPA (lane 2), tPA-NPs formed without any cross-linker (lane 3) readily released most of the tPA protein, as observed by the protein's largely unhindered migration which was similar to the free protein (Fig. 4.1B). When glutaraldehyde was added to a final concentration of 0.06% (lane 4), no free tPA was able to migrate into the gel, indicating that tPA-NPs were effectively cross linked with 0.06% glutaraldehyde. Higher concentrations of glutaraldehyde (lanes 6 and 7) resulted in a heterogeneous migration of protein into the gel that made protein encapsulation difficult to interpret.

DLS was used to determine the size of the tPA-NPs (Table 1). All NPs ranged in size from 40-60 nm and had relatively low to moderate polydispersity. Ter119-NPs was relatively smaller (~ 50 nm) in diameter compared to ERY1-NP (~60nm). All NPs demonstrated a relatively narrow size distribution (Fig. 4.1C).

Ter119 antibody functionalized NPs exhibited prolonged circulation compared to other treatments by efficiently binding to RBCs after intravenous delivery

A single intravenous injection of FITC labeled tPA and tPA-NPs was performed in Balb/c mice and blood samples were assessed for RBC binding efficiencies of NPs by flow cytometry (Fig. 4.2A). Targeting NPs to RBCs using Ter119 ligand significantly prolonged circulation of tPA compared to ERY1-NPs, Bare NPs or free tPA (Fig. 4.2B). The Ter119-NPs achieved >98 % of RBC binding immediately after injection and labeling efficiencies of >95 % could be seen up to 3 days post-injection. Also, 85 % of RBC bound Ter119-NPs were observed on day 4, but it sharply declined to ~30 % on day 5. In contrast, ERY1-NPs exhibited about 3-5 % binding up to an hour post injection and cleared rapidly beyond detection. Unbound drug (tPA) and Bare NPs

showed ~2.5 % binding to RBCs at time 0, however, fluorescence signals were undetected afterward. At all-time points, the mean fluorescence intensity (MFI) of Ter119-NP was significantly higher than tPA, Bare NPs, and ERY1-NPs until 5 days and dropped close to the MFIs of the other cohorts on day 6 (Fig. 4.2C). Additionally, the MFI of FITC positive RBCs decreased from days 3 through 5, suggesting that the Ter119-NPs showed enhanced detachment from the RBC surface after 72 hours (Fig. 4.2D).

Ter119-NPs showed high stability and durability of RBC complexation during confocal microscopy

To demonstrate attachment of FITC labeled NPs encapsulated with tPA to RBCs, blood samples from mice were imaged under confocal microscope. No detectable FITC emission from the RBCs of tPA and Bare NP treated mice was noted (Fig. 4.3A). In contrast, Ter119-NP demonstrated the brightest signal from 0 h-5 days after injection (Fig. 4.3B). ERY1-NPs showed moderate fluorescence till an hour, but the detectable signal was not evident at later time points**.** Ter119-NP attachment was not associated with morphological deformation and alterations compared to control (Fig. 4.3B). Additionally, the RBC count, RBC distribution width [403], and hemoglobin content remained unaltered for the 7-day period of observation (Table 4.2). The complete blood count parameters were within the range of reference values from Charles River Laboratories database for BALB/c mice [32,542]. Fluorescence intensity of Ter119-NPs appeared as scattered, green fluorescent spots on RBC membrane after 72h.

Ter119-NPs demonstrated delayed clearance from blood compared to bare NP

Mice were injected with FITC labeled tPA and tPA-NPs and blood samples were subjected to spectrophotometric analysis. Determination of % injected dose (ID) in the blood samples based on normalization of FITC fluorescence intensity to time 0h indicated rapid clearance for (tPA, Bare NPs, and ERY1-NPs; >95% of ID in <1h) (Fig. 4.4A; inset). Ter119-NPs exhibited

markedly prolonged circulation time (about 85% of ID in circulation up to 48 h) (Fig. 4.4A). The clearance kinetics was somewhat rapid after 48h, however ~60% and 25% of ID was evident on days 3 and 4 post-injection, respectively. The average time for Ter119-NPs to reach 50% of their injected dose was ~3.5 days. In contrast to Ter119-NPs, ERY1-NPs demonstrate rapid clearance kinetics. Overall, the area under curve (AUC) of Ter119-NPs was >150-folds compared to tPA, Bare NP and ERY1-NP (Fig. 4.4B). AUC of ERY1-NPs was ~1.2-folds greater than Bare NPs and tPA, whereas Bare NPs and tPAs demonstrated similar clearance profile.

Biodistribution of NPs by non-invasive *in vivo* imaging

To assess biodistribution kinetics of RBC bound *vs.* unbound particles, Balb/c mice were injected with NIR tagged tPA and tPA-NPs (Bare NP, ERY1-NP, and Ter119-NP) and imaged longitudinally for 5 days post-injection using XtremeII *in vivo* imaging system (Fig. 4.5A). Animals injected with NIR-tPA showed high fluorescence in the bladder at 1h followed by very low to no signal from the bladder at 24h post-injection. Fluorescent signals were not observed in the liver and the spleen of tPA cohorts suggesting rapid elimination via the urinary route. In contrast, mice infused with NIR labeled tPA-NPs, irrespective of the NP type, showed weak fluorescent signal in urinary bladder at 1 hour and a bright fluorescent signal in the liver and spleen at 24h post injection (Fig. 4.5B). Subsequent daily imaging of the NP cohorts with the same acquisition parameters revealed a gradual decrease in the fluorescence signal from the liver with the intensities becoming undetectable at 5 days. For Bare NP, ERY1-NP, and Ter119-NP, elimination via hepato-biliary route was predominantly observed. Most importantly, Ter119-NPs avoided the liver and spleen accumulation at early time points relative to ERY1-NPs or Bare NPs, as evidenced by fluorescence intensities.

***Ex vivo* organ imaging suggested lower accumulation of Ter119-NPs than Bare NPs and ERY1-NPs in liver and spleen**

To further define the relative differences in biodistribution and elimination of NIR labelled tPA and tPA-NPs, we sacrificed the mice one-week post-injection and performed *ex vivo* ROI analysis of NIR fluorescence in the harvested organs of interest. In tPA cohorts, maximal fluorescence intensity was observed in kidney (~60%) while the liver and spleen accounted for remaining 40% of the fluorescence (Fig. 4.6A-C). Organs from all the NP cohorts demonstrated strongest signal in the liver followed by spleen, kidneys, lungs, heart and LNs. However, fluorescence intensity in livers of Ter119-NP treated mice demonstrated 1.7 folds less intensity than Bare NP and 1.3 folds less than that of ERY1-NP (Fig. 4.6B). Though these observations clearly suggested an initial uptake of the NPs by the RES system followed by hepatobiliary excretion, Ter119-NPs exhibited relatively lower accumulation in the RES system than Bare NPs and ERY1-NPs.

Systemic targeting of Ter119 conjugated NPs to RBCs did not cause adverse innate and adaptive immune responses

Antigen-specific IFN-γ secreting CD4+ T cells in the spleen and CD8+ T cells in the LN were significantly decreased by ~2.5 and 1.5-folds in the tPA, Bare NP, and ERY1-NP groups compared to control mice (Fig. 4.7A-D). The percentage of CD4+ T and CD8+ T cells expressing IFN-γ was 19.6% ± 1.4 and 2.9% ± 0.4 in the spleen and 54.5% ± 1.2 and 0.7% ± 0.04 in the LNs of Ter119-NP cohorts and they were similar to the naïve control mice. Additionally, no obvious signs of toxic reactions or inflammatory responses that could be attributed to the systemic injection of NPs were found in hematology. The fraction of leukocytes and their subsets in blood was within the normal reference range suggesting that Ter119-NPs bound to RBCs did not provoke systemic innate and adaptive immune responses in spite of an intravenous route of administration (Table 4.2).

Intravenous administration of Ter119-NPs was biocompatible and safe to major organs

To assess the effect of RBC targeting Ter119-NPs on major organs, histological examination of liver, spleen, kidney, lung, and brain was performed 7 days post intravenous administration of the NPs. Liver and spleen sections from all the treated groups did not reveal any inflammation or fibrosis and their microscopic architecture was comparable to control (Fig. 4.8A). Similarly, kidney, lung, and brain in tPA and NP groups did not show any evidence of pathologic changes compared to control. Further evaluation of liver function tests indicated normal levels of total protein, albumin, albumin to globulin ratio, ALT, and AST in serum from treated mice (Fig. 4.8B).

Discussion

Prior research has shown that encapsulation of therapeutic agents in NPs can enhance targeted therapy in a region of interest compared to conventional approaches [543,544]. Although beneficial, less than 5-10% of NP injectable dose is typically retained in circulation over 24h after intravenous injection, thereby underscoring a need for additional innovations in formulation chemistry to improve NP retention in body [379,545,546] [547,548]. One approach to address this can be by attaching therapeutics to harvested RBCs via adsorption or ligand-receptor interaction, and their re-injection into the donor subjects [379,529-531,549]. Several recent studies have shown the feasibility of this approach against a variety of chronic diseases [531,550-552,379,385,543,553]. We have shown that *ex-vivo* attachment of NPs to RBCs especially via the GPA membrane receptor do not induce oxidative stress or impact the oxygen carrying capacities [540,554]. Although *ex-vivo* loading of RBCs with drugs and NPs has merits, the need of donor or autologous blood restricts the treatment option to blood transfusion settings, preventing widespread clinical use [527,555]. To overcome this barrier, in this study, we investigated the feasibility of direct and real-time labeling of RBCs with NPs *in vivo* for enhancing circulation kinetics, bio-distribution, and bio-compatibility of therapeutic agents.

As a model therapeutic, we utilized tPA, an FDA approved agent commonly used in clinics to dissolve blood clots. A key current limitation of tPA is its short circulation half-life (<10 min) [556]. Thus, to enhance its half-life, neutrally charged PEG grafted onto a cationic PLL backbone nanomaterial was utilized to load tPA and generate core-shell NPs [554]. The NPs were also equipped with Ter119 antibody and ERY1 peptide for active targeting of RBC membrane receptor. Ter119 antibody is an IgG2b class monoclonal antibody. It targets the Ter119 antigen associated with GPAs on erythrocyte membrane [557]. ERY1 is a 12 amino acid long peptide sequence that directly labels the GPAs on RBCs [536,558]. We found that ERY1 peptide or Ter119 antibody functionalization of NPs increased their hydrodynamic diameter slightly (~10 nm) compared to unliganded NPs (Table 1). To investigate whether the increase in NP size influenced RBC targeting and half-life *in vivo*, the NPs were injected in mice via intravenous route, and the RBC targeting was assessed by flow cytometry and confocal microscopy. In contrast to ERY1-NP and bare NPs (<3% labeling efficiency), the Ter119-NP remarkably labeled >98% of circulating RBCs within a few minutes after intravenous injection (Fig. 4.2). Importantly, the Ter119-NPs remained bound to ~95% of RBCs up to 3 days post injection, and retained ~60 % injected dose (ID), demonstrating durable binding with RBCs in circulation. In contrast, ERY1-NP demonstrated weak RBC association and cleared rapidly from the circulation under the shear stress (Fig. 4.3). The dramatic increase in the elimination half-life of TER119-NPs (~3.5 days) was also a significant improvement from prior reported NPs approaches with polystyrene and poly(DL-lactide-co-glycolide (PLGA) NPs that retained 5-30% of ID in the circulation over 2 days [396,559]. Based on this premise, we propose that real-time targeting of Ter119 membrane protein can be leveraged for dramatically improving circulatory retention of NPs from hours to days.

For clinical translation, it is important that the binding of NPs to RBCs does not induce hemolysis or modulate the cellular functions [560 561]. As a first step, we evaluated the effect of NPs on blood

cell counts, and MCHC (Table 4.2). We found that the adhesion of Ter119-NP to RBCs did not result in adverse effects on RBC morphology and cell counts. This is in contrast to a prior study that showed development of anemia *in vivo* [562]. Most likely, the modification of Ter119 antibody using DTT before NP formulation enhanced tolerance *in vivo*, however, this phenomenon will require more detailed mechanistic investigations in future [563,564]. Also, the NPs exhibited predominant accumulation in liver and spleen. In contrast, free tPA was cleared by renal route (Fig. 4.5 and 4.6). Larger particles (~20-50 nm) are primarily cleared by the hepatobiliary and fecal routes and the smaller particles typically show clearance by renal mechanisms (3-6 nm), thus we believe that the NPs maintained its stability *in vivo* and altered the biodistribution profile of tPA [565,566,567,568]. Importantly, amongst all group, Ter119 NPs demonstrated a relatively slower accumulation in liver and spleen at early time points without activating the immune system (Fig. 4.7 and Table 4.2). This indicates that RBC attachment of NPs prevent inflammation and cardiovascular stress, while also improving retention in circulation [546,569]. This finding was supported by the histopathological examination of various organs where NPs did not cause intracerebral hemorrhage and major organ toxicities (Fig. 4.8).

In conclusion, our study shows that the Ter119-NPs are capable of achieving stable and durable targeting to RBCs after intravenous injection, and this novel technology can effectively evade the RES to prolong NP circulation time. Future studies comparing the therapeutic efficacies of RBC targeted NPs with conventional NPs can shed more lights on clinical translation potential in various disease models.

Table 4.1. NP size and PDI determined by DLS.

	Bare NP	ERY1-NP	Ter119-NP
Diameter (nm)	40.5 ± 7.6	60.4 ± 9.1	51.2 ± 3.4
PDI	0.084 ± 0.104	0.252 ± 0.104	0.285 ± 0.102

Table 4.2. Hematological parameters were not altered by intravenous delivery of TNPs.

Parameter	Ter119-NP	ERY1-NP	Bare NP	tPA	Reference value
RBC (x10^6 /μL)	9.72±0.30	8.84±0.36	8.03±0.25	8.87±0.17	5-9.5
Hb (g/dL)	14.97±0.44	13.83±0.52	11.73±0.54	13.60±0.34	10.9-16.3
HCT (%)	47.67±2.07	43.50±1.21	37.80±1.38	42.23±1.01	37.4-51.7
MCV (fL)	49.00±0.66	49.30±0.66	47±0.43	47.63±0.30	48-56
MCH (pg/dL)	15.40±0.05	15.67±0.05	14.56±0.21	15.33±0.11	11.9-19
MCHC (g/dL)	31.47±0.46	31.77±0.32	31±0.37	32.20±0.16	25.9-35.1
Platelet (x10^3 /μL)	818.33±167.57	756.00±168.49	1284.33±39.26	463.67±92.43	1084-1992
WBC (x10^3 /μL)	4.03±1.37	3.51±0.15	8.65±1.88	4.10±0.56	3-14.2
Neutrophil (x10^3 /μL)	1.44±0.30	1.39±0.22	4.06±1.03	1.81±0.42	0.46-2.2
Lymphocyte (x10^3 /μL)	2.43±1.1	1.85±0.35	3.55±0.56	2.10±0.48	3-2-11.2
Monocyte (x10^3 /μL)	0.11±0.3	0.20±0	0.94±0.38	0.13±0.03	0.4-1.43
Eosinophil (x10^3 /μL)	0.04±0.2	0.05±0.01	0.097±0.04	0.05±0.01	0-0.38
Basophil (x10^3 /μL)	0.00±0	0.02±0.01	0±0	0.01±0	0-0.09

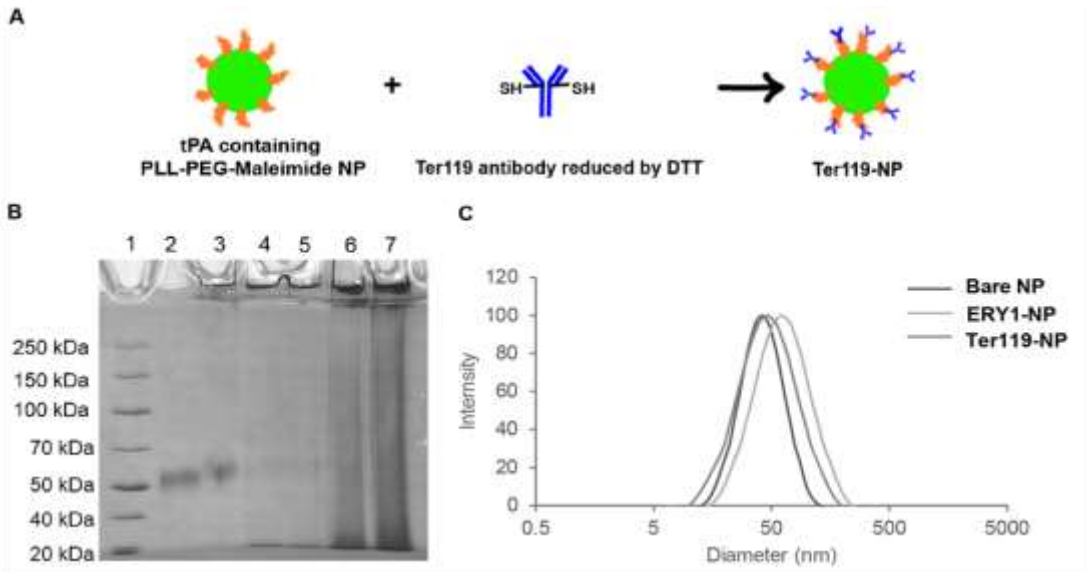

Fig. 4.1. Synthesis, encapsulation and characterization of NPs. (A) Schematic of Ter119-antibody conjugation to the surface of PLL-PEG-Maleimide NP. (B) SDS-PAGE of tPA NPs with glutaraldehyde titration. Lane 1: Ladder; Lane 2: tPA; Lane 3: tPA NPs 0% glutaraldehyde; Lane 4: tPA NPs 0.06% glutaraldehyde; Lane 5: tPA NPs 0.08% glutaraldehyde; Lane 6: tPA-NPs 0.12% glutaraldehyde; Lane 7: tPA-NPs 0.25% glutaraldehyde. (C) Size distribution of Bare NPs, ERY1-NPs, and Ter119-NPs determined by DLS. The mean particle size of Ter119-NPs was approximately 50 nm and with a PDI of 0.285.

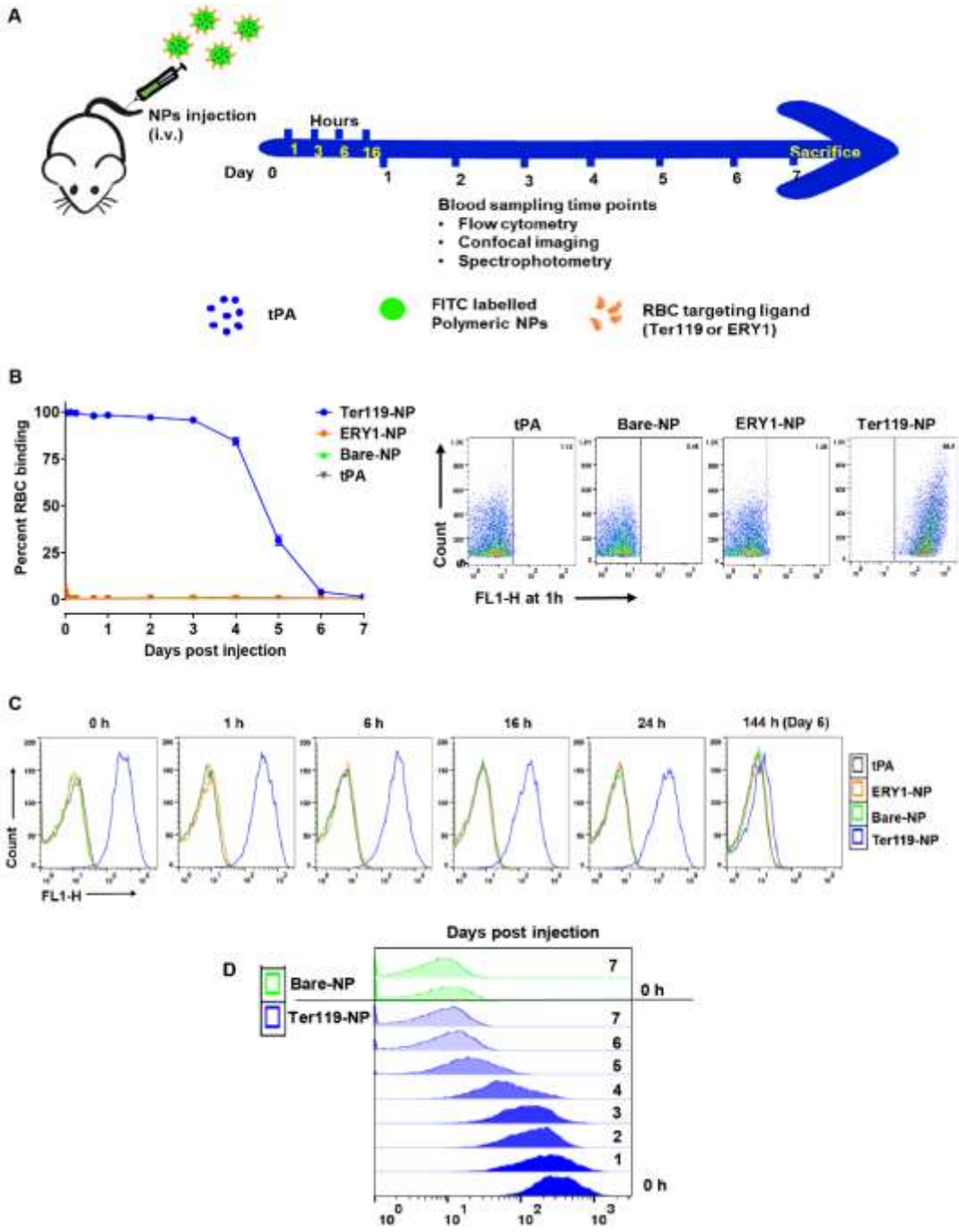

Fig. 4.2. Clinically translatable prolonged circulation of polymeric NPs is achieved by targeting Ter119-NPs to RBCs. BALB/c mice were randomized into the following groups: tPA, Bare NP, ERY1-NP and Ter119-NP. (A) Mice in each cohort received 90 µg of tPA or tPA loaded NPs labeled with FITC by tail vein injection as shown by the schematic. Flow cytometric analysis of blood (n=3 for each time point) was performed at different time points over a period

of 7 days. (B) Percentage of RBCs bound to tPA loaded polymeric NPs. % RBC binding in circulation was quantified based on FITC fluorescence as a function of change in time. Data are shown as mean ± SEM. (C) Histograms representing relative differences of median fluorescence intensity (MFI) between the groups from 0, 1, 6, 16, 24, and 144 hours. (D) Gradual decrease in the MFI of Ter119-NP bound to RBCs over a period of 7 days depicted by histograms.

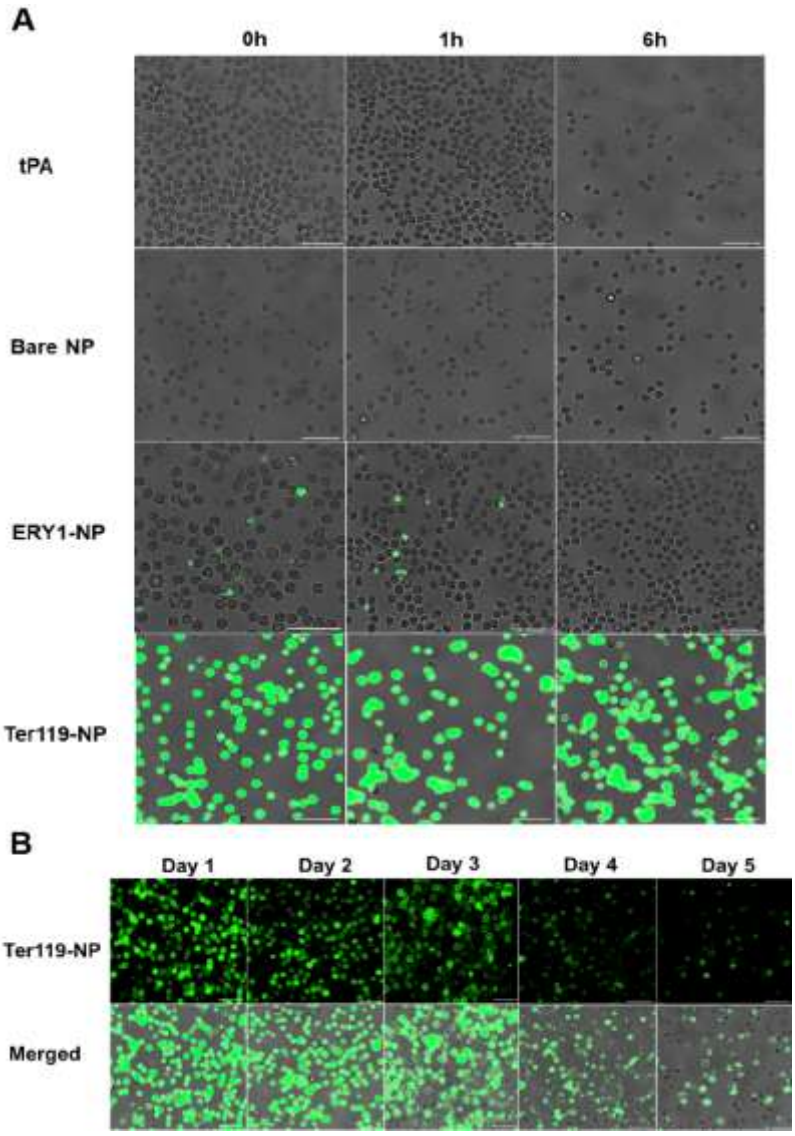

Fig. 4.3. Real-time tracking of Ter119-NP attachment to RBCs by confocal microscopy. Blood samples from mice (n=3 per time point) injected intravenously with FITC tPA or tPA-NPs were observed under confocal microscope. (A) Merged images of FITC labeled NP/free tPA and

bright field optical images. Blood samples from Ter119-NP cohorts showed bright green fluorescent spots from 0 to 6 h compared to tPA, Bare NP, and ERY1-NP. (B) Time dependent decrease in fluorescence signal from FITC positive RBCs bound to Ter119-NPs over a period of 5 days post injection. No RBC membrane damage was observed. Scale bar is 20 µm.

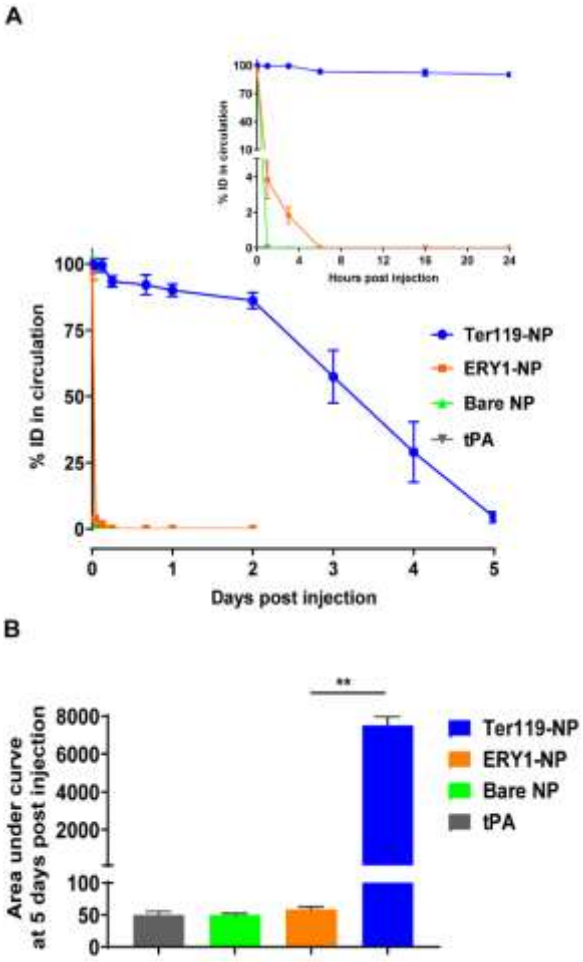

Fig. 4.4. RBC targeting Ter119-NPs augmented circulation half-life of the NPs. Mice were injected IV with FITC tPA or tPA loaded NPs and blood was collected at different time intervals (n=3 per time point). FITC was used as fluorescence probe in tPA or NPs and change in fluorescence was measured by spectrophotometer. (A) Time dependent *in vivo* circulation of tPA-NPs represented as the percentage of injected dose (%ID). %ID was calculated from the change in fluorescence intensity at time 't' h relative to time 0 h. Inset: magnified representation of early

time points. (B) The area under curve (AUC) of tPA-NPs versus tPA at 5 days post injection. Each data point represents mean ± S.E.M ($n = 3$). Statistics were determined by ANOVA with Tukey's post-hoc correction (** $p<0.01$).

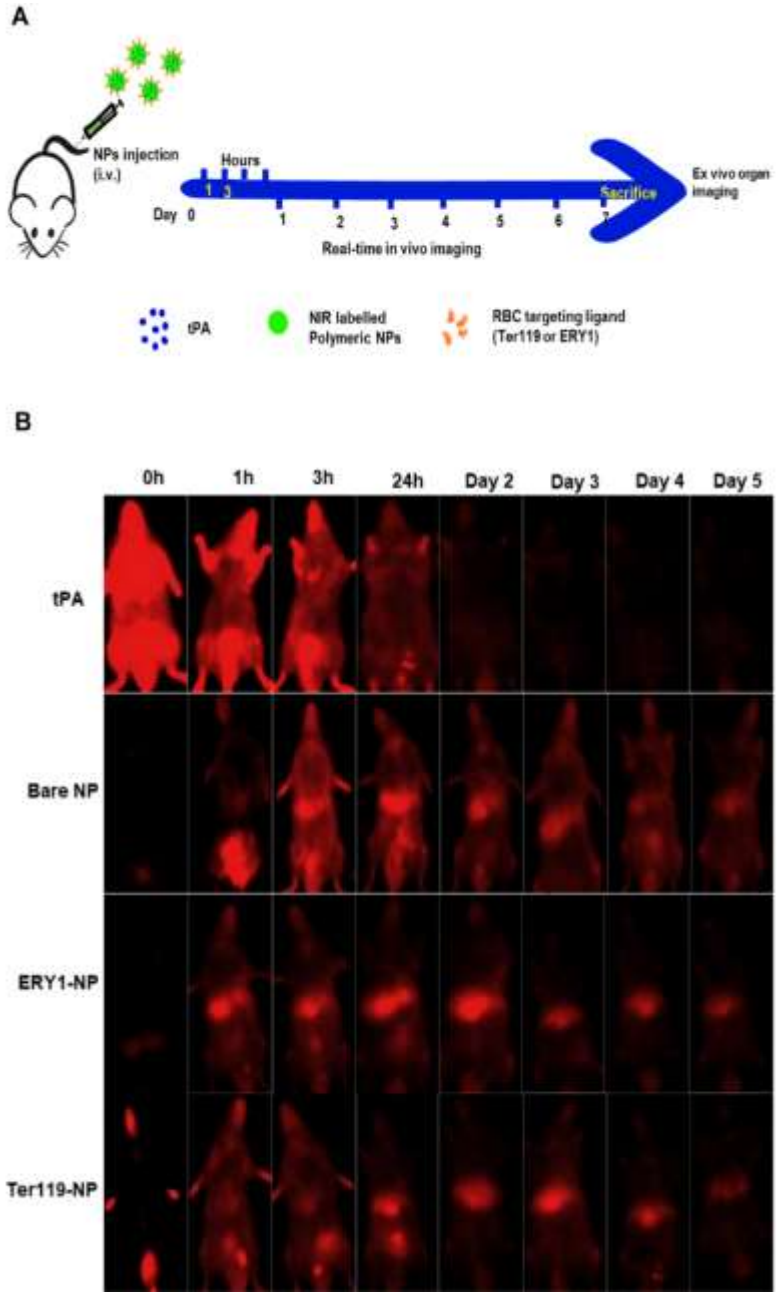

Fig. 4.5. Non-invasive real time *in vivo* fluorescence imaging in mice after IV injection of NIR labeled tPA-NPs. (A) Experimental design for evaluation of biodistribution of NPs using *in*

vivo imaging of mice injected with NIR tPA and tPA-NPs. (B) Longitudinal whole body imaging of mice in different groups (n=3) was performed to assess the biodistribution and elimination of polymeric nanoparticles over time. Mice in Ter119-NP cohorts showed a delay in hepatic accumulation as compared to Bare NPs and ERY1-NPs. Same acquisition parameters were maintained for all the time points of imaging.

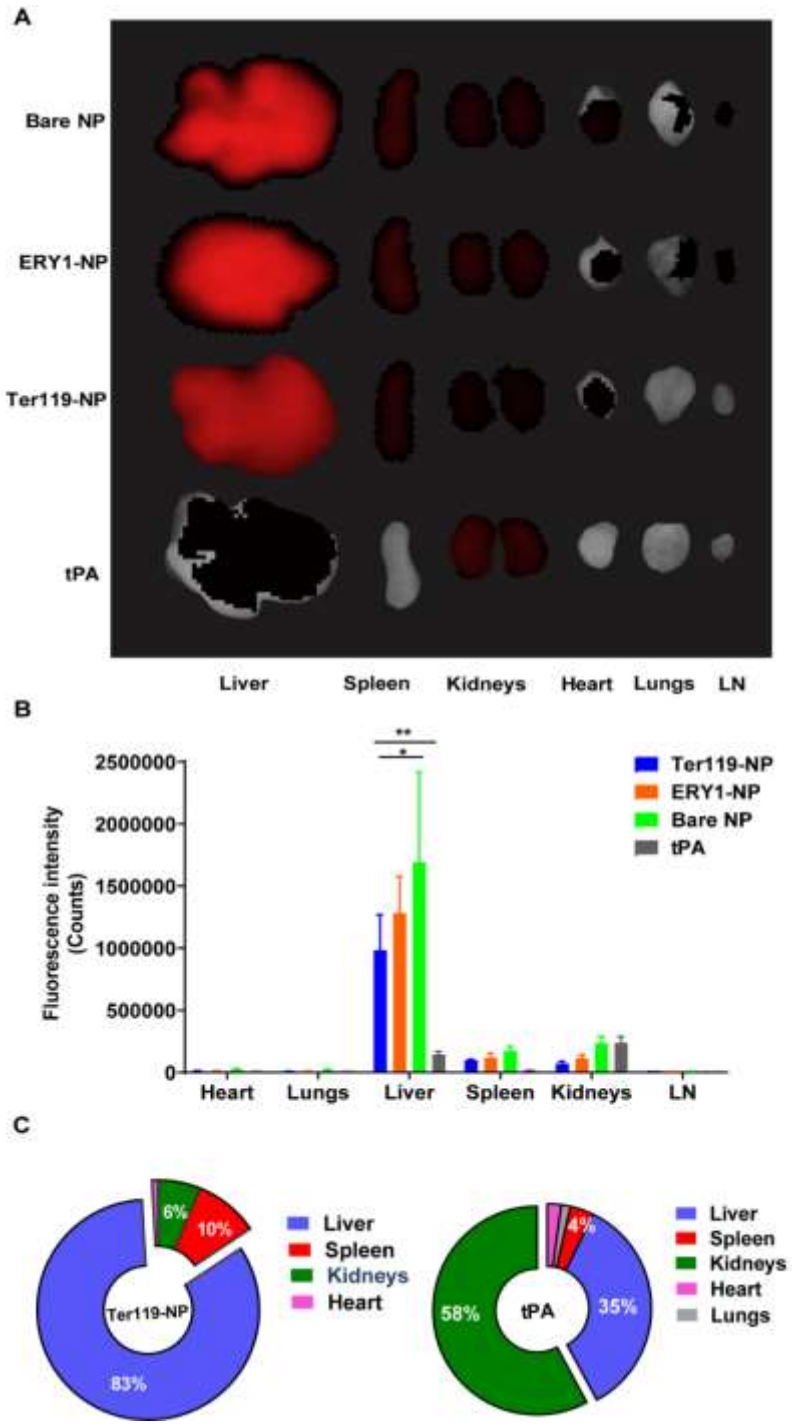

Fig. 4.6. *Ex-vivo* NIR fluorescence imaging of isolated organs on day 7 post injection. Mice were injected with 90 µg NIR labelled tPA or tPA-NPs via tail vein and sacrificed on day 7 post injection. (A) In each cohort, organs of interest namely liver, spleen, kidneys, heart, lungs, and LNs were harvested and imaged *ex-vivo* on day 7 after injection. Each panel represents merged

images of fluorescence of NIR emission and X-ray. (B) ROI analysis of the harvested organs in *ex vivo* fluorescence imaging (n=3). Data are represented as mean ± SEM. Statistics were determined by ANOVA with Tukey's post-hoc correction (* $p<0.05$, ** $p<0.01$). (C) Average percent fluorescent intensity representing the biodistribution of Ter119-NPs and tPA in the harvested organs.

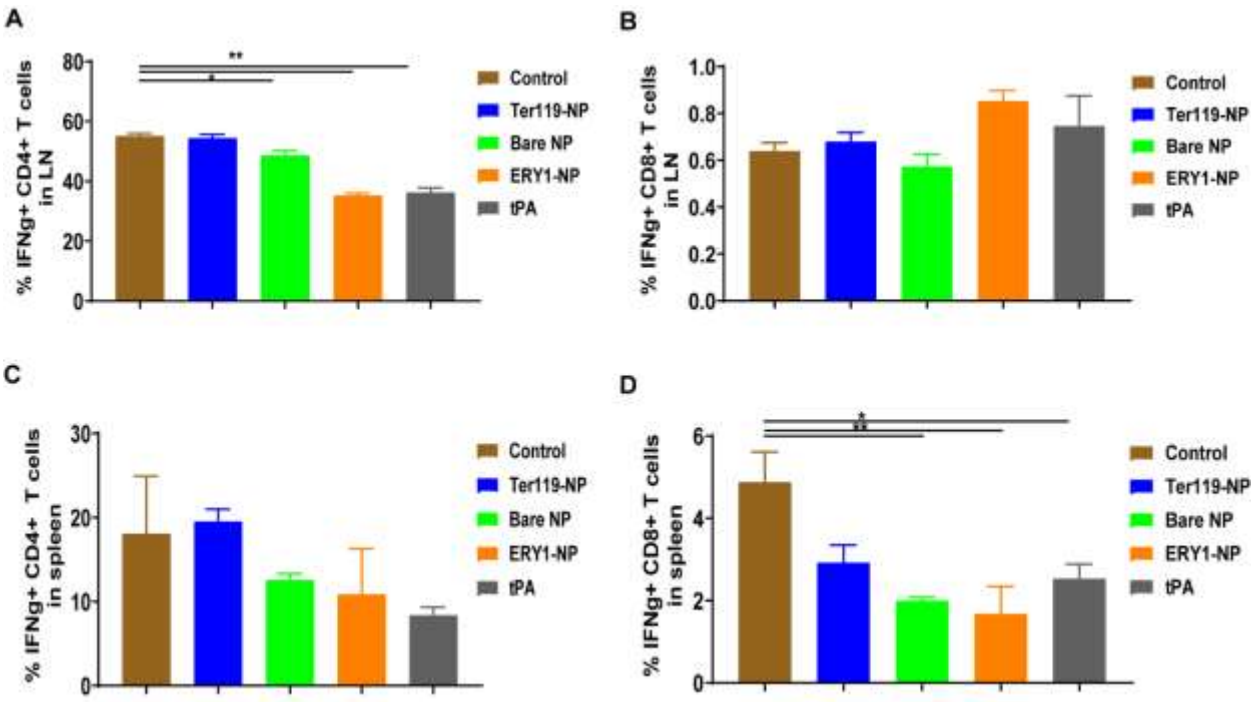

Fig. 4.7. RBCs-bound Ter119-NPs did not cause adverse immune response. Balb/c mice injected with NPs or tPA were sacrificed 7 days post injection. Spleens and superficial lymph nodes (LN) were harvested and single cell suspensions were stimulated *ex-vivo* with antigens in the presence of Brefeldin A to assess NP specific immune response in the mice. The following were used as the antigens (5 µg/ml) in the respective groups: tPA protein for tPA, Bare NP, ERY1-NP, or Ter119-NP for the respective cohorts. The graphs represent percent of IFN—γ secreting T cells after *ex vivo* stimulation, (A,B) CD4+ IFN-γ and CD8+ IFN-γ T cells respectively in the LN (n=3) and (C,D) CD4+ IFN-γ and CD8+ IFN-γ T cells in the spleen (n=3-5). Naive Balb/c mice that did not receive any injection were kept as untreated control for baseline value comparison. Data are shown as mean ± SEM, Statistics were determined by ANOVA with Tukey's post-hoc correction. Comparisons were performed between UC and treatments. * $p < 0.05$, ** $p < 0.01$.

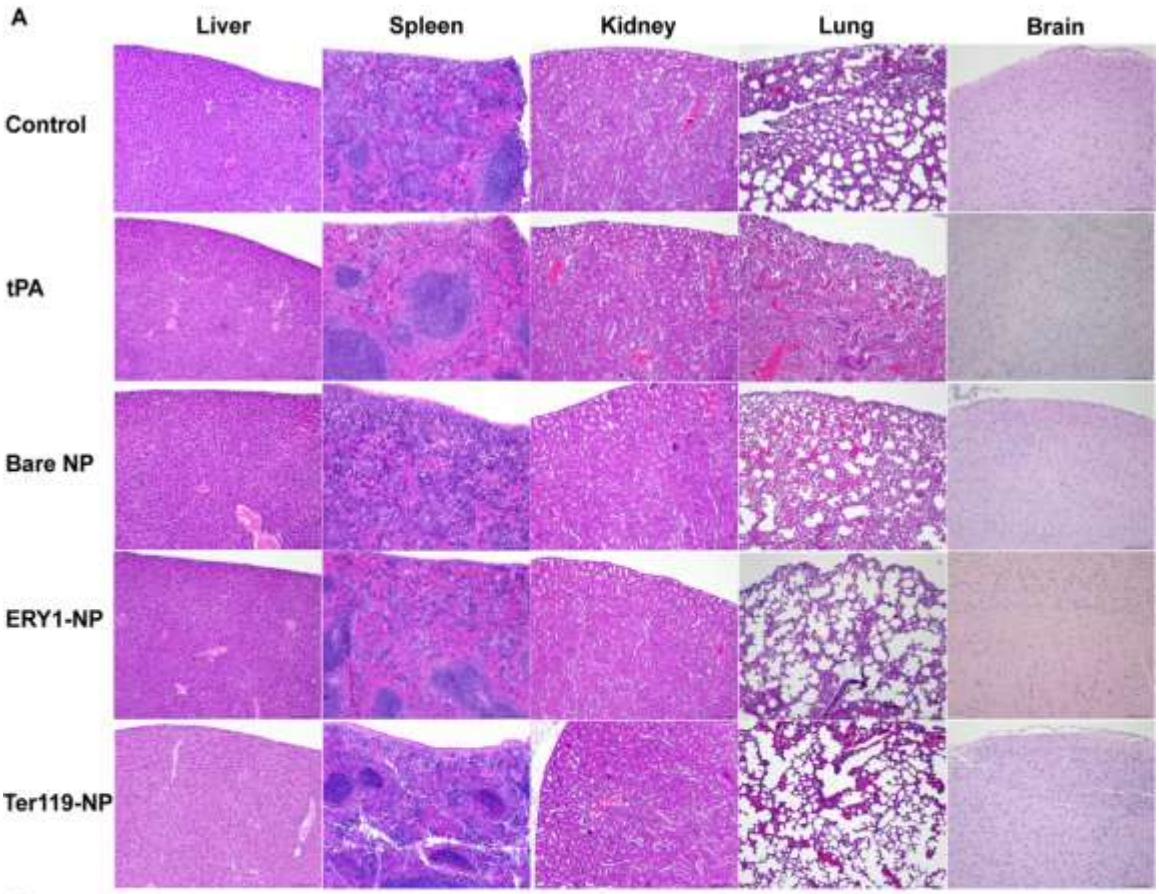

B

Parameter	tPA	Bare NP	ERY1-NP	Ter119-NP
Total protein	3.86 ± 0.03	3.97 ± 0.08	4.43 ± 0.38	4.23 ± 0.28
Albumin	2.33 ± 0.03	1.87 ± 0.15	2.6 ± 0.2	2.5 ± 0.1
Albumin/globulin	1.52 ± 0.05	0.89 ± 0.09	1.42 ± 0.03	1.46 ± 0.10
ALT	86.67 ± 13.86	18.67 ± 0.88	39.67 ± 13.42	32 ± 10.53
AST	155 ± 12	77.67 ± 10.91	133.67 ± 60.74	94 ± 12.01

Fig. 4.8. Ter119-NP is not toxic to major organs upon intravenous administration. (A) Histological sections of mice (n=3) liver, spleen, kidney, lung, and brain 7 days after intravenous administration of NPs did not show any pathological lesions compared to untreated control group. (B) Biochemical analysis of serum from treated mice (n=3) for total protein, albumin, albumin to globulin ratio, ALT and AST suggested that the parameters were in the normal range.

CHAPTER V

SUMMARY AND FUTURE PERSPECTIVES

Melanoma is an aggressive form of skin cancer that responds poorly to conventional cancer therapies. In the last decade, FDA approved immune checkpoint inhibitor therapy have revolutionized the field of cancer immunotherapy. Immune checkpoint therapy is successful only in 30-40% of melanoma patients and the rest either respond poorly or do not respond at all. Factors responsible for the failure of immunotherapy in advanced melanoma patients are poor antigen expression on tumor cells, defective antigen presentation mechanisms, expression of immune checkpoints, and poor baseline tumor specific cytotoxic T cell population.

Novel therapeutics that can reprogram tumor immune microenvironment are needed to treat aggressive malignancies. We hypothesized that an increase in immune cell infiltration in tumor and their activation by exogenous activators will generate robust melanoma specific immunity. We treated clinically relevant poorly immunogenic B16F10 melanoma with focused ultrasound-based hyperthermia (thermal) or histotripsy (mechanical) with and without local CD40 stimulation and assessed immune mechanisms. Efficacy of these treatment approaches in sensitizing large refractory melanoma to dual anti-CTLA-4 and anti-PD-L1 checkpoint therapy was evaluated in bilateral B16F10 model. Both hyperthermia and histotripsy treatments in combination with CD40 agonism were successful in reprogramming tumor microenvironment, leading to robust melanoma specific immune response. Combined histotripsy and CD40 therapy sensitized refractor melanoma tumors to immune checkpoint therapy and significantly prolonged survival of mice. Additionally, this dissertation also demonstrates the potential of targeting of RBCs using an intravenously injectable polymeric nanoparticles as a cell targeting therapeutic approach. Findings from this work are described below.

Chapter II

In this chapter, we explored the role of local FUS hyperthermia and in situ anti-CD40 agonist antibody treatment in improving melanoma specific systemic immune response in mice. FUS and

CD40 alone were able to delay tumor growth but FUS40 was superior in delaying progression of both treated and untreated abscopal tumor. The efficacy improvement with FUS40 therapy was also reflected in immune cell profiling, whereas the FUS40 treated tumors had a higher infiltration of cytotoxic Granzyme B+ CD8+ T cells and anti-tumoral M1 macrophages. We found that combined FUS40 therapy was able to preserve functional status of CD8+ T cells in tumors and had a high frequency of Granzyme B+ PD-1- CD8+ T cells. Splenocyte stimulation assay suggested that FUS40 cohorts had significantly higher percentage of activated IL-2 and IFN-γ secreting melanoma specific CD8+ T cells. Generation of melanoma specific systemic immune response correlated with better suppression of untreated tumor growth in FUS40 cohorts than others. These findings suggest that FUS40 therapy can be a novel approach to improve immunogenicity of poorly immunogenic tumors.

Chapter III

In this chapter, we assessed the efficiency of non-invasive ultrasound-based histotripsy (HT) technique and anti-CD40 agonist antibody in sensitizing large refractory B16F10 melanoma to immune checkpoint blockade. Mechanical fragmentation of tumors by HT resulted in an upregulation of CCL8, CSFR1, ICAM2 and VCAM1. Upregulation of these chemokines and cell adhesion molecules in tumors correlated with an increase in immune cell recruitment. Combination of CD40 plus HT (HT40) further enhanced the immune profile of tumors. HT40 treated tumors had higher infiltration of activated granzyme B secreting CD8+ T cells compared to untreated controls and tumor associated macrophage population shifted towards anti-tumoral M1 macrophages. Upregulation of CXCL9 in HT40 tumors was associated with high T cell recruitment and homing. HT40 cohorts demonstrated generation of melanoma specific systemic immunity and had high number of CD4+ T effector/memory cells. Together with these changes, there was an increase in expression of immune checkpoint PD-L1 in the treated tumors. Reprogramming of the tumor immune environment in HT40 cohorts resulted in sensitization of

tumors to anti-CTLA-4 and anti-PD-L1 therapy and significantly prolonged survival of otherwise refractory mice. Our findings suggest that priming of advanced stage melanoma with histotripsy and CD40 activator can unlock the full potential of immune checkpoint inhibitors in hard to treat cases.

Chapter IV

In this chapter, we explored the potential of erythrocyte targeting polymeric nanoparticles in improving blood retention time of model thrombolytic drug. Tissue plasminogen activator or tPA gets cleared from the circulation in <10 minutes after injection. We encapsulated tPA in polymeric NPs to protect it from serum inhibitors and decorated these NPs with RBC targeting ligand anti-Ter119 antibody. Ter119-NPs targeted >98% of RBCs immediately after intravenous injection. Ter119-NP displayed enhanced blood retention time such that 80% of the injected dose was still in circulation after 2 days. These findings suggested formation of a durable RBC-NP complex *in vivo*. In spite, of strong and persistent binding to RBCs, Ter119-NPs did not cause detrimental changes in either RBC morphology or function. *In vivo* longitudinal imaging showed delayed and gradual accumulation of NPs in liver and spleen in Ter119-NP cohorts compare to other groups. *In vivo* imaging data also suggested hepatobiliary route of clearance for NPs while renal clearance was the dominant route of excretion for free tPA. Ter119-NPs can be a potent drug delivery system to extend the circulation life of drugs used in various vascular ailments.

Future perspectives

Findings from our studies suggest that focused ultrasound and CD40 combination reprograms tumor immune profile and preserves functional status of CD8+ T cells. However, in spite of melanoma specific immunity generation, FUS40 and HT40 therapy did not eradicate the tumors completely. Based on gene profile data from HT40 treated tumors, an upregulation of CTLA-4 and anti-PD-L1 and immunosuppressive checkpoints namely Lag3 and Tim3 was noted. We

would consider testing the efficacy of Lag3 and Tim3 inhibitors in melanoma after priming the tumors with FUS40 or HT40. We did not test our FUS40 and HT40 approaches in other more immunogenic tumor models or genetically modified tumor models that are close to human malignancies. Evaluation of our therapies in different tumor models may shed more light on clinical translation potential of our approach. Both FUS40 and HT40 therapy were able to generate melanoma specific immunity, supporting effective antigen presentation with these therapies but we do not know if CD40 stimulation prior to focused ultrasound will be better than the current approach. We had covered 50% of tumor mass with HT therapy, this may not be the ideal volume to be covered in large tumors and may need to be further explored. It may be valuable to optimize FUS, HT and CD40 sequence to achieve best therapeutic outcome. We saw survival improvement when tumors were primed with HT40 prior to systemic checkpoint blockade. It may be worth exploring the feasibility of *in situ* immune checkpoint blockade along with local HT40 or FUS40 therapy. *In situ* checkpoint inhibition approach may reduce the side effects associated with systemic administration of immune checkpoint inhibitors.

Recently new isoforms of CD40 antibody have been developed that are more potent than the current CD40 antibody. Validation of new CD40 isoforms with FUS and HT can further improve our treatment outcomes. Therapy that works in one type of cancer may not work in other. It may be valuable to try other immune adjuvants like CpG, OX40 or FDA approved IL-2 or IFN-α in combination with FUS and HT, to develop novel immunotherapy combinations that can cover the majority of cancer patients.

We had attempted delivering tPA loaded Ter119-polymeric NPs to target RBCs in blood circulation for extending the circulation half-life of the therapeutic. The results from this work are highly exciting with the RBC-NP complex circulating in blood for >3 days. The *in vivo* drug release, activity of the NP loaded drug (tPA), and therapeutic value of the RBC-NP complex need to be evaluated in further studies. This work also has the potential to provide insights for

delivering NPs loaded with chemotherapeutics, gene, or protein-based anti-cancer agents to target RBCs, achieve sustained release of drug, improve drug pharmacokinetics, and enhance its efficacy against chronic inflammatory disorders and metastatic cancers.

REFERENCES

1 Grumezescu, A. M. Nano-and Microscale Drug Delivery Systems: Design and Fabrication. (William Andrew, 2017).

2 Cichorek, M., Wachulska, M., Stasiewicz, A. & Tymińska, A. Skin melanocytes: biology and development. Advances in Dermatology and Allergology/Postępy Dermatologii I Alergologii 30, 30 (2013).

3 Lin, J. Y. & Fisher, D. E. Melanocyte biology and skin pigmentation. Nature 445, 843-850 (2007).

4 Brozyna, A. et al. Mechanism of UV-related carcinogenesis and its contribution to nevi/melanoma. Expert review of dermatology 2, 451-469 (2007).

5 Chin, L., Garraway, L. A. & Fisher, D. E. Malignant melanoma: genetics and therapeutics in the genomic era. Genes Dev 20, 2149-2182 (2006).

6 Haass, N. K. & Herlyn, M. Normal Human Melanocyte Homeostasis as a Paradigm for Understanding Melanoma. Journal of Investigative Dermatology Symposium Proceedings 10, 153-163, doi:https://doi.org/10.1111/j.1087-0024.2005.200407.x (2005).

7 Bandarchi, B., Ma, L., Navab, R., Seth, A. & Rasty, G. From melanocyte to metastatic malignant melanoma. Dermatol Res Pract 2010, 583748, doi:10.1155/2010/583748 (2010).

8 Sandru, A., Voinea, S., Panaitescu, E. & Blidaru, A. Survival rates of patients with metastatic malignant melanoma. J Med Life 7, 572-576 (2014).

9 Cummins, D. L. et al. in Mayo clinic proceedings. 500-507 (Elsevier).

10 Count, R. C. R. C. R. Melanoma Incidence and Mortality, United States–2012-2016.

11 Siegel, R. L., Miller, K. D. & Jemal, A. Cancer statistics, 2020. CA: a cancer journal for clinicians 70, 7-30 (2020).

12 Wilson, M. A. & Schuchter, L. M. Chemotherapy for Melanoma. Cancer Treat Res 167, 209-229, doi:10.1007/978-3-319-22539-5_8 (2016).

13 Kim, C. et al. Long-term survival in patients with metastatic melanoma treated with DTIC or temozolomide. Oncologist 15, 765-771, doi:10.1634/theoncologist.2009-0237 (2010).

14 Middleton, M. R. et al. Randomized phase III study of temozolomide versus dacarbazine in the treatment of patients with advanced metastatic malignant melanoma. J Clin Oncol 18, 158-166, doi:10.1200/jco.2000.18.1.158 (2000).

15 Miklavcic, D. et al. Electrochemotherapy: technological advancements for efficient electroporation-based treatment of internal tumors. Med Biol Eng Comput 50, 1213-1225, doi:10.1007/s11517-012-0991-8 (2012).

16 Matthiessen, L. W. et al. Management of cutaneous metastases using electrochemotherapy. Acta Oncol 50, 621-629, doi:10.3109/0284186x.2011.573626 (2011).

17 Baldea, I. & Filip, A. G. Photodynamic therapy in melanoma--an update. J Physiol Pharmacol 63, 109-118 (2012).

18 Austin, E., Mamalis, A., Ho, D. & Jagdeo, J. Laser and light-based therapy for cutaneous and soft-tissue metastases of malignant melanoma: a systematic review. Arch Dermatol Res 309, 229-242, doi:10.1007/s00403-017-1720-9 (2017).

19 Henderson, B. W. & Dougherty, T. J. How does photodynamic therapy work? Photochem Photobiol 55, 145-157, doi:10.1111/j.1751-1097.1992.tb04222.x (1992).

20 Brown, S. B., Brown, E. A. & Walker, I. The present and future role of photodynamic therapy in cancer treatment. Lancet Oncol 5, 497-508, doi:10.1016/s1470-2045(04)01529-3 (2004).

21 Huang, Y. Y. et al. Melanoma resistance to photodynamic therapy: new insights. Biol Chem 394, 239-250, doi:10.1515/hsz-2012-0228 (2013).

22 Biteghe, F. N. & Davids, L. M. A combination of photodynamic therapy and chemotherapy displays a differential cytotoxic effect on human metastatic melanoma cells. J Photochem Photobiol B 166, 18-27, doi:10.1016/j.jphotobiol.2016.11.004 (2017).

23 Lugowska, I., Teterycz, P. & Rutkowski, P. Immunotherapy of melanoma. Contemp Oncol (Pozn) 22, 61-67, doi:10.5114/wo.2018.73889 (2018).

24 Creagan, E. T. et al. Phase II trials of recombinant leukocyte A interferon in disseminated malignant melanoma: results in 96 patients. Cancer Treat Rep 70, 619-624 (1986).

25 Leach, D. R., Krummel, M. F. & Allison, J. P. Enhancement of Antitumor Immunity by CTLA-4 Blockade. Science 271, 1734, doi:10.1126/science.271.5256.1734 (1996).

26 Hanson, D. C. et al. Preclinical in vitro characterization of anti-CTLA4 therapeutic antibody CP-675,206. Cancer Research 64, 877 (2004).

27 Ribas, A. et al. Intratumoral immune cell infiltrates, FoxP3, and indoleamine 2,3-dioxygenase in patients with melanoma undergoing CTLA4 blockade. Clin Cancer Res 15, 390-399, doi:10.1158/1078-0432.Ccr-08-0783 (2009).

28 Beatty, G. L. et al. CD40 Agonists Alter Tumor Stroma and Show Efficacy Against Pancreatic Carcinoma in Mice and Humans. Science 331, 1612, doi:10.1126/science.1198443 (2011).

29 Okazaki, T. & Honjo, T. PD-1 and PD-1 ligands: from discovery to clinical application. Int Immunol 19, 813-824, doi:10.1093/intimm/dxm057 (2007).

30 Mahoney, K. M., Rennert, P. D. & Freeman, G. J. Combination cancer immunotherapy and new immunomodulatory targets. Nat Rev Drug Discov 14, 561-584, doi:10.1038/nrd4591 (2015).

31 Zou, M. Z. et al. A Multifunctional Biomimetic Nanoplatform for Relieving Hypoxia to Enhance Chemotherapy and Inhibit the PD-1/PD-L1 Axis. Small 14, 1801120 (2018).

32 Robert, C. et al. Nivolumab in previously untreated melanoma without BRAF mutation. N Engl J Med 372, 320-330, doi:10.1056/NEJMoa1412082 (2015).

33 Robert, C. et al. Pembrolizumab versus ipilimumab in advanced melanoma (KEYNOTE-006): post-hoc 5-year results from an open-label, multicentre, randomised, controlled, phase 3 study. The Lancet Oncology 20, 1239-1251 (2019).

34 Larkin, J. et al. Combined Nivolumab and Ipilimumab or Monotherapy in Untreated Melanoma. N Engl J Med 373, 23-34, doi:10.1056/NEJMoa1504030 (2015).

35 Le, D. T. et al. Mismatch repair deficiency predicts response of solid tumors to PD-1 blockade. Science 357, 409-413, doi:10.1126/science.aan6733 (2017).

36 Schumacher, T. N. & Schreiber, R. D. Neoantigens in cancer immunotherapy. Science 348, 69, doi:10.1126/science.aaa4971 (2015).

37 Hamid, O. et al. Safety and tumor responses with lambrolizumab (anti-PD-1) in melanoma. N Engl J Med 369, 134-144, doi:10.1056/NEJMoa1305133 (2013).

38 McDermott, D. F. et al. Atezolizumab, an Anti-Programmed Death-Ligand 1 Antibody, in Metastatic Renal Cell Carcinoma: Long-Term Safety, Clinical Activity, and Immune Correlates From a Phase Ia Study. J Clin Oncol 34, 833-842, doi:10.1200/jco.2015.63.7421 (2016).

39 Motzer, R. J. et al. Nivolumab for Metastatic Renal Cell Carcinoma: Results of a Randomized Phase II Trial. J Clin Oncol 33, 1430-1437, doi:10.1200/jco.2014.59.0703 (2015).

40 Tietze, J. K. et al. The proportion of circulating CD45RO(+)CD8(+) memory T cells is correlated with clinical response in melanoma patients treated with ipilimumab. Eur J Cancer 75, 268-279, doi:10.1016/j.ejca.2016.12.031 (2017).

41 Wistuba-Hamprecht, K. et al. Peripheral CD8 effector-memory type 1 T-cells correlate with outcome in ipilimumab-treated stage IV melanoma patients. Eur J Cancer 73, 61-70, doi:10.1016/j.ejca.2016.12.011 (2017).

42 Milhem, M. et al. Abstract CT144: Intratumoral toll-like receptor 9 (TLR9) agonist, CMP-001, in combination with pembrolizumab can reverse resistance to PD-1 inhibition in a phase Ib trial in subjects with advanced melanoma. Cancer Research 78, CT144-CT144, doi:10.1158/1538-7445.AM2018-CT144 (2018).

43 Gonzalez, H., Hagerling, C. & Werb, Z. Roles of the immune system in cancer: from tumor initiation to metastatic progression. Genes Dev 32, 1267-1284, doi:10.1101/gad.314617.118 (2018).

44 Escors, D. Tumour Immunogenicity, Antigen Presentation, and Immunological Barriers in Cancer Immunotherapy. New Journal of Science 2014, 734515, doi:10.1155/2014/734515 (2014).

45 Schreiber, T. H., Raez, L., Rosenblatt, J. D. & Podack, E. R. Tumor immunogenicity and responsiveness to cancer vaccine therapy: the state of the art. Seminars in immunology 22, 105-112, doi:10.1016/j.smim.2010.02.001 (2010).

46 Blankenstein, T., Coulie, P. G., Gilboa, E. & Jaffee, E. M. The determinants of tumour immunogenicity. Nat Rev Cancer 12, 307-313, doi:10.1038/nrc3246 (2012).

47 Berglund, A. et al. Methylation of immune synapse genes modulates tumor immunogenicity. The Journal of clinical investigation 130, 974-980 (2020).

48 Capietto, A.-H., Jhunjhunwala, S. & Delamarre, L. Characterizing neoantigens for personalized cancer immunotherapy. Current opinion in immunology 46, 58-65 (2017).

49 Conway, J. R., Kofman, E., Mo, S. S., Elmarakeby, H. & Van Allen, E. Genomics of response to immune checkpoint therapies for cancer: implications for precision medicine. Genome medicine 10, 93-93, doi:10.1186/s13073-018-0605-7 (2018).

50 Yarchoan, M., Johnson, B. A., 3rd, Lutz, E. R., Laheru, D. A. & Jaffee, E. M. Targeting neoantigens to augment antitumour immunity. Nat Rev Cancer 17, 209-222, doi:10.1038/nrc.2016.154 (2017).

51 Dong, Z.-Y. et al. EGFR mutation correlates with uninflamed phenotype and weak immunogenicity, causing impaired response to PD-1 blockade in non-small cell lung cancer. Oncoimmunology 6, e1356145 (2017).

52 Knocke, S. et al. Tailored tumor immunogenicity reveals regulation of CD4 and CD8 T cell responses against cancer. Cell reports 17, 2234-2246 (2016).

53 Martincorena, I. & Campbell, P. J. Somatic mutation in cancer and normal cells. Science 349, 1483-1489, doi:10.1126/science.aab4082 (2015).

54 Errol, C. F. et al. DNA Repair and Mutagenesis, Second Edition. (American Society of Microbiology, 2006).

55 Dunn, G. P., Koebel, C. M. & Schreiber, R. D. Interferons, immunity and cancer immunoediting. Nat Rev Immunol 6, 836-848, doi:10.1038/nri1961 (2006).

56 Chalmers, Z. R. et al. Analysis of 100,000 human cancer genomes reveals the landscape of tumor mutational burden. Genome Med 9, 34, doi:10.1186/s13073-017-0424-2 (2017).

57 Kim, J. Y. et al. Tumor Mutational Burden and Efficacy of Immune Checkpoint Inhibitors: A Systematic Review and Meta-Analysis. Cancers (Basel) 11, 1798, doi:10.3390/cancers11111798 (2019).

58 Dong, Z. Y. et al. Potential Predictive Value of TP53 and KRAS Mutation Status for Response to PD-1 Blockade Immunotherapy in Lung Adenocarcinoma. Clin Cancer Res 23, 3012-3024, doi:10.1158/1078-0432.Ccr-16-2554 (2017).

59 Galuppini, F. et al. Tumor mutation burden: from comprehensive mutational screening to the clinic. Cancer Cell Int 19, 209-209, doi:10.1186/s12935-019-0929-4 (2019).

60 Snyder, A. et al. Genetic basis for clinical response to CTLA-4 blockade in melanoma. The New England journal of medicine 371, 2189-2199, doi:10.1056/NEJMoa1406498 (2014).

61 Lechner, M. G. et al. Immunogenicity of murine solid tumor models as a defining feature of in vivo behavior and response to immunotherapy. J Immunother 36, 477-489, doi:10.1097/01.cji.0000436722.46675.4a (2013).

62 Gaudino, S. J. & Kumar, P. Cross-Talk Between Antigen Presenting Cells and T Cells Impacts Intestinal Homeostasis, Bacterial Infections, and Tumorigenesis. Frontiers in Immunology 10, doi:10.3389/fimmu.2019.00360 (2019).

63 Garris, C. S. et al. Successful Anti-PD-1 Cancer Immunotherapy Requires T Cell-Dendritic Cell Crosstalk Involving the Cytokines IFN-γ and IL-12. Immunity 49, 1148-1161.e1147, doi:https://doi.org/10.1016/j.immuni.2018.09.024 (2018).

64 Faltus, J., Boggess, B. & Bruzga, R. The use of diagnostic musculoskeletal ultrasound to document soft tissue treatment mobilization of a quadriceps femoris muscle tear: a case report. Int J Sports Phys Ther 7, 342-349 (2012).

65 Ozgönenel, L., Aytekin, E. & Durmuşoglu, G. A double-blind trial of clinical effects of therapeutic ultrasound in knee osteoarthritis. Ultrasound Med Biol 35, 44-49, doi:10.1016/j.ultrasmedbio.2008.07.009 (2009).

66 Wong, R. A., Schumann, B., Townsend, R. & Phelps, C. A. A survey of therapeutic ultrasound use by physical therapists who are orthopaedic certified specialists. Phys Ther 87, 986-994, doi:10.2522/ptj.20050392 (2007).

67 Chiang, Y.-P., Wang, T.-G. & Hsieh, S.-F. Application of Ultrasound in Sports Injury. Journal of Medical Ultrasound 21, 1-8, doi:https://doi.org/10.1016/j.jmu.2013.01.008 (2013).

68 Sengupta, S. & Balla, V. K. A review on the use of magnetic fields and ultrasound for non-invasive cancer treatment. J Adv Res 14, 97-111, doi:10.1016/j.jare.2018.06.003 (2018).

69 Hickey, R. C., Fry, W. J., Meyers, R., Fry, F. J. & Bradbury, J. T. Human Pituitary Irradiation with Focused Ultrasound: An Initial Report on Effect in Advanced Breast Cancer. Archives of Surgery 83, 620-633, doi:10.1001/archsurg.1961.01300160132016 (1961).

70 Kim, Y.-s., Rhim, H., Choi, M. J., Lim, H. K. & Choi, D. High-intensity focused ultrasound therapy: an overview for radiologists. Korean J Radiol 9, 291-302, doi:10.3348/kjr.2008.9.4.291 (2008).

71 Dalecki, D. Mechanical Bioeffects of Ultrasound. Annual Review of Biomedical Engineering 6, 229-248, doi:10.1146/annurev.bioeng.6.040803.140126 (2004).

72 Harari, P. M. et al. Development of scanned focussed ultrasound hyperthermia: Clinical response evaluation clinical response evaluation. International Journal of Radiation Oncology* Biology* Physics 21, 831-840 (1991).

73 Hand, J., Vernon, C. & Prior, M. Early experience of a commercial scanned focused ultrasound hyperthermia system. International journal of hyperthermia 8, 587-607 (1992).

74 Court, K. A. et al. HSP70 Inhibition Synergistically Enhances the Effects of Magnetic Fluid Hyperthermia in Ovarian Cancer. Mol Cancer Ther 16, 966-976, doi:10.1158/1535-7163.Mct-16-0519 (2017).

75 Ma, Y. et al. Anticancer chemotherapy-induced intratumoral recruitment and differentiation of antigen-presenting cells. Immunity 38, 729-741, doi:10.1016/j.immuni.2013.03.003 (2013).

76 King, M. A., Leon, L. R., Morse, D. A. & Clanton, T. L. Unique cytokine and chemokine responses to exertional heat stroke in mice. J Appl Physiol (1985) 122, 296-306, doi:10.1152/japplphysiol.00667.2016 (2017).

77 Harjunpää, H., Llort Asens, M., Guenther, C. & Fagerholm, S. C. Cell Adhesion Molecules and Their Roles and Regulation in the Immune and Tumor Microenvironment. Frontiers in Immunology 10, doi:10.3389/fimmu.2019.01078 (2019).

78 Ostberg, J. R., Kabingu, E. & Repasky, E. A. Thermal regulation of dendritic cell activation and migration from skin explants. Int J Hyperthermia 19, 520-533, doi:10.1080/02656730310001607986 (2003).

79 Chen, Q., Fisher, D. T., Kucinska, S. A., Wang, W. C. & Evans, S. S. Dynamic control of lymphocyte trafficking by fever-range thermal stress. Cancer immunology, immunotherapy : CII 55, 299-311, doi:10.1007/s00262-005-0022-9 (2006).

80 Chaussy, C., Tilki, D. & Thüroff, S. Transrectal high-intensity focused ultrasound for the treatment of localized prostate cancer: current role. (2013).

81 Uchida, T. et al. Five years experience of transrectal high-intensity focused ultrasound using the Sonablate device in the treatment of localized prostate cancer. international Journal of Urology 13, 228-233 (2006).

82 Uchida, T. et al. Five years experience of transrectal high-intensity focused ultrasound using the Sonablate device in the treatment of localized prostate cancer. Int J Urol 13, 228-233, doi:10.1111/j.1442-2042.2006.01272.x (2006).

83 Wu, F. et al. A randomised clinical trial of high-intensity focused ultrasound ablation for the treatment of patients with localised breast cancer. British Journal of Cancer 89, 2227-2233, doi:10.1038/sj.bjc.6601411 (2003).

84 Li, H. et al. [High-intensity focused ultrasound inhibits tumor metastasis in a melanoma-bearing mouse model]. Nan Fang Yi Ke Da Xue Xue Bao 35, 223-228 (2015).

85 Maxwell, A. D. et al. Cavitation clouds created by shock scattering from bubbles during histotripsy. J Acoust Soc Am 130, 1888-1898, doi:10.1121/1.3625239 (2011).

86 Brujan, E. A. The role of cavitation microjets in the therapeutic applications of ultrasound. Ultrasound Med Biol 30, 381-387, doi:10.1016/j.ultrasmedbio.2003.10.019 (2004).

87 Khokhlova, V. A. et al. Effects of nonlinear propagation, cavitation, and boiling in lesion formation by high intensity focused ultrasound in a gel phantom. J Acoust Soc Am 119, 1834-1848, doi:10.1121/1.2161440 (2006).

88 Brujan, E. A., Ikeda, T. & Matsumoto, Y. On the pressure of cavitation bubbles. Experimental Thermal and Fluid Science 32, 1188-1191, doi:https://doi.org/10.1016/j.expthermflusci.2008.01.006 (2008).

89 Hoogenboom, M. et al. Mechanical High-Intensity Focused Ultrasound Destruction of Soft Tissue: Working Mechanisms and Physiologic Effects. Ultrasound in Medicine & Biology 41, 1500-1517, doi:https://doi.org/10.1016/j.ultrasmedbio.2015.02.006 (2015).

90 Wang, Y. N., Khokhlova, T., Bailey, M., Hwang, J. H. & Khokhlova, V. Histological and biochemical analysis of mechanical and thermal bioeffects in boiling histotripsy lesions induced by high intensity focused ultrasound. Ultrasound Med Biol 39, 424-438, doi:10.1016/j.ultrasmedbio.2012.10.012 (2013).

91 Jonathan, R. S. et al. In vivo histotripsy brain treatment. Journal of Neurosurgery JNS 131, 1331-1338, doi:10.3171/2018.4.JNS172652 (2018).

92 Parsons, J. E., Cain, C. A., Abrams, G. D. & Fowlkes, J. B. Pulsed cavitational ultrasound therapy for controlled tissue homogenization. Ultrasound in medicine & biology 32, 115-129 (2006).

93 Xu, Z., Fowlkes, J. B., Rothman, E. D., Levin, A. M. & Cain, C. A. Controlled ultrasound tissue erosion: The role of dynamic interaction between insonation and microbubble activity. The Journal of the Acoustical Society of America 117, 424-435 (2005).

94 Hall, T. L. et al. Histotripsy of rabbit renal tissue in vivo: temporal histologic trends. J Endourol 21, 1159-1166, doi:10.1089/end.2007.9915 (2007).

95 Lake, A. M. et al. Histotripsy: minimally invasive technology for prostatic tissue ablation in an in vivo canine model. Urology 72, 682-686, doi:10.1016/j.urology.2008.01.037 (2008).

96 Hempel, C. R. et al. Histotripsy fractionation of prostate tissue: local effects and systemic response in a canine model. J Urol 185, 1484-1489, doi:10.1016/j.juro.2010.11.044 (2011).

97 Worlikar, T. et al. Histotripsy for Non-Invasive Ablation of Hepatocellular Carcinoma (HCC) Tumor in a Subcutaneous Xenograft Murine Model. Conf Proc IEEE Eng Med Biol Soc 2018, 6064-6067, doi:10.1109/embc.2018.8513650 (2018).

98 Schade, G. R. et al. Boiling Histotripsy Ablation of Renal Cell Carcinoma in the Eker Rat Promotes a Systemic Inflammatory Response. Ultrasound in Medicine & Biology 45, 137-147, doi:https://doi.org/10.1016/j.ultrasmedbio.2018.09.006 (2019).

99 Qu, S. et al. Non-thermal histotripsy tumor ablation promotes abscopal immune responses that enhance cancer immunotherapy. Journal for ImmunoTherapy of Cancer 8, e000200, doi:10.1136/jitc-2019-000200 (2020).

100 Silvestrini, M. T. et al. Priming is key to effective incorporation of image-guided thermal ablation into immunotherapy protocols. JCI Insight 2, e90521-e90521, doi:10.1172/jci.insight.90521 (2017).

101 Silvestrini, M. T. et al. Priming is key to effective incorporation of image-guided thermal ablation into immunotherapy protocols. JCI Insight 2, doi:10.1172/jci.insight.90521 (2017).

102 Diamond, M. S. et al. Type I interferon is selectively required by dendritic cells for immune rejection of tumors. The Journal of experimental medicine 208, 1989-2003, doi:10.1084/jem.20101158 (2011).

103 Fuertes, M. B. et al. Host type I IFN signals are required for antitumor CD8+ T cell responses through CD8{alpha}+ dendritic cells. The Journal of experimental medicine 208, 2005-2016, doi:10.1084/jem.20101159 (2011).

104 Rajčáni, J. & Szathmary, S. Peptide Vaccines: New Trends for Avoiding the Autoimmune Response. The Open Infectious Diseases Journal 10 (2018).

105 Escors, D. Tumour immunogenicity, antigen presentation and immunological barriers in cancer immunotherapy. New J Sci 2014, doi:10.1155/2014/734515 (2014).

106 Menares, E. et al. Tissue-resident memory CD8+ T cells amplify anti-tumor immunity by triggering antigen spreading through dendritic cells. Nature communications 10, 1-12 (2019).

107 Liechtenstein, T., Dufait, I., Lanna, A., Breckpot, K. & Escors, D. MODULATING CO-STIMULATION DURING ANTIGEN PRESENTATION TO ENHANCE CANCER IMMUNOTHERAPY. Immunol Endocr Metab Agents Med Chem 12, 224-235, doi:10.2174/187152212802001875 (2012).

108 Gardner, A. & Ruffell, B. Dendritic Cells and Cancer Immunity. Trends Immunol 37, 855-865, doi:10.1016/j.it.2016.09.006 (2016).

109 Grywalska, E., Pasiarski, M., Góźdź, S. & Roliński, J. Immune-checkpoint inhibitors for combating T-cell dysfunction in cancer. OncoTargets and therapy 11, 6505 (2018).

110 Dominguez, D. et al. Exogenous IL-33 restores dendritic cell activation and maturation in established cancer. The Journal of Immunology 198, 1365-1375 (2017).

111 Fiorentino, D. F. et al. IL-10 acts on the antigen-presenting cell to inhibit cytokine production by Th1 cells. The Journal of Immunology 146, 3444 (1991).

112 Gabrilovich, D. et al. Vascular endothelial growth factor inhibits the development of dendritic cells and dramatically affects the differentiation of multiple hematopoietic lineages in vivo. Blood 92, 4150-4166 (1998).

113 Shi, Y. et al. Suppression of vascular endothelial growth factor abrogates the immunosuppressive capability of murine gastric cancer cells and elicits antitumor immunity. Febs j 281, 3882-3893, doi:10.1111/febs.12923 (2014).

114 Brown, R. D. et al. Dendritic cells from patients with myeloma are numerically normal but functionally defective as they fail to up-regulate CD80 (B7-1) expression after huCD40LT stimulation because of inhibition by transforming growth factor-beta1 and interleukin-10. Blood 98, 2992-2998, doi:10.1182/blood.v98.10.2992 (2001).

115 Lou, Y. et al. Antitumor activity mediated by CpG: the route of administration is critical. J Immunother 34, 279-288, doi:10.1097/CJI.0b013e31820d2a05 (2011).

116 den Brok, M. H. M. G. M. et al. Synergy between In situ Cryoablation and TLR9 Stimulation Results in a Highly Effective In vivo Dendritic Cell Vaccine. Cancer Research 66, 7285, doi:10.1158/0008-5472.CAN-06-0206 (2006).

117 Yasmin-Karim, S. et al. Radiation and Local Anti-CD40 Generate an Effective in situ Vaccine in Preclinical Models of Pancreatic Cancer. Frontiers in immunology 9, 2030-2030, doi:10.3389/fimmu.2018.02030 (2018).

118 van Kooten, C. & Banchereau, J. CD40-CD40 ligand. Journal of leukocyte biology 67, 2-17 (2000).

119 Clark, E. A. A Short History of the B-Cell-Associated Surface Molecule CD40. Frontiers in immunology 5, 472-472, doi:10.3389/fimmu.2014.00472 (2014).

120 van Kooten, C. & Banchereau, J. Functions of CD40 on B cells, dendritic cells and other cells. Curr Opin Immunol 9, 330-337 (1997).

121 Bourgeois, C., Rocha, B. & Tanchot, C. A role for CD40 expression on CD8+ T cells in the generation of CD8+ T cell memory. Science 297, 2060-2063 (2002).

122 Klaus, G. G., Choi, M. S., Lam, E. W.-F., Johnson-Leger, C. & Cliff, J. CD40: a pivotal receptor in the determination of life/death decisions in B lymphocytes. International reviews of immunology 15, 5-31 (1997).

123 Henn, V. et al. CD40 ligand on activated platelets triggers an inflammatory reaction of endothelial cells. Nature 391, 591-594 (1998).

124 Higuchi, T. et al. Cutting Edge: Ectopic expression of CD40 ligand on B cells induces lupus-like autoimmune disease. The Journal of Immunology 168, 9-12 (2002).

125 Elgueta, R. et al. Molecular mechanism and function of CD40/CD40L engagement in the immune system. Immunol Rev 229, 152-172, doi:10.1111/j.1600-065X.2009.00782.x (2009).

126 Lanzavecchia, A. Licence to kill. Nature 393, 413-414, doi:10.1038/30845 (1998).

127 Ara, A., Ahmed, K. A. & Xiang, J. Multiple effects of CD40-CD40L axis in immunity against infection and cancer. Immunotargets Ther 7, 55-61, doi:10.2147/ITT.S163614 (2018).

128 Pullen, S. S. et al. CD40− tumor necrosis factor receptor-associated factor (TRAF) interactions: regulation of CD40 signaling through multiple TRAF binding sites and TRAF hetero-oligomerization. Biochemistry 37, 11836-11845 (1998).

129 Banchereau, J. & Steinman, R. M. Dendritic cells and the control of immunity. Nature 392, 245-252 (1998).

130 Frleta, D. et al. Distinctive maturation of in vitro versus in vivo anti-CD40 mAb-matured dendritic cells in mice. Journal of Immunotherapy 26, 72-84 (2003).

131 Quezada, S. A., Jarvinen, L. Z., Lind, E. F. & Noelle, R. J. CD40/CD154 Interactions at the Interface of Tolerance and Immunity. Annual review of immunology 22, 307-328, doi:10.1146/annurev.immunol.22.012703.104533 (2004).

132 Wong, P. & Pamer, E. G. Feedback regulation of pathogen-specific T cell priming. Immunity 18, 499-511 (2003).

133 Josien, R. et al. TRANCE, a tumor necrosis factor family member, enhances the longevity and adjuvant properties of dendritic cells in vivo. The Journal of experimental medicine 191, 495-502 (2000).

134 Miga, A. J. et al. Dendritic cell longevity and T cell persistence is controlled by CD154-CD40 interactions. European journal of immunology 31, 959-965 (2001).

135 Wong, B. R. et al. TRANCE (tumor necrosis factor [TNF]-related activation-induced cytokine), a new TNF family member predominantly expressed in T cells, is a dendritic cell–specific survival factor. The Journal of experimental medicine 186, 2075-2080 (1997).

136 Cremer, I. et al. Long-lived immature dendritic cells mediated by TRANCE-RANK interaction. Blood, The Journal of the American Society of Hematology 100, 3646-3655 (2002).

137 Ouaaz, F., Arron, J., Zheng, Y., Choi, Y. & Beg, A. A. Dendritic cell development and survival require distinct NF-κB subunits. Immunity 16, 257-270 (2002).

138 Ghosh, S. & Karin, M. Missing pieces in the NF-κB puzzle. cell 109, S81-S96 (2002).

139 Pomerantz, J. L. & Baltimore, D. Two pathways to NF-κB. Molecular cell 10, 693-695 (2002).

140 Macatonia, S. E. et al. Dendritic cells produce IL-12 and direct the development of Th1 cells from naive CD4+ T cells. Journal of immunology (Baltimore, Md. : 1950) 154, 5071-5079 (1995).

141 Grumont, R. et al. c-Rel regulates interleukin 12 p70 expression in CD8+ dendritic cells by specifically inducing p35 gene transcription. The Journal of experimental medicine 194, 1021-1032 (2001).

142 Dejardin, E. et al. The lymphotoxin-beta receptor induces different patterns of gene expression via two NF-kappaB pathways. Immunity 17, 525-535, doi:10.1016/s1074-7613(02)00423-5 (2002).

143 Saccani, S., Pantano, S. & Natoli, G. Modulation of NF-κB activity by exchange of dimers. Molecular cell 11, 1563-1574 (2003).

144 Ballesteros-Tato, A., León, B., Lund, F. E. & Randall, T. D. CD4+ T helper cells use CD154-CD40 interactions to counteract T reg cell-mediated suppression of CD8+ T cell responses to influenza. The Journal of experimental medicine 210, 1591-1601, doi:10.1084/jem.20130097 (2013).

145 Hubo, M. et al. Costimulatory molecules on immunogenic versus tolerogenic human dendritic cells. Frontiers in immunology 4, 82-82, doi:10.3389/fimmu.2013.00082 (2013).

146 Rouard, H. et al. IL-12 secreting dendritic cells are required for optimum activation of human secondary lymphoid tissue T cells. Journal of Immunotherapy 25, 324-333 (2002).

147 Decken, K. et al. Interleukin-12 is essential for a protective Th1 response in mice infected with Cryptococcus neoformans. Infect Immun 66, 4994-5000 (1998).

148 Raker, V. K., Domogalla, M. P. & Steinbrink, K. Tolerogenic Dendritic Cells for Regulatory T Cell Induction in Man. Front Immunol 6, 569, doi:10.3389/fimmu.2015.00569 (2015).

149 Enk, A. H., Jonuleit, H., Saloga, J. & Knop, J. Dendritic cells as mediators of tumor-induced tolerance in metastatic melanoma. International journal of cancer 73, 309-316 (1997).

150 Jonuleit, H., Schmitt, E., Steinbrink, K. & Enk, A. H. Dendritic cells as a tool to induce anergic and regulatory T cells. Trends Immunol 22, 394-400, doi:10.1016/S1471-4906(01)01952-4 (2001).

151 Vonderheide, R. H. & Glennie, M. J. Agonistic CD40 Antibodies and Cancer Therapy. Clinical Cancer Research 19, 1035, doi:10.1158/1078-0432.CCR-12-2064 (2013).

152 Tong, A. W. & Stone, M. J. Prospects for CD40-directed experimental therapy of human cancer. Cancer gene therapy 10, 1 (2003).

153 Horton, H. M. et al. Fc-engineered anti-CD40 antibody enhances multiple effector functions and exhibits potent in vitro and in vivo antitumor activity against hematologic malignancies. Blood, The Journal of the American Society of Hematology 116, 3004-3012 (2010).

154 Oflazoglu, E. et al. Macrophages and Fc-receptor interactions contribute to the antitumour activities of the anti-CD40 antibody SGN-40. British journal of cancer 100, 113-117 (2009).

155 Restifo, N. P. et al. Molecular mechanisms used by tumors to escape immune recognition: Immunogenetherapy and the cell biology of major histocompatibility complex class I. Journal of Immunotherapy 14, 182-190, doi:10.1097/00002371-199310000-00004 (1993).

156 Suh, W. K. et al. Interaction of MHC class I molecules with the transporter associated with antigen processing. Science 264, 1322-1326, doi:10.1126/science.8191286 (1994).

157 Khanna, R. et al. Engagement of CD40 antigen with soluble CD40 ligand up-regulates peptide transporter expression and restores endogenous processing function in Burkitt's lymphoma cells. Journal of immunology (Baltimore, Md. : 1950) 159, 5782-5785 (1997).

158 Antoniades, C., Bakogiannis, C., Tousoulis, D., Antonopoulos, A. S. & Stefanadis, C. The CD40/CD40 Ligand System. Linking Inflammation With Atherothrombosis 54, 669-677, doi:10.1016/j.jacc.2009.03.076 (2009).

159 Danese, S., Sans, M. & Fiocchi, C. The CD40/CD40L costimulatory pathway in inflammatory bowel disease. Gut 53, 1035-1043, doi:10.1136/gut.2003.026278 (2004).

160 Foy, T. M. et al. In vivo CD40-gp39 interactions are essential for thymus-dependent humoral immunity. II. Prolonged suppression of the humoral immune response by an antibody to the ligand for CD40, gp39. The Journal of experimental medicine 178, 1567-1575 (1993).

161 Turner, J. G. et al. Anti-CD40 Antibody Induces Antitumor and Antimetastatic Effects: The Role of NK Cells. The Journal of Immunology 166, 89-94, doi:10.4049/jimmunol.166.1.89 (2001).

162 Lum, H. D. et al. Tumoristatic effects of anti-CD40 mAb-activated macrophages involve nitric oxide and tumour necrosis factor-alpha. Immunology 118, 261-270, doi:10.1111/j.1365-2567.2006.02366.x (2006).

163 Buhtoiarov, I. N. et al. CD40 ligation activates murine macrophages via an IFN-γ-dependent mechanism resulting in tumor cell destruction in vitro. The Journal of Immunology 174, 6013-6022 (2005).

164 Strowig, T., Brilot, F. & Münz, C. Noncytotoxic functions of NK cells: direct pathogen restriction and assistance to adaptive immunity. Journal of immunology (Baltimore, Md. : 1950) 180, 7785-7791, doi:10.4049/jimmunol.180.12.7785 (2008).

165 Ferlazzo, G. et al. Distinct roles of IL-12 and IL-15 in human natural killer cell activation by dendritic cells from secondary lymphoid organs. Proc Natl Acad Sci U S A 101, 16606-16611, doi:10.1073/pnas.0407522101 (2004).

166 Orange, J. S. & Biron, C. A. An absolute and restricted requirement for IL-12 in natural killer cell IFN-gamma production and antiviral defense. Studies of natural killer and T cell responses in contrasting viral infections. The Journal of Immunology 156, 1138-1142 (1996).

167 Tomihara, K. et al. Gene transfer of the CD40-ligand to human dendritic cells induces NK-mediated antitumor effects against human carcinoma cells. Int J Cancer 120, 1491-1498, doi:10.1002/ijc.22518 (2007).

168 Trivedi, R. & Mishra, D. P. Trailing TRAIL Resistance: Novel Targets for TRAIL Sensitization in Cancer Cells. Frontiers in Oncology 5, doi:10.3389/fonc.2015.00069 (2015).

169 Bose, A. & Baral, R. Natural killer cell mediated cytotoxicity of tumor cells initiated by neem leaf preparation is associated with CD40–CD40L–mediated endogenous production of interleukin-12. Human Immunology 68, 823-831, doi:https://doi.org/10.1016/j.humimm.2007.08.002 (2007).

170 Byrne, K. T. & Vonderheide, R. H. CD40 Stimulation Obviates Innate Sensors and Drives T Cell Immunity in Cancer. Cell Rep 15, 2719-2732, doi:10.1016/j.celrep.2016.05.058 (2016).

171 Nowak, A. K., Robinson, B. W. S. & Lake, R. A. Synergy between Chemotherapy and Immunotherapy in the Treatment of Established Murine Solid Tumors. Cancer Research 63, 4490 (2003).

172 Nowak, A., Mahendran, S., van der Most, R. & Lake, R. Cisplatin and pemetrexed synergises with immunotherapy to result in cures in established murine malignant mesothelioma. Cancer Research 68, 2073 (2008).

173 O'Hara, M. H. et al. Abstract CT004: A Phase Ib study of CD40 agonistic monoclonal antibody APX005M together with gemcitabine (Gem) and nab-paclitaxel (NP) with or without nivolumab (Nivo) in untreated metastatic ductal pancreatic adenocarcinoma (PDAC) patients. Cancer research 79, CT004-CT004, doi:10.1158/1538-7445.am2019-ct004 (2019).

174 Siolas, D. et al. (American Society of Clinical Oncology, 2016).

175 Vonderheide, R. H. et al. Clinical activity and immune modulation in cancer patients treated with CP-870,893, a novel CD40 agonist monoclonal antibody. J Clin Oncol 25, 876-883, doi:10.1200/jco.2006.08.3311 (2007).

176 Johnson, P. et al. Clinical and biological effects of an agonist anti-CD40 antibody: a Cancer Research UK phase I study. Clin Cancer Res 21, 1321-1328, doi:10.1158/1078-0432.Ccr-14-2355 (2015).

177 Grilley-Olson, J. E. et al. SEA-CD40, a non-fucosylated CD40 agonist: Interim results from a phase 1 study in advanced solid tumors. Journal of Clinical Oncology 36, 3093-3093, doi:10.1200/JCO.2018.36.15_suppl.3093 (2018).

178 Nowak, A. et al. A phase 1b clinical trial of the CD40-activating antibody CP-870,893 in combination with cisplatin and pemetrexed in malignant pleural mesothelioma. Annals of Oncology 26, 2483-2490 (2015).

179 Bajor, D. L. et al. Long-term outcomes of a phase I study of agonist CD40 antibody and CTLA-4 blockade in patients with metastatic melanoma. Oncoimmunology 7, e1468956-e1468956, doi:10.1080/2162402X.2018.1468956 (2018).

180 Turner, M. D., Nedjai, B., Hurst, T. & Pennington, D. J. Cytokines and chemokines: At the crossroads of cell signalling and inflammatory disease. Biochimica et Biophysica Acta (BBA) - Molecular Cell Research 1843, 2563-2582, doi:https://doi.org/10.1016/j.bbamcr.2014.05.014 (2014).

181 Wilson, C. J., Finch, C. E. & Cohen, H. J. Cytokines and Cognition—The Case for A Head-to-Toe Inflammatory Paradigm. Journal of the American Geriatrics Society 50, 2041-2056, doi:10.1046/j.1532-5415.2002.50619.x (2002).

182 Landskron, G., De la Fuente, M., Thuwajit, P., Thuwajit, C. & Hermoso, M. A. Chronic Inflammation and Cytokines in the Tumor Microenvironment. Journal of Immunology Research 2014, 149185, doi:10.1155/2014/149185 (2014).

183 Gresser, I. Biologic effects of interferons. Journal of Investigative Dermatology 95, 66-71 (1990).

184 Isaacs, A. & Lindenmann, J. Virus interference. I. The interferon. Proceedings of the Royal Society of London. Series B-Biological Sciences 147, 258-267 (1957).

185 Wack, A., Terczyńska-Dyla, E. & Hartmann, R. Guarding the frontiers: the biology of type III interferons. Nature immunology 16, 802 (2015).

186 Castro, F., Cardoso, A. P., Gonçalves, R. M., Serre, K. & Oliveira, M. J. Interferon-Gamma at the Crossroads of Tumor Immune Surveillance or Evasion. Frontiers in Immunology 9, doi:10.3389/fimmu.2018.00847 (2018).

187 Shankaran, V. et al. IFNγ and lymphocytes prevent primary tumour development and shape tumour immunogenicity. Nature 410, 1107-1111 (2001).

188 Kaplan, D. H. et al. Demonstration of an interferon γ-dependent tumor surveillance system in immunocompetent mice. Proceedings of the national academy of sciences 95, 7556-7561 (1998).

189 Kelker, H. C. et al. Three molecular weight forms of natural human interferon-gamma revealed by immunoprecipitation with monoclonal antibody. Journal of Biological Chemistry 259, 4301-4304 (1984).

190 Ealick, S. E. et al. Three-dimensional structure of recombinant human interferon-gamma. Science 252, 698-702 (1991).

191 Darwich, L. et al. Secretion of interferon-γ by human macrophages demonstrated at the single-cell level after costimulation with interleukin (IL)-12 plus IL-18. Immunology 126, 386-393, doi:10.1111/j.1365-2567.2008.02905.x (2009).

192 Ohteki, T. et al. Interleukin 12–dependent Interferon γ Production by CD8α+Lymphoid Dendritic Cells. Journal of Experimental Medicine 189, 1981-1986, doi:10.1084/jem.189.12.1981 (1999).

193 Keppel, M. P., Saucier, N., Mah, A. Y., Vogel, T. P. & Cooper, M. A. Activation-Specific Metabolic Requirements for NK Cell IFN-γ Production. The Journal of Immunology 194, 1954-1962, doi:10.4049/jimmunol.1402099 (2015).

194 Matsushita, H. et al. Cytotoxic T Lymphocytes Block Tumor Growth Both by Lytic Activity and IFNγ-Dependent Cell-Cycle Arrest. Cancer Immunology Research 3, 26-36, doi:10.1158/2326-6066.Cir-14-0098 (2015).

195 Kasahara, T., Hooks, J. J., Dougherty, S. F. & Oppenheim, J. J. Interleukin 2-mediated immune interferon (IFN-gamma) production by human T cells and T cell subsets. The Journal of Immunology 130, 1784-1789 (1983).

196 Chan, S. H. et al. Induction of interferon gamma production by natural killer cell stimulatory factor: characterization of the responder cells and synergy with other inducers. Journal of Experimental Medicine 173, 869-879, doi:10.1084/jem.173.4.869 (1991).

197 Ye, J., Ortaido, J. R., Conlon, K., Winkler-Pickett, R. & Young, H. A. Cellular and molecular mechanisms of IFN-γ production induced by IL-2 and IL-12 in a human NK cell line. Journal of leukocyte biology 58, 225-233, doi:10.1002/jlb.58.2.225 (1995).

198 Takeda, K. et al. Defective NK Cell Activity and Th1 Response in IL-18–Deficient Mice. Immunity 8, 383-390, doi:https://doi.org/10.1016/S1074-7613(00)80543-9 (1998).

199 Carson, W. E. et al. Endogenous production of interleukin 15 by activated human monocytes is critical for optimal production of interferon-gamma by natural killer cells in vitro. The Journal of Clinical Investigation 96, 2578-2582, doi:10.1172/JCI118321 (1995).

200 Munder, M., Mallo, M., Eichmann, K. & Modolell, M. Murine Macrophages Secrete Interferon γ upon Combined Stimulation with Interleukin (IL)-12 and IL-18: A Novel Pathway of Autocrine Macrophage Activation. Journal of Experimental Medicine 187, 2103-2108, doi:10.1084/jem.187.12.2103 (1998).

201 Fricke, I. et al. Mycobacteria Induce IFN-γ Production in Human Dendritic Cells via Triggering of TLR2. The Journal of Immunology 176, 5173-5182, doi:10.4049/jimmunol.176.9.5173 (2006).

202 Majoros, A. et al. Canonical and Non-Canonical Aspects of JAK–STAT Signaling: Lessons from Interferons for Cytokine Responses. Frontiers in Immunology 8, doi:10.3389/fimmu.2017.00029 (2017).

203 Shirayoshi, Y., Burke, P. A., Appella, E. & Ozato, K. Interferon-induced transcription of a major histocompatibility class I gene accompanies binding of inducible nuclear factors to the interferon consensus sequence. Proceedings of the National Academy of Sciences 85, 5884-5888, doi:10.1073/pnas.85.16.5884 (1988).

204 Amaldi, I., Reith, W., Berte, C. & Mach, B. Induction of HLA class II genes by IFN-gamma is transcriptional and requires a trans-acting protein. The Journal of Immunology 142, 999-1004 (1989).

205 Zhao, M. et al. MHC class II transactivator (CIITA) expression is upregulated in multiple myeloma cells by IFN-γ. Molecular Immunology 44, 2923-2932, doi:https://doi.org/10.1016/j.molimm.2007.01.009 (2007).

206 Deffrennes, V. et al. Constitutive Expression of MHC Class II Genes in Melanoma Cell Lines Results from the Transcription of Class II Transactivator Abnormally Initiated from Its B Cell-Specific Promoter. The Journal of Immunology 167, 98-106, doi:10.4049/jimmunol.167.1.98 (2001).

207 Maraskovsky, E., Chen, W. F. & Shortman, K. IL-2 and IFN-gamma are two necessary lymphokines in the development of cytolytic T cells. Journal of immunology (Baltimore, Md. : 1950) 143, 1210-1214 (1989).

208 Curtsinger, J. M., Agarwal, P., Lins, D. C. & Mescher, M. F. Autocrine IFN-γ Promotes Naive CD8 T Cell Differentiation and Synergizes with IFN-α To Stimulate Strong Function. The Journal of Immunology 189, 659-668, doi:10.4049/jimmunol.1102727 (2012).

209 Walter, W., Lingnau, K., Schmitt, E., Loos, M. & Maeurer, M. J. MHC class II antigen presentation pathway in murine tumours: tumour evasion from immunosurveillance? British Journal of Cancer 83, 1192-1201, doi:10.1054/bjoc.2000.1415 (2000).

210 Akbar, S. M., Inaba, K. & Onji, M. Upregulation of MHC class II antigen on dendritic cells from hepatitis B virus transgenic mice by interferon-gamma: abrogation of immune response defect to a T-cell-dependent antigen. Immunology 87, 519-527, doi:10.1046/j.1365-2567.1996.516576.x (1996).

211 Nathan, C. F., Murray, H. W., Wiebe, M. E. & Rubin, B. Y. Identification of interferon-gamma as the lymphokine that activates human macrophage oxidative metabolism and antimicrobial activity. The Journal of experimental medicine 158, 670-689 (1983).

212 Shiloh, M. U. et al. Phenotype of mice and macrophages deficient in both phagocyte oxidase and inducible nitric oxide synthase. Immunity 10, 29-38 (1999).

213 Pfefferkorn, E. Interferon gamma blocks the growth of Toxoplasma gondii in human fibroblasts by inducing the host cells to degrade tryptophan. Proceedings of the National Academy of Sciences 81, 908-912 (1984).

214 Laha, T. T., Hawley, M., Rock, K. L. & Goldberg, A. L. Gamma-interferon causes a selective induction of the lysosomal proteases, cathepsins B and L, in macrophages. FEBS letters 363, 85-89 (1995).

215 Bromberg, J. F., Horvath, C. M., Wen, Z., Schreiber, R. D. & Darnell, J. E. Transcriptionally active Stat1 is required for the antiproliferative effects of both interferon alpha and interferon gamma. Proceedings of the national academy of sciences 93, 7673-7678 (1996).

216 Chin, Y. E. et al. Cell growth arrest and induction of cyclin-dependent kinase inhibitor p21WAF1/CIP1 mediated by STAT1. Science 272, 719-722 (1996).

217 Takeda, K. et al. Critical role for tumor necrosis factor–related apoptosis-inducing ligand in immune surveillance against tumor development. The Journal of experimental medicine 195, 161-169 (2002).

218 Xu, X., Fu, X.-Y., Plate, J. & Chong, A. S. IFN-γ induces cell growth inhibition by Fas-mediated apoptosis: requirement of STAT1 protein for up-regulation of Fas and FasL expression. Cancer research 58, 2832-2837 (1998).

219 Liu, F. et al. TNFα cooperates with IFN-γ to repress Bcl-xL expression to sensitize metastatic colon carcinoma cells to TRAIL-mediated apoptosis. PloS one 6 (2011).

220 Thapa, R. J. et al. NF-κB protects cells from gamma interferon-induced RIP1-dependent necroptosis. Molecular and cellular biology 31, 2934-2946 (2011).

221 Kammertoens, T. et al. Tumour ischaemia by interferon-γ resembles physiological blood vessel regression. Nature 545, 98-102 (2017).

222 Hayakawa, Y. et al. IFN-γ–mediated inhibition of tumor angiogenesis by natural killer T-cell ligand, α-galactosylceramide. Blood, The Journal of the American Society of Hematology 100, 1728-1733 (2002).

223 Groom, J. R. & Luster, A. D. CXCR3 ligands: redundant, collaborative and antagonistic functions. Immunology and cell biology 89, 207-215 (2011).

224 Melero, I., Rouzaut, A., Motz, G. T. & Coukos, G. T-cell and NK-cell infiltration into solid tumors: a key limiting factor for efficacious cancer immunotherapy. Cancer discovery 4, 522-526 (2014).

225 Nakajima, C. et al. A role of interferon-γ (IFN-γ) in tumor immunity: T cells with the capacity to reject tumor cells are generated but fail to migrate to tumor sitesin IFN-γ-deficient mice. Cancer research 61, 3399-3405 (2001).

226 Zimmerman, M. et al. IFN-γ upregulates survivin and Ifi202 expression to induce survival and proliferation of tumor-specific T cells. PloS one 5 (2010).

227 Cripps, J. G., Wang, J., Maria, A., Blumenthal, I. & Gorham, J. D. Type 1 T helper cells induce the accumulation of myeloid-derived suppressor cells in the inflamed Tgfb1 knockout mouse liver. Hepatology 52, 1350-1359 (2010).

228 Mundy-Bosse, B. L. et al. Myeloid-derived suppressor cell inhibition of the IFN response in tumor-bearing mice. Cancer research 71, 5101-5110 (2011).

229 Abiko, K. et al. IFN-γ from lymphocytes induces PD-L1 expression and promotes progression of ovarian cancer. British journal of cancer 112, 1501-1509 (2015).

230 Abiko, K. et al. PD-L1 on tumor cells is induced in ascites and promotes peritoneal dissemination of ovarian cancer through CTL dysfunction. Clinical cancer research 19, 1363-1374 (2013).

231 Leonard, W. J. Cytokines and immunodeficiency diseases. Nature Reviews Immunology 1, 200-208 (2001).

232 Yui, M. A., Sharp, L. L., Havran, W. L. & Rothenberg, E. V. Preferential activation of an IL-2 regulatory sequence transgene in TCRγδ and NKT cells: subset-specific differences in IL-2 regulation. The Journal of Immunology 172, 4691-4699 (2004).

233 Nelson, B. H. & Willerford, D. M. in Advances in immunology Vol. 70 1-81 (Elsevier, 1998).

234 Nelson, B. H. IL-2, Regulatory T Cells, and Tolerance. The Journal of Immunology 172, 3983, doi:10.4049/jimmunol.172.7.3983 (2004).

235 Malek, T. R. The biology of interleukin-2. Annu. Rev. Immunol. 26, 453-479 (2008).

236 Kalia, V. & Sarkar, S. Regulation of Effector and Memory CD8 T Cell Differentiation by IL-2—A Balancing Act. Frontiers in Immunology 9, doi:10.3389/fimmu.2018.02987 (2018).

237 Kalia, V. et al. Prolonged interleukin-2Rα expression on virus-specific CD8+ T cells favors terminal-effector differentiation in vivo. Immunity 32, 91-103 (2010).

238 Gong, D. & Malek, T. R. Cytokine-dependent Blimp-1 expression in activated T cells inhibits IL-2 production. The Journal of Immunology 178, 242-252 (2007).

239 Yang, C. Y. et al. The transcriptional regulators Id2 and Id3 control the formation of distinct memory CD8+ T cell subsets. Nature immunology 12, 1221 (2011).

240 Crompton, J. G., Sukumar, M. & Restifo, N. P. Uncoupling T-cell expansion from effector differentiation in cell-based immunotherapy. Immunological reviews 257, 264-276 (2014).

241 Finlay, D. & Cantrell, D. A. Metabolism, migration and memory in cytotoxic T cells. Nature Reviews Immunology 11, 109-117 (2011).

242 Waugh, C., Sinclair, L., Finlay, D., Bayascas, J. R. & Cantrell, D. Phosphoinositide (3, 4, 5)-triphosphate binding to phosphoinositide-dependent kinase 1 regulates a protein kinase B/Akt signaling threshold that dictates T-cell migration, not proliferation. Molecular and cellular biology 29, 5952-5962 (2009).

243 Lord, J. D., McIntosh, B. C., Greenberg, P. D. & Nelson, B. H. The IL-2 receptor promotes lymphocyte proliferation and induction of the c-myc, bcl-2, and bcl-x genes through the trans-activation domain of Stat5. The Journal of Immunology 164, 2533-2541 (2000).

244 Malek, T. R. & Castro, I. Interleukin-2 receptor signaling: at the interface between tolerance and immunity. Immunity 33, 153-165, doi:10.1016/j.immuni.2010.08.004 (2010).

245 Kim, H.-P., Kelly, J. & Leonard, W. J. The basis for IL-2-induced IL-2 receptor α chain gene regulation: importance of two widely separated IL-2 response elements. Immunity 15, 159-172 (2001).

246 Malek, T. R. & Bayer, A. L. Tolerance, not immunity, crucially depends on IL-2. Nature Reviews Immunology 4, 665-674, doi:10.1038/nri1435 (2004).

247 Almeida, A. R., Zaragoza, B. & Freitas, A. A. Indexation as a novel mechanism of lymphocyte homeostasis: the number of CD4+ CD25+ regulatory T cells is indexed to the number of IL-2-producing cells. The Journal of Immunology 177, 192-200 (2006).

248 Scheffold, A., Hühn, J. & Höfer, T. Regulation of CD4+ CD25+ regulatory T cell activity: it takes (IL-) two to tango. European journal of immunology 35, 1336-1341 (2005).

249 Busse, D. et al. Competing feedback loops shape IL-2 signaling between helper and regulatory T lymphocytes in cellular microenvironments. Proceedings of the National Academy of Sciences 107, 3058-3063, doi:10.1073/pnas.0812851107 (2010).

250 Passerini, L. et al. STAT5-signaling cytokines regulate the expression of FOXP3 in CD4+CD25+ regulatory T cells and CD4+CD25- effector T cells. Int Immunol 20, 421-431, doi:10.1093/intimm/dxn002 (2008).

251 Toomer, K. H. et al. Essential and non-overlapping IL-2Rα-dependent processes for thymic development and peripheral homeostasis of regulatory T cells. Nature Communications 10, 1037, doi:10.1038/s41467-019-08960-1 (2019).

252 Redeker, A. et al. The Quantity of Autocrine IL-2 Governs the Expansion Potential of CD8⁺ T Cells. The Journal of Immunology 195, 4792-4801, doi:10.4049/jimmunol.1501083 (2015).

253 Feau, S., Arens, R., Togher, S. & Schoenberger, S. P. Autocrine IL-2 is required for secondary population expansion of CD8+ memory T cells. Nature Immunology 12, 908-913, doi:10.1038/ni.2079 (2011).

254 Curtsinger, J. M. & Mescher, M. F. Inflammatory cytokines as a third signal for T cell activation. Curr Opin Immunol 22, 333-340, doi:10.1016/j.coi.2010.02.013 (2010).

255 Kobayashi, M. et al. Identification and purification of natural killer cell stimulatory factor (NKSF), a cytokine with multiple biologic effects on human lymphocytes. The Journal of experimental medicine 170, 827-845 (1989).

256 Stern, A. S. et al. Purification to homogeneity and partial characterization of cytotoxic lymphocyte maturation factor from human B-lymphoblastoid cells. Proceedings of the National Academy of Sciences 87, 6808-6812 (1990).

257 Schmitt, N. et al. Human dendritic cells induce the differentiation of interleukin-21-producing T follicular helper-like cells through interleukin-12. Immunity 31, 158-169, doi:10.1016/j.immuni.2009.04.016 (2009).

258 Yoshimoto, T. et al. LPS-stimulated SJL macrophages produce IL-12 and IL-18 that inhibit IgE production in vitro by induction of IFN-gamma production from CD3intIL-2R beta+ T cells. Journal of immunology (Baltimore, Md. : 1950) 161, 1483-1492 (1998).

259 Ma, X. & Trinchieri, G. Regulation of interleukin-12 production in antigen-presenting cells. Adv Immunol 79, 55-92, doi:10.1016/s0065-2776(01)79002-5 (2001).

260 Taoufik, Y. et al. Human microglial cells express a functional IL-12 receptor and produce IL-12 following IL-12 stimulation. European journal of immunology 31, 3228-3239, doi:10.1002/1521-4141(200111)31:11<3228::aid-immu3228>3.0.co;2-7 (2001).

261 Wenink, M. H. et al. TLR2 promotes Th2/Th17 responses via TLR4 and TLR7/8 by abrogating the type I IFN amplification loop. Journal of immunology (Baltimore, Md. : 1950) 183, 6960-6970, doi:10.4049/jimmunol.0900713 (2009).

262 Zhang, Y. et al. Tim-3 Negatively Regulates IL-12 Expression by Monocytes in HCV Infection. PLOS ONE 6, e19664, doi:10.1371/journal.pone.0019664 (2011).

263 Presky, D. H. et al. A functional interleukin 12 receptor complex is composed of two beta-type cytokine receptor subunits. Proc Natl Acad Sci U S A 93, 14002-14007, doi:10.1073/pnas.93.24.14002 (1996).

264 Grohmann, U. et al. IL-12 acts directly on DC to promote nuclear localization of NF-kappaB and primes DC for IL-12 production. Immunity 9, 315-323, doi:10.1016/s1074-7613(00)80614-7 (1998).

265 Airoldi, I. et al. Expression and function of IL-12 and IL-18 receptors on human tonsillar B cells. Journal of immunology (Baltimore, Md. : 1950) 165, 6880-6888, doi:10.4049/jimmunol.165.12.6880 (2000).

266 Trinchieri, G. Interleukin-12 and the regulation of innate resistance and adaptive immunity. Nature Reviews Immunology 3, 133-146, doi:10.1038/nri1001 (2003).

267 Presky, D. H. et al. A functional interleukin 12 receptor complex is composed of two β-type cytokine receptor subunits. Proceedings of the National Academy of Sciences 93, 14002-14007, doi:10.1073/pnas.93.24.14002 (1996).

268 Thierfelder, W. E. et al. Requirement for Stat4 in interleukin-12-mediated responses of natural killer and T cells. Nature 382, 171-174, doi:10.1038/382171a0 (1996).

269 Kelsall, B. L., Stüber, E., Neurath, M. & Strober, W. Interleukin-12 production by dendritic cells. The role of CD40-CD40L interactions in Th1 T-cell responses. Ann N Y Acad Sci 795, 116-126, doi:10.1111/j.1749-6632.1996.tb52660.x (1996).

270 Wesa, A. K. & Galy, A. IL-1 beta induces dendritic cells to produce IL-12. Int Immunol 13, 1053-1061, doi:10.1093/intimm/13.8.1053 (2001).

271 Hayes, M. P., Murphy, F. J. & Burd, P. R. Interferon-gamma-dependent inducible expression of the human interleukin-12 p35 gene in monocytes initiates from a TATA-containing promoter distinct from the CpG-rich promoter active in Epstein-Barr virus-transformed lymphoblastoid cells. Blood 91, 4645-4651 (1998).

272 Felzmann, T. et al. Functional maturation of dendritic cells by exposure to CD40L transgenic tumor cells, fibroblasts or keratinocytes. Cancer Letters 168, 145-154, doi:https://doi.org/10.1016/S0304-3835(01)00526-2 (2001).

273 Bellone, G. et al. Tumor-associated transforming growth factor-beta and interleukin-10 contribute to a systemic Th2 immune phenotype in pancreatic carcinoma patients. Am J Pathol 155, 537-547, doi:10.1016/s0002-9440(10)65149-8 (1999).

274 Aste-Amezaga, M., D'Andrea, A., Kubin, M. & Trinchieri, G. Cooperation of natural killer cell stimulatory factor/interleukin-12 with other stimuli in the induction of cytokines and cytotoxic cell-associated molecules in human T and NK cells. Cell Immunol 156, 480-492, doi:10.1006/cimm.1994.1192 (1994).

275 Salcedo, T. W., Azzoni, L., Wolf, S. F. & Perussia, B. Modulation of perforin and granzyme messenger RNA expression in human natural killer cells. Journal of immunology (Baltimore, Md. : 1950) 151, 2511-2520 (1993).

276 Micallef, M. J. et al. Interferon-gamma-inducing factor enhances T helper 1 cytokine production by stimulated human T cells: synergism with interleukin-12 for interferon-gamma production. European journal of immunology 26, 1647-1651, doi:10.1002/eji.1830260736 (1996).

277 Hsieh, C. S. et al. Development of TH1 CD4+ T cells through IL-12 produced by Listeria-induced macrophages. Science 260, 547-549, doi:10.1126/science.8097338 (1993).

278 Prochazkova, J., Pokorna, K. & Holan, V. IL-12 inhibits the TGF-β-dependent T cell developmental programs and skews the TGF-β-induced differentiation into a Th1-like direction. Immunobiology 217, 74-82, doi:10.1016/j.imbio.2011.07.032 (2012).

279 Chowdhury, F. Z., Ramos, H. J., Davis, L. S., Forman, J. & Farrar, J. D. IL-12 selectively programs effector pathways that are stably expressed in human CD8+ effector memory T cells in vivo. Blood 118, 3890-3900, doi:10.1182/blood-2011-05-357111 (2011).

280 Grohmann, U. et al. A tumor-associated and self antigen peptide presented by dendritic cells may induce T cell anergy in vivo, but IL-12 can prevent or revert the anergic state. Journal of immunology (Baltimore, Md. : 1950) 158, 3593-3602 (1997).

281 Okamura, H., Tsutsui, H., Kashiwamura, S., Yoshimoto, T. & Nakanishi, K. Interleukin-18: a novel cytokine that augments both innate and acquired immunity. Adv Immunol 70, 281-312, doi:10.1016/s0065-2776(08)60389-2 (1998).

282 Grohmann, U. et al. Positive regulatory role of IL-12 in macrophages and modulation by IFN-gamma. Journal of immunology (Baltimore, Md. : 1950) 167, 221-227, doi:10.4049/jimmunol.167.1.221 (2001).

283 Dias, S., Boyd, R. & Balkwill, F. IL-12 regulates VEGF and MMPs in a murine breast cancer model. Int J Cancer 78, 361-365, doi:10.1002/(sici)1097-0215(19981029)78:3<361::Aid-ijc17>3.0.Co;2-9 (1998).

284 Kanegane, C. et al. Contribution of the CXC chemokines IP-10 and Mig to the antitumor effects of IL-12. Journal of leukocyte biology 64, 384-392, doi:10.1002/jlb.64.3.384 (1998).

285 Dahmani, A. & Delisle, J.-S. TGF-β in T Cell Biology: Implications for Cancer Immunotherapy. Cancers (Basel) 10, 194, doi:10.3390/cancers10060194 (2018).

286 Shull, M. M. et al. Targeted disruption of the mouse transforming growth factor-beta 1 gene results in multifocal inflammatory disease. Nature 359, 693-699, doi:10.1038/359693a0 (1992).

287 Kulkarni, A. B. et al. Transforming growth factor beta 1 null mutation in mice causes excessive inflammatory response and early death. Proc Natl Acad Sci U S A 90, 770-774, doi:10.1073/pnas.90.2.770 (1993).

288 Li, M. O., Wan, Y. Y., Sanjabi, S., Robertson, A. K. & Flavell, R. A. Transforming growth factor-beta regulation of immune responses. Annual review of immunology 24, 99-146, doi:10.1146/annurev.immunol.24.021605.090737 (2006).

289 David, C. J. & Massagué, J. Contextual determinants of TGFβ action in development, immunity and cancer. Nat Rev Mol Cell Biol 19, 419-435, doi:10.1038/s41580-018-0007-0 (2018).

290 Zitvogel, L., Tesniere, A. & Kroemer, G. Cancer despite immunosurveillance: immunoselection and immunosubversion. Nat Rev Immunol 6, 715-727, doi:10.1038/nri1936 (2006).

291 Flavell, R. A., Sanjabi, S., Wrzesinski, S. H. & Licona-Limón, P. The polarization of immune cells in the tumour environment by TGFbeta. Nat Rev Immunol 10, 554-567, doi:10.1038/nri2808 (2010).

292 Branton, M. H. & Kopp, J. B. TGF-beta and fibrosis. Microbes Infect 1, 1349-1365, doi:10.1016/s1286-4579(99)00250-6 (1999).

293 Sanjabi, S., Oh, S. A. & Li, M. O. Regulation of the Immune Response by TGF-β: From Conception to Autoimmunity and Infection. Cold Spring Harb Perspect Biol 9, doi:10.1101/cshperspect.a022236 (2017).

294 Travis, M. A. & Sheppard, D. TGF-β activation and function in immunity. Annual review of immunology 32, 51-82, doi:10.1146/annurev-immunol-032713-120257 (2014).

295 Annes, J. P., Munger, J. S. & Rifkin, D. B. Making sense of latent TGFbeta activation. J Cell Sci 116, 217-224, doi:10.1242/jcs.00229 (2003).

296 Constam, D. B. Regulation of TGFβ and related signals by precursor processing. Seminars in Cell & Developmental Biology 32, 85-97, doi:https://doi.org/10.1016/j.semcdb.2014.01.008 (2014).

297 Travis, M. A. et al. Loss of integrin alpha(v)beta8 on dendritic cells causes autoimmunity and colitis in mice. Nature 449, 361-365, doi:10.1038/nature06110 (2007).

298 Wang, R., Wan, Q., Kozhaya, L., Fujii, H. & Unutmaz, D. Identification of a regulatory T cell specific cell surface molecule that mediates suppressive signals and induces Foxp3 expression. PLoS One 3, e2705, doi:10.1371/journal.pone.0002705 (2008).

299 Feng, X. H. & Derynck, R. Specificity and versatility in tgf-beta signaling through Smads. Annu Rev Cell Dev Biol 21, 659-693, doi:10.1146/annurev.cellbio.21.022404.142018 (2005).

300 Massagué, J., Seoane, J. & Wotton, D. Smad transcription factors. Genes Dev 19, 2783-2810, doi:10.1101/gad.1350705 (2005).

301 Inman, G. J., Nicolás, F. J. & Hill, C. S. Nucleocytoplasmic Shuttling of Smads 2, 3, and 4 Permits Sensing of TGF-β Receptor Activity. Molecular Cell 10, 283-294, doi:https://doi.org/10.1016/S1097-2765(02)00585-3 (2002).

302 Mu, Y., Gudey, S. K. & Landström, M. Non-Smad signaling pathways. Cell Tissue Res 347, 11-20, doi:10.1007/s00441-011-1201-y (2012).

303 Sad, S. & Mosmann, T. R. Single IL-2-secreting precursor CD4 T cell can develop into either Th1 or Th2 cytokine secretion phenotype. The Journal of Immunology 153, 3514-3522 (1994).

304 Hemmers, S. et al. TGF-? signalling is required for CD4? T cell homeostasis but dispensable for regulatory T cell function. (2013).

305 Zhang, N. & Bevan, M. J. TGF-β signaling to T cells inhibits autoimmunity during lymphopenia-driven proliferation. Nature immunology 13, 667 (2012).

306 Gorelik, L., Constant, S. & Flavell, R. A. Mechanism of transforming growth factor β–induced inhibition of T helper type 1 differentiation. The Journal of experimental medicine 195, 1499-1505 (2002).

307 Lin, J. T., Martin, S. L., Xia, L. & Gorham, J. D. TGF-β1 uses distinct mechanisms to inhibit IFN-γ expression in CD4+ T cells at priming and at recall: differential involvement of Stat4 and T-bet. The Journal of Immunology 174, 5950-5958 (2005).

308 Chen, C.-H. et al. Transforming growth factor β blocks Tec kinase phosphorylation, Ca2+ influx, and NFATc translocation causing inhibition of T cell differentiation. The Journal of experimental medicine 197, 1689-1699 (2003).

309 Tzachanis, D. et al. Tob is a negative regulator of activation that is expressed in anergic and quiescent T cells. Nature immunology 2, 1174-1182 (2001).

310 McKarns, S. C., Schwartz, R. H. & Kaminski, N. E. Smad3 is essential for TGF-β1 to suppress IL-2 production and TCR-induced proliferation, but not IL-2-induced proliferation. The Journal of Immunology 172, 4275-4284 (2004).

311 Wolfraim, L. A., Walz, T. M., James, Z., Fernandez, T. & Letterio, J. J. p21Cip1 and p27Kip1 act in synergy to alter the sensitivity of naive T cells to TGF-β-mediated G1 arrest through modulation of IL-2 responsiveness. The Journal of Immunology 173, 3093-3102 (2004).

312 Genestier, L., Kasibhatla, S., Brunner, T. & Green, D. R. Transforming growth factor β1 inhibits Fas ligand expression and subsequent activation-induced cell death in T cells via downregulation of c-Myc. The Journal of experimental medicine 189, 231-239 (1999).

313 Batlle, E. & Massagué, J. Transforming Growth Factor-β Signaling in Immunity and Cancer. Immunity 50, 924-940, doi:https://doi.org/10.1016/j.immuni.2019.03.024 (2019).

314 Strainic, M. G., Shevach, E. M., An, F., Lin, F. & Medof, M. E. Absence of signaling into CD4+ cells via C3aR and C5aR enables autoinductive TGF-β1 signaling and induction of Foxp3+ regulatory T cells. Nature immunology 14, 162 (2013).

315 Windhagen, A. et al. Modulation of cytokine patterns of human autoreactive T cell clones by a single amino acid substitution of their peptide ligand. Immunity 2, 373-380 (1995).

316 Ravi, R. et al. Bifunctional immune checkpoint-targeted antibody-ligand traps that simultaneously disable TGFβ enhance the efficacy of cancer immunotherapy. Nature communications 9, 741-741, doi:10.1038/s41467-017-02696-6 (2018).

317 Battaglia, A. et al. Interleukin-21 (IL-21) synergizes with IL-2 to enhance T-cell receptor-induced human T-cell proliferation and counteracts IL-2/transforming growth factor-β-induced regulatory T-cell development. Immunology 139, 109-120, doi:10.1111/imm.12061 (2013).

318 Wei, J. et al. Antagonistic nature of T helper 1/2 developmental programs in opposing peripheral induction of Foxp3+ regulatory T cells. Proceedings of the National Academy of Sciences 104, 18169-18174 (2007).

319 Budhu, S. et al. Blockade of surface-bound TGF-β on regulatory T cells abrogates suppression of effector T cell function in the tumor microenvironment. Sci. Signal. 10, eaak9702 (2017).

320 Nandan, D. & Reiner, N. E. TGF-beta attenuates the class II transactivator and reveals an accessory pathway of IFN-gamma action. The Journal of Immunology 158, 1095-1101 (1997).

321 Papaspyridonos, M. et al. Id1 suppresses anti-tumour immune responses and promotes tumour progression by impairing myeloid cell maturation. Nature communications 6, 1-13 (2015).

322 Castriconi, R. et al. Transforming growth factor β1 inhibits expression of NKp30 and NKG2D receptors: consequences for the NK-mediated killing of dendritic cells. Proceedings of the National Academy of Sciences 100, 4120-4125 (2003).

323 Zhang, F. et al. TGF-β induces M2-like macrophage polarization via SNAIL-mediated suppression of a pro-inflammatory phenotype. Oncotarget 7, 52294-52306, doi:10.18632/oncotarget.10561 (2016).

324 Voskoboinik, I., Whisstock, J. C. & Trapani, J. A. Perforin and granzymes: function, dysfunction and human pathology. Nature Reviews Immunology 15, 388-400, doi:10.1038/nri3839 (2015).

325 Cullen, S. P. & Martin, S. J. Mechanisms of granule-dependent killing. Cell Death & Differentiation 15, 251-262, doi:10.1038/sj.cdd.4402244 (2008).

326 Praper, T. et al. Human perforin permeabilizing activity, but not binding to lipid membranes, is affected by pH. Mol Immunol 47, 2492-2504, doi:10.1016/j.molimm.2010.06.001 (2010).

327 Voskoboinik, I. et al. Calcium-dependent plasma membrane binding and cell lysis by perforin are mediated through its C2 domain: A critical role for aspartate residues 429, 435, 483, and 485 but not 491. J Biol Chem 280, 8426-8434, doi:10.1074/jbc.M413303200 (2005).

328 Law, R. H. et al. The structural basis for membrane binding and pore formation by lymphocyte perforin. Nature 468, 447-451, doi:10.1038/nature09518 (2010).

329 Shatursky, O. et al. The mechanism of membrane insertion for a cholesterol-dependent cytolysin: a novel paradigm for pore-forming toxins. Cell 99, 293-299, doi:10.1016/s0092-8674(00)81660-8 (1999).

330 Sattar, R., Ali, S. A. & Abbasi, A. Bioinformatics of granzymes: sequence comparison and structural studies on granzyme family by homology modeling. Biochemical and biophysical research communications 308, 726-735 (2003).

331 Susanto, O., Trapani, J. A. & Brasacchio, D. Controversies in granzyme biology. Tissue Antigens 80, 477-487, doi:10.1111/tan.12014 (2012).

332 Wensink, A. C., Hack, C. E. & Bovenschen, N. Granzymes Regulate Proinflammatory Cytokine Responses. The Journal of Immunology 194, 491-497, doi:10.4049/jimmunol.1401214 (2015).

333 Walle, L. V. & Lamkanfi, M. Pyroptosis. Current Biology 26, R568-R572 (2016).

334 Franchi, L., Eigenbrod, T., Muñoz-Planillo, R. & Nuñez, G. The inflammasome: a caspase-1-activation platform that regulates immune responses and disease pathogenesis. Nature immunology 10, 241-247, doi:10.1038/ni.1703 (2009).

335 Bergsbaken, T., Fink, S. L. & Cookson, B. T. Pyroptosis: host cell death and inflammation. Nat Rev Microbiol 7, 99-109, doi:10.1038/nrmicro2070 (2009).

336 Kovacs, S. B. & Miao, E. A. Gasdermins: Effectors of Pyroptosis. Trends Cell Biol 27, 673-684, doi:10.1016/j.tcb.2017.05.005 (2017).

337 Sborgi, L. et al. GSDMD membrane pore formation constitutes the mechanism of pyroptotic cell death. The EMBO journal 35, 1766-1778 (2016).

338 Zhou, Z. et al. Granzyme A from cytotoxic lymphocytes cleaves GSDMB to trigger pyroptosis in target cells. Science 368, eaaz7548, doi:10.1126/science.aaz7548 (2020).

339 Martinvalet, D., Zhu, P. & Lieberman, J. Granzyme A induces caspase-independent mitochondrial damage, a required first step for apoptosis. Immunity 22, 355-370, doi:10.1016/j.immuni.2005.02.004 (2005).

340 Beresford, P. J. et al. Granzyme A activates an endoplasmic reticulum-associated caspase-independent nuclease to induce single-stranded DNA nicks. J Biol Chem 276, 43285-43293, doi:10.1074/jbc.M108137200 (2001).

341 Chowdhury, D. & Lieberman, J. Death by a thousand cuts: granzyme pathways of programmed cell death. Annual review of immunology 26, 389-420, doi:10.1146/annurev.immunol.26.021607.090404 (2008).

342 Heusel, J. W., Wesselschmidt, R. L., Shresta, S., Russell, J. H. & Ley, T. J. Cytotoxic lymphocytes require granzyme B for the rapid induction of DNA fragmentation and apoptosis in allogeneic target cells. Cell 76, 977-987 (1994).

343 Pardo, J. et al. Apoptotic pathways are selectively activated by granzyme A and/or granzyme B in CTL-mediated target cell lysis. The Journal of cell biology 167, 457-468 (2004).

344 Cullen, S. P., Brunet, M. & Martin, S. J. Granzymes in cancer and immunity. Cell Death & Differentiation 17, 616-623, doi:10.1038/cdd.2009.206 (2010).

345 Cullen, S. P., Adrain, C., Lüthi, A. U., Duriez, P. J. & Martin, S. J. Human and murine granzyme B exhibit divergent substrate preferences. The Journal of cell biology 176, 435-444 (2007).

346 Adrain, C., Murphy, B. M. & Martin, S. J. Molecular ordering of the caspase activation cascade initiated by the cytotoxic T lymphocyte/natural killer (CTL/NK) protease granzyme B. Journal of Biological Chemistry 280, 4663-4673 (2005).

347 Heibein, J. A. et al. Granzyme B-mediated cytochrome c release is regulated by the Bcl-2 family members bid and Bax. The Journal of experimental medicine 192, 1391-1402, doi:10.1084/jem.192.10.1391 (2000).

348 Alimonti, J. B., Shi, L., Baijal, P. K. & Greenberg, A. H. Granzyme B induces BID-mediated cytochrome c release and mitochondrial permeability transition. Journal of Biological Chemistry 276, 6974-6982 (2001).

349 Barry, M. et al. Granzyme B short-circuits the need for caspase 8 activity during granule-mediated cytotoxic T-lymphocyte killing by directly cleaving Bid. Molecular and cellular biology 20, 3781-3794 (2000).

350 Fellows, E., Gil-Parrado, S., Jenne, D. E. & Kurschus, F. C. Natural killer cell–derived human granzyme H induces an alternative, caspase-independent cell-death program. Blood, The Journal of the American Society of Hematology 110, 544-552 (2007).

351 Waterhouse, N. J. & Trapani, J. A. H is for helper: granzyme H helps granzyme B kill adenovirus-infected cells. Trends Immunol 28, 373-375 (2007).

352 Hou, Q. et al. Granzyme H induces apoptosis of target tumor cells characterized by DNA fragmentation and Bid-dependent mitochondrial damage. Molecular Immunology 45, 1044-1055, doi:https://doi.org/10.1016/j.molimm.2007.07.032 (2008).

353 Grossman, W. J. et al. The orphan granzymes of humans and mice. Curr Opin Immunol 15, 544-552, doi:10.1016/s0952-7915(03)00099-2 (2003).

354 Zhao, T. et al. Granzyme K cleaves the nucleosome assembly protein SET to induce single-stranded DNA nicks of target cells. Cell Death & Differentiation 14, 489-499, doi:10.1038/sj.cdd.4402040 (2007).

355 Bratke, K., Kuepper, M., Bade, B., Virchow Jr, J. C. & Luttmann, W. Differential expression of human granzymes A, B, and K in natural killer cells and during CD8+ T cell differentiation in peripheral blood. European journal of immunology 35, 2608-2616 (2005).

356 Sayers, T. J. et al. The restricted expression of granzyme M in human lymphocytes. Journal of immunology (Baltimore, Md. : 1950) 166, 765-771, doi:10.4049/jimmunol.166.2.765 (2001).

357 Lu, H. et al. Granzyme M Directly Cleaves Inhibitor of Caspase-Activated DNase (CAD) to Unleash CAD Leading to DNA Fragmentation. The Journal of Immunology 177, 1171-1178, doi:10.4049/jimmunol.177.2.1171 (2006).

358 Bovenschen, N. et al. NK Cell Protease Granzyme M Targets α-Tubulin and Disorganizes the Microtubule Network. The Journal of Immunology 180, 8184-8191, doi:10.4049/jimmunol.180.12.8184 (2008).

359 Pham, C. T. N., MacIvor, D. M., Hug, B. A., Heusel, J. & Ley, T. J. Long-range disruption of gene expression by a selectable marker cassette. Proc Natl Acad Sci U S A 93, 13090-13095, doi:10.1073/pnas.93.23.13090 (1996).

360 Shi, L., Wu, L., Wang, S. & Fan, Z. Granzyme F induces a novel death pathway characterized by Bid-independent cytochrome c release without caspase activation. Cell Death Differ 16, 1694-1706, doi:10.1038/cdd.2009.101 (2009).

361 Davis, M. E., Chen, Z. G. & Shin, D. M. Nanoparticle therapeutics: an emerging treatment modality for cancer. Nat Rev Drug Discov 7, 771-782, doi:10.1038/nrd2614 (2008).

362 Zhang, L. et al. Nanoparticles in medicine: therapeutic applications and developments. Clinical pharmacology & therapeutics 83, 761-769 (2008).

363 Park, J. et al. PEGylated PLGA nanoparticles for the improved delivery of doxorubicin. Nanomedicine 5, 410-418, doi:10.1016/j.nano.2009.02.002 (2009).

364 Wang, X. et al. HFT-T, a targeting nanoparticle, enhances specific delivery of paclitaxel to folate receptor-positive tumors. ACS Nano 3, 3165-3174, doi:10.1021/nn900649v (2009).

365 Petros, R. A. & DeSimone, J. M. Strategies in the design of nanoparticles for therapeutic applications. Nature Reviews Drug Discovery 9, 615-627, doi:10.1038/nrd2591 (2010).

366 Torchilin, V. P. Recent advances with liposomes as pharmaceutical carriers. Nature reviews Drug discovery 4, 145-160 (2005).

367 Ulrich, A. S. Biophysical aspects of using liposomes as delivery vehicles. Bioscience reports 22, 129-150 (2002).

368 Gabizon, A., Dagan, A., Goren, D., Barenholz, Y. & Fuks, Z. Liposomes as in vivo carriers of adriamycin: reduced cardiac uptake and preserved antitumor activity in mice. Cancer Res 42, 4734-4739 (1982).

369 Koning, G. A. & Storm, G. Targeted drug delivery systems for the intracellular delivery of macromolecular drugs. Drug Discov Today 8, 482-483, doi:10.1016/s1359-6446(03)02699-0 (2003).

370 Fontana, G., Licciardi, M., Mansueto, S., Schillaci, D. & Giammona, G. Amoxicillin-loaded polyethylcyanoacrylate nanoparticles: influence of PEG coating on the particle size, drug release rate and phagocytic uptake. Biomaterials 22, 2857-2865 (2001).

371 Gabizon, A. et al. Pharmacokinetic and imaging studies in patients receiving a formulation of liposome-associated adriamycin. Br J Cancer 64, 1125-1132, doi:10.1038/bjc.1991.476 (1991).

372 Berry, G. et al. The use of cardiac biopsy to demonstrate reduced cardiotoxicity in AIDS Kaposi's sarcoma patients treated with pegylated liposomal doxorubicin. Ann Oncol 9, 711-716, doi:10.1023/a:1008216430806 (1998).

373 Batist, G. Cardiac safety of liposomal anthracyclines. Cardiovasc Toxicol 7, 72-74, doi:10.1007/s12012-007-0014-4 (2007).

374 Gabizon, A. et al. Prolonged circulation time and enhanced accumulation in malignant exudates of doxorubicin encapsulated in polyethylene-glycol coated liposomes. Cancer Res 54, 987-992 (1994).

375 Allen, T. M. Long-circulating (sterically stabilized) liposomes for targeted drug delivery. Trends Pharmacol Sci 15, 215-220, doi:10.1016/0165-6147(94)90314-x (1994).

376 Moghimi, S. M. & Szebeni, J. Stealth liposomes and long circulating nanoparticles: critical issues in pharmacokinetics, opsonization and protein-binding properties. Prog Lipid Res 42, 463-478, doi:10.1016/s0163-7827(03)00033-x (2003).

377 Barenholz, Y. Doxil(R)--the first FDA-approved nano-drug: lessons learned. J Control Release 160, 117-134, doi:10.1016/j.jconrel.2012.03.020 (2012).

378 Zhang, X.-y. & Zhang, P.-y. Polymersomes in Nanomedicine - A Review. Curr Med Chem 13, 124-129, doi:10.2174/157341371266616101814451 9 (2017).

379 Chambers, E. & Mitragotri, S. Prolonged circulation of large polymeric nanoparticles by non-covalent adsorption on erythrocytes. Journal of Controlled Release 100, 111-119, doi:https://doi.org/10.1016/j.jconrel.2004.08.005 (2004).

380 Gunawan, C., Lim, M., Marquis, C. P. & Amal, R. Nanoparticle–protein corona complexes govern the biological fates and functions of nanoparticles. Journal of Materials Chemistry B 2, 2060-2083, doi:10.1039/C3TB21526A (2014).

381 Nie, S. Understanding and overcoming major barriers in cancer nanomedicine. Nanomedicine (Lond) 5, 523-528, doi:10.2217/nnm.10.23 (2010).

382 Verhoef, J. J. F. & Anchordoquy, T. J. Questioning the Use of PEGylation for Drug Delivery. Drug Deliv Transl Res 3, 499-503, doi:10.1007/s13346-013-0176-5 (2013).

383 Simon, B. H., Ando, H. Y. & Gupta, P. K. Circulation time and body distribution of 14C-labeled amino-modified polystyrene nanoparticles in mice. J Pharm Sci 84, 1249-1253, doi:10.1002/jps.2600841020 (1995).

384 Chambers, E. & Mitragotri, S. Long Circulating Nanoparticles via Adhesion on Red Blood Cells: Mechanism and Extended Circulation. Experimental Biology and Medicine 232, 958-966, doi:10.3181/00379727-232-2320958 (2007).

385 Muzykantov, V. R. Drug delivery by red blood cells: vascular carriers designed by mother nature. Expert Opin Drug Deliv 7, 403-427, doi:10.1517/17425241003610633 (2010).

386 Beatty, G. L. et al. CD40 agonists alter tumor stroma and show efficacy against pancreatic carcinoma in mice and humans. Science (New York, N.Y.) 331, 1612-1616, doi:10.1126/science.1198443 (2011).

387 Villa, C. H. et al. Delivery of drugs bound to erythrocytes: new avenues for an old intravascular carrier. Ther Deliv 6, 795-826, doi:10.4155/tde.15.34 (2015).

388 Humphreys, J. D. & Ihler, G. Enhanced stability of erythrocyte-entrapped glucocerebrosidase activity. The Journal of laboratory and clinical medicine 96, 682-692 (1980).

389 Garin, M., Rossi, L., Luque, J. & Magnani, M. Lactate catabolism by enzyme-loaded red blood cells. Biotechnology and applied biochemistry 22, 295-303 (1995).

390 Tajerzadeh, H. & Hamidi, M. Evaluation of hypotonic preswelling method for encapsulation of enalaprilat in intact human erythrocytes. Drug development and industrial pharmacy 26, 1247-1257 (2000).

391 Turrini, F., Arese, P., Yuan, J. & Low, P. Clustering of integral membrane proteins of the human erythrocyte membrane stimulates autologous IgG binding, complement deposition, and phagocytosis. Journal of Biological Chemistry 266, 23611-23617 (1991).

392 Chiarantini, L., Rossi, L., Fraternale, A. & Magnani, M. Modulated red blood cell survival by membrane protein clustering. Molecular and cellular biochemistry 144, 53-59 (1995).

393 Muzykantov, V. R., Zaltsman, A. B., Smirnon, M. D., Samokhin, G. P. & Morgan, B. P. Target-sensitive immunoerythrocytes: interaction of biotinylated red blood cells with immobilized avidin induces their lysis by complement. Biochimica et Biophysica Acta (BBA)-Biomembranes 1279, 137-143 (1996).

394 Magnani, M., Mancini, U., Bianchi, M. & Fazi, A. in The Use of Resealed Erythrocytes as Carriers and Bioreactors 189-194 (Springer, 1992).

395 Murciano, J.-C. et al. Prophylactic fibrinolysis through selective dissolution of nascent clots by tPA-carrying erythrocytes. Nature Biotechnology 21, 891-896, doi:10.1038/nbt846 (2003).

396 Anselmo, A. C. et al. Delivering Nanoparticles to Lungs while Avoiding Liver and Spleen through Adsorption on Red Blood Cells. ACS Nano 7, 11129-11137, doi:10.1021/nn404853z (2013).

397 Zaitsev, S. et al. Targeting of a mutant plasminogen activator to circulating red blood cells for prophylactic fibrinolysis. J Pharmacol Exp Ther 332, 1022-1031, doi:10.1124/jpet.109.159194 (2010).

398 Whiteman, D. C., Green, A. C. & Olsen, C. M. The Growing Burden of Invasive Melanoma: Projections of Incidence Rates and Numbers of New Cases in Six Susceptible Populations through 2031. Journal of Investigative Dermatology 136, 1161-1171, doi:https://doi.org/10.1016/j.jid.2016.01.035 (2016).

399 Seidel, J. A., Otsuka, A. & Kabashima, K. Anti-PD-1 and Anti-CTLA-4 Therapies in Cancer: Mechanisms of Action, Efficacy, and Limitations. Frontiers in oncology 8, 86-86, doi:10.3389/fonc.2018.00086 (2018).

400 Taggart, D. et al. Anti–PD-1/anti–CTLA-4 efficacy in melanoma brain metastases depends on extracranial disease and augmentation of CD8⁺ T cell trafficking. 115, E1540-E1549, doi:10.1073/pnas.1714089115 %J Proceedings of the National Academy of Sciences (2018).

401 Chae, Y. K. et al. Current landscape and future of dual anti-CTLA4 and PD-1/PD-L1 blockade immunotherapy in cancer; lessons learned from clinical trials with melanoma and non-small cell lung cancer (NSCLC). Journal for ImmunoTherapy of Cancer 6, 39, doi:10.1186/s40425-018-0349-3 (2018).

402 Hashimoto, M. et al. CD8 T Cell Exhaustion in Chronic Infection and Cancer: Opportunities for Interventions. Annual review of medicine 69, 301-318, doi:10.1146/annurev-med-012017-043208 (2018).

403 Hammerich, L., Bhardwaj, N., Kohrt, H. E. & Brody, J. D. In situ vaccination for the treatment of cancer. Immunotherapy 8, 315-330, doi:10.2217/imt.15.120 (2016).

404 Hammerich, L., Binder, A. & Brody, J. D. In situ vaccination: Cancer immunotherapy both personalized and off-the-shelf. Molecular oncology 9, 1966-1981, doi:10.1016/j.molonc.2015.10.016 (2015).

405 Clark, E. A. et al. CDw40 and BLCa-specific monoclonal antibodies detect two distinct molecules which transmit progression signals to human B lymphocytes. European journal of immunology 18, 451-457, doi:10.1002/eji.1830180320 (1988).

406 Stout, R. D., Suttles, J., Xu, J., Grewal, I. S. & Flavell, R. A. Impaired T cell-mediated macrophage activation in CD40 ligand-deficient mice. Journal of immunology (Baltimore, Md. : 1950) 156, 8-11 (1996).

407 Fransen, M. F., Sluijter, M., Morreau, H., Arens, R. & Melief, C. J. M. Local Activation of CD8 T Cells and Systemic Tumor Eradication without Toxicity via Slow Release and Local Delivery of Agonistic CD40 Antibody. 17, 2270-2280, doi:10.1158/1078-0432.CCR-10-2888 %J Clinical Cancer Research (2011).

408 Gladue, R. P. et al. The CD40 agonist antibody CP-870,893 enhances dendritic cell and B-cell activity and promotes anti-tumor efficacy in SCID-hu mice. Cancer immunology, immunotherapy : CII 60, 1009-1017, doi:10.1007/s00262-011-1014-6 (2011).

409 Cella, M. et al. Ligation of CD40 on dendritic cells triggers production of high levels of interleukin-12 and enhances T cell stimulatory capacity: T-T help via APC activation. 184, 747-752, doi:10.1084/jem.184.2.747 %J The Journal of Experimental Medicine (1996).

410 Schoenberger, S. P., Toes, R. E., van der Voort, E. I., Offringa, R. & Melief, C. J. T-cell help for cytotoxic T lymphocytes is mediated by CD40-CD40L interactions. Nature 393, 480-483, doi:10.1038/31002 (1998).

411 Rakhmilevich, A. L., Alderson, K. L. & Sondel, P. M. T-cell-independent antitumor effects of CD40 ligation. International reviews of immunology 31, 267-278, doi:10.3109/08830185.2012.698337 (2012).

412 Rakhmilevich, A. L., Buhtoiarov, I. N., Malkovsky, M. & Sondel, P. M. J. C. I., Immunotherapy. CD40 ligation in vivo can induce T cell independent antitumor effects even against immunogenic tumors. 57, 1151-1160, doi:10.1007/s00262-007-0447-4 (2008).

413 Ngiow, S. F. et al. Agonistic CD40 mAb-Driven IL12 Reverses Resistance to Anti-PD1 in a T-cell-Rich Tumor. Cancer research 76, 6266-6277, doi:10.1158/0008-5472.Can-16-2141 (2016).

414 Hu, Z. et al. Investigation of HIFU-induced anti-tumor immunity in a murine tumor model. Journal of translational medicine 5, 34, doi:10.1186/1479-5876-5-34 (2007).

415 Bandyopadhyay, S. & Quinn, T. J. Low-Intensity Focused Ultrasound Induces Reversal of Tumor-Induced T Cell Tolerance and Prevents Immune Escape. 196, 1964-1976, doi:10.4049/jimmunol.1500541 (2016).

416 Honeychurch, J., Glennie, M. J., Johnson, P. W. & Illidge, T. M. Anti-CD40 monoclonal antibody therapy in combination with irradiation results in a CD8 T-cell-dependent immunity to B-cell lymphoma. Blood 102, 1449-1457, doi:10.1182/blood-2002-12-3717 (2003).

417 Fan, Y., Kuai, R., Xu, Y., Ochyl, L. J. & Irvine, D. J. Immunogenic Cell Death Amplified by Co-localized Adjuvant Delivery for Cancer Immunotherapy. 17, 7387-7393, doi:10.1021/acs.nanolett.7b03218 (2017).

418 De Palma, R. et al. Therapeutic effectiveness of recombinant cancer vaccines is associated with a prevalent T-cell receptor alpha usage by melanoma-specific CD8+ T lymphocytes. Cancer research 64, 8068-8076, doi:10.1158/0008-5472.can-04-0067 (2004).

419 Breshears, M. A., Eberle, R. & Ritchey, J. W. Temporal Progression of Viral Replication and Gross and Histological Lesions in Balb/c Mice Inoculated Epidermally with Saimiriine herpesvirus 1 (SaHV-1). Journal of Comparative Pathology 133, 103-113, doi:https://doi.org/10.1016/j.jcpa.2005.01.012 (2005).

420 Dannenmann, S. R. et al. Tumor-associated macrophages subvert T-cell function and correlate with reduced survival in clear cell renal cell carcinoma. Oncoimmunology 2, e23562-e23562, doi:10.4161/onci.23562 (2013).

421 Maimela, N. R., Liu, S. & Zhang, Y. Fates of CD8+ T cells in Tumor Microenvironment. Computational and structural biotechnology journal 17, 1-13, doi:10.1016/j.csbj.2018.11.004 (2018).

422 Hoves, S. et al. Rapid activation of tumor-associated macrophages boosts preexisting tumor immunity. The Journal of experimental medicine 215, 859-876, doi:10.1084/jem.20171440 (2018).

423 Jackaman, C. et al. Targeting macrophages rescues age-related immune deficiencies in C57BL/6J geriatric mice. Aging cell 12, 345-357, doi:10.1111/acel.12062 (2013).

424 Lin, L. et al. CCL18 from tumor-associated macrophages promotes angiogenesis in breast cancer. Oncotarget 6, 34758-34773, doi:10.18632/oncotarget.5325 (2015).

425 Medina-Echeverz, J. et al. Systemic Agonistic Anti-CD40 Treatment of Tumor-Bearing Mice Modulates Hepatic Myeloid-Suppressive Cells and Causes Immune-Mediated Liver Damage. Cancer immunology research 3, 557-566, doi:10.1158/2326-6066.CIR-14-0182 (2015).

426 Diem, S. et al. Tumor infiltrating lymphocytes in lymph node metastases of stage III melanoma correspond to response and survival in nine patients treated with ipilimumab at the time of stage IV disease. Cancer immunology, immunotherapy : CII 67, 39-45, doi:10.1007/s00262-017-2061-4 (2018).

427 Liu, F. et al. Boosting high-intensity focused ultrasound-induced anti-tumor immunity using a sparse-scan strategy that can more effectively promote dendritic cell maturation. Journal of translational medicine 8, 7, doi:10.1186/1479-5876-8-7 (2010).

428 Huang, X. et al. M-HIFU inhibits tumor growth, suppresses STAT3 activity and enhances tumor specific immunity in a transplant tumor model of prostate cancer. PloS one 7, e41632, doi:10.1371/journal.pone.0041632 (2012).

429 Zhang, Y., Deng, J., Feng, J. & Wu, F. Enhancement of antitumor vaccine in ablated hepatocellular carcinoma by high-intensity focused ultrasound. World journal of gastroenterology 16, 3584-3591 (2010).

430 de Smet, M. et al. Magnetic resonance guided high-intensity focused ultrasound mediated hyperthermia improves the intratumoral distribution of temperature-sensitive liposomal Doxorubicin. Investigative radiology 48, 395-405, doi:10.1097/RLI.0b013e3182806940 (2013).

431 Ranjan, A. et al. Image-guided drug delivery with magnetic resonance guided high intensity focused ultrasound and temperature sensitive liposomes in a rabbit Vx2 tumor model. Journal of Controlled Release 158, 487-494 (2012).

432 Manzoor, A. A. et al. Overcoming limitations in nanoparticle drug delivery: triggered, intravascular release to improve drug penetration into tumors. Cancer research 72, 5566-5575, doi:10.1158/0008-5472.CAN-12-1683 (2012).

433 Formenti, S. C. & Demaria, S. Combining radiotherapy and cancer immunotherapy: a paradigm shift. Journal of the National Cancer Institute 105, 256-265, doi:10.1093/jnci/djs629 (2013).

434 Kang, J., Demaria, S. & Formenti, S. Current clinical trials testing the combination of immunotherapy with radiotherapy. Journal for immunotherapy of cancer 4, 51, doi:10.1186/s40425-016-0156-7 (2016).

435 Chen, T., Guo, J., Han, C., Yang, M. & Cao, X. Heat shock protein 70, released from heat-stressed tumor cells, initiates antitumor immunity by inducing tumor cell chemokine production and activating dendritic cells via TLR4 pathway. Journal of immunology (Baltimore, Md. : 1950) 182, 1449-1459 (2009).

436 Chen, T., Guo, J., Yang, M., Zhu, X. & Cao, X. Chemokine-containing exosomes are released from heat-stressed tumor cells via lipid raft-dependent pathway and act as efficient tumor vaccine. Journal of immunology (Baltimore, Md. : 1950) 186, 2219-2228, doi:10.4049/jimmunol.1002991 (2011).

437 Yi, J. S., Cox, M. A. & Zajac, A. J. T-cell exhaustion: characteristics, causes and conversion. 129, 474-481, doi:10.1111/j.1365-2567.2010.03255.x (2010).

438 Liao, W., Lin, J.-X. & Leonard, W. J. Interleukin-2 at the crossroads of effector responses, tolerance, and immunotherapy. Immunity 38, 13-25, doi:10.1016/j.immuni.2013.01.004 (2013).

439 Mellor-Heineke, S. et al. Elevated Granzyme B in Cytotoxic Lymphocytes is a Signature of Immune Activation in Hemophagocytic Lymphohistiocytosis. Frontiers in immunology 4, 72, doi:10.3389/fimmu.2013.00072 (2013).

440 Chikuma, S. et al. PD-1-mediated suppression of IL-2 production induces CD8+ T cell anergy in vivo. Journal of immunology (Baltimore, Md. : 1950) 182, 6682-6689, doi:10.4049/jimmunol.0900080 (2009).

441 Ji, R. R. et al. An immune-active tumor microenvironment favors clinical response to ipilimumab. Cancer immunology, immunotherapy : CII 61, 1019-1031, doi:10.1007/s00262-011-1172-6 (2012).

442 Gajewski, T. F., Louahed, J. & Brichard, V. G. Gene signature in melanoma associated with clinical activity: a potential clue to unlock cancer immunotherapy. Cancer journal (Sudbury, Mass.) 16, 399-403, doi:10.1097/PPO.0b013e3181eacbd8 (2010).

443 Hamid, O. et al. A prospective phase II trial exploring the association between tumor microenvironment biomarkers and clinical activity of ipilimumab in advanced melanoma. Journal of translational medicine 9, 204, doi:10.1186/1479-5876-9-204 (2011).

444 Wiehagen, K. R. et al. Combination of CD40 Agonism and CSF-1R Blockade Reconditions Tumor-Associated Macrophages and Drives Potent Antitumor Immunity. 5, 1109-1121, doi:10.1158/2326-6066.CIR-17-0258 %J Cancer Immunology Research (2017).

445 Baer, C. et al. Suppression of microRNA activity amplifies IFN-γ-induced macrophage activation and promotes anti-tumour immunity. Nature Cell Biology 18, 790, doi:10.1038/ncb3371

https://www.nature.com/articles/ncb3371#supplementary-information (2016).

446 Qian, B. Z. & Pollard, J. W. Macrophage diversity enhances tumor progression and metastasis. Cell 141, 39-51, doi:10.1016/j.cell.2010.03.014 (2010).

447 Sasidharan Nair, V. & Elkord, E. Immune checkpoint inhibitors in cancer therapy: a focus on T-regulatory cells. Immunology and cell biology 96, 21-33, doi:10.1111/imcb.1003 (2018).

448 Sakai, K. et al. Association of tumour-infiltrating regulatory T cells with adverse outcomes in dogs with malignant tumours. Veterinary and comparative oncology, doi:10.1111/vco.12383 (2018).

449 Zhu, Q., Wu, X., Wu, Y. & Wang, X. Interaction between Treg cells and tumor-associated macrophages in the tumor microenvironment of epithelial ovarian cancer. Oncology reports 36, 3472-3478, doi:10.3892/or.2016.5136 (2016).

450 Gupta, A. et al. Radiotherapy Promotes Tumor-Specific Effector CD8⁺ T Cells via Dendritic Cell Activation. The Journal of Immunology 189, 558, doi:10.4049/jimmunol.1200563 (2012).

451 Golden, E. B. et al. Radiation fosters dose-dependent and chemotherapy-induced immunogenic cell death. Oncoimmunology 3, e28518, doi:10.4161/onci.28518 (2014).

452 Gameiro, S. R. et al. Radiation-induced immunogenic modulation of tumor enhances antigen processing and calreticulin exposure, resulting in enhanced T-cell killing. Oncotarget 5, 403-416, doi:10.18632/oncotarget.1719 (2014).

453 Clery, R. et al. Outcomes after salvage radical prostatectomy and first-line radiation therapy or HIFU for recurrent localized prostate cancer: results from a multicenter study. World journal of urology, doi:10.1007/s00345-019-02683-0 (2019).

454 Chen, T., Guo, J., Han, C., Yang, M. & Cao, X. Heat Shock Protein 70, Released from Heat-Stressed Tumor Cells, Initiates Antitumor Immunity by Inducing Tumor Cell Chemokine Production and Activating Dendritic Cells via TLR4 Pathway. The Journal of Immunology 182, 1449, doi:10.4049/jimmunol.182.3.1449 (2009).

455 Toraya-Brown, S. et al. Local hyperthermia treatment of tumors induces CD8(+) T cell-mediated resistance against distal and secondary tumors. Nanomedicine : nanotechnology, biology, and medicine 10, 1273-1285, doi:10.1016/j.nano.2014.01.011 (2014).

456 Behrouzkia, Z., Joveini, Z., Keshavarzi, B., Eyvazzadeh, N. & Aghdam, R. Z. Hyperthermia: How Can It Be Used? Oman Med J 31, 89-97, doi:10.5001/omj.2016.19 (2016).

457 Rao, W., Deng, Z. S. & Liu, J. A review of hyperthermia combined with radiotherapy/chemotherapy on malignant tumors. Critical reviews in biomedical engineering 38, 101-116 (2010).

458 Datta, N. R. et al. Local hyperthermia combined with radiotherapy and-/or chemotherapy: recent advances and promises for the future. Cancer treatment reviews 41, 742-753, doi:10.1016/j.ctrv.2015.05.009 (2015).

459 Hargadon, K. M., Johnson, C. E. & Williams, C. J. Immune checkpoint blockade therapy for cancer: An overview of FDA-approved immune checkpoint inhibitors. International immunopharmacology 62, 29-39 (2018).

460 Massard, C. et al. Safety and efficacy of durvalumab (MEDI4736), an anti–programmed cell death ligand-1 immune checkpoint inhibitor, in patients with advanced urothelial bladder cancer. Journal of Clinical Oncology 34, 3119 (2016).

461 Ott, P. A., Hodi, F. S. & Robert, C. (AACR, 2013).

462 Gajewski, T. F. in Seminars in oncology. 663-671 (Elsevier).

463 Mellman, I., Coukos, G. & Dranoff, G. Cancer immunotherapy comes of age. Nature 480, 480-489, doi:10.1038/nature10673 (2011).

464 Smyth, M. J., Ngiow, S. F., Ribas, A. & Teng, M. W. Combination cancer immunotherapies tailored to the tumour microenvironment. Nature reviews Clinical oncology 13, 143 (2016).

465 Janco, J. M. T., Lamichhane, P., Karyampudi, L. & Knutson, K. L. Tumor-infiltrating dendritic cells in cancer pathogenesis. The Journal of Immunology 194, 2985-2991 (2015).

466 Bertrand, F. et al. TNFα blockade overcomes resistance to anti-PD-1 in experimental melanoma. Nature communications 8, 1-13 (2017).

467 Robert, C. et al. Pembrolizumab versus Ipilimumab in Advanced Melanoma. N Engl J Med 372, 2521-2532, doi:10.1056/NEJMoa1503093 (2015).

468 Lee, C. et al. Targeting of M2-like tumor-associated macrophages with a melittin-based pro-apoptotic peptide. Journal for immunotherapy of cancer 7, 147 (2019).

469 Bodey, B., Bodey Jr, B., Siegel, S. E. & Kaiser, H. E. Failure of cancer vaccines: the significant limitations of this approach to immunotherapy. Anticancer research 20, 2665-2676 (2000).

470 Gujar, S. A., Marcato, P., Pan, D. & Lee, P. W. Reovirus virotherapy overrides tumor antigen presentation evasion and promotes protective antitumor immunity. Molecular cancer therapeutics 9, 2924-2933 (2010).

471 Garris, C. S. et al. Successful anti-PD-1 cancer immunotherapy requires T cell-dendritic cell crosstalk involving the cytokines IFN-γ and IL-12. Immunity 49, 1148-1161. e1147 (2018).

472 Daud, A. I. et al. Tumor immune profiling predicts response to anti-PD-1 therapy in human melanoma. J Clin Invest 126, 3447-3452, doi:10.1172/jci87324 (2016).

473 Ferris, R. L., Whiteside, T. L. & Ferrone, S. Immune Escape Associated with Functional Defects in Antigen-Processing Machinery in Head and Neck Cancer. Clinical Cancer Research 12, 3890-3895, doi:10.1158/1078-0432.Ccr-05-2750 (2006).

474 Palucka, K. & Banchereau, J. Dendritic cells: a link between innate and adaptive immunity. J Clin Immunol 19, 12-25, doi:10.1023/a:1020558317162 (1999).

475 Beatty, G. L. & Gladney, W. L. Immune Escape Mechanisms as a Guide for Cancer Immunotherapy. Clinical Cancer Research 21, 687-692, doi:10.1158/1078-0432.Ccr-14-1860 (2015).

476 Ting Koh, Y., Luz García-Hernández, M. & Martin Kast, W. in Cancer Drug Resistance (ed Beverly A. Teicher) 577-602 (Humana Press, 2006).

477 Singh, M. P. et al. In-situ vaccination using focused ultrasound heating and anti-CD-40 agonistic antibody enhances T-cell mediated local and abscopal effects in murine melanoma. Int J Hyperthermia 36, 64-73, doi:10.1080/02656736.2019.1663280 (2019).

478 Rosberger, D. F. et al. Immunomodulation in choroidal melanoma: reversal of inverted CD4/CD8 ratios following treatment with ultrasonic hyperthermia. Biotechnol Ther 5, 59-68 (1994).

479 Sethuraman, S. N. et al. Novel calreticulin-nanoparticle in combination with focused ultrasound induces immunogenic cell death in melanoma to enhance antitumor immunity. Theranostics 10, 3397 (2020).

480 Hu, Z. et al. Investigation of HIFU-induced anti-tumor immunity in a murine tumor model. J Transl Med 5, 34 (2007).

481 Eranki, A. et al. Mechanical fractionation of tissues using microsecond-long HIFU pulses on a clinical MR-HIFU system. International Journal of Hyperthermia 34, 1213-1224 (2018).

482 Eranki, A. et al. High Intensity Focused Ultrasound (HIFU) Triggers Immune Sensitization of Refractory Murine Neuroblastoma to Checkpoint Inhibitor Therapy. Clinical Cancer Research, clincanres.1604.2019, doi:10.1158/1078-0432.Ccr-19-1604 (2019).

483 Simon, J. C. et al. Ultrasonic atomization of tissue and its role in tissue fractionation by high intensity focused ultrasound. Physics in Medicine & Biology 57, 8061 (2012).

484 Khokhlova, T. D. et al. Controlled tissue emulsification produced by high intensity focused ultrasound shock waves and millisecond boiling. The Journal of the Acoustical Society of America 130, 3498-3510 (2011).

485 Ziadloo, A. et al. Enhanced homing permeability and retention of bone marrow stromal cells by noninvasive pulsed focused ultrasound. Stem Cells 30, 1216-1227, doi:10.1002/stem.1099 (2012).

486 Pahk, K. J. et al. Boiling Histotripsy-induced Partial Mechanical Ablation Modulates Tumour Microenvironment by Promoting Immunogenic Cell Death of Cancers. Scientific Reports 9, 9050, doi:10.1038/s41598-019-45542-z (2019).

487 Petersen, T. R., Dickgreber, N. & Hermans, I. F. Tumor antigen presentation by dendritic cells. Crit Rev Immunol 30, 345-386, doi:10.1615/critrevimmunol.v30.i4.30 (2010).

488 Schade, G. R. et al. Boiling Histotripsy Ablation of Renal Cell Carcinoma in the Eker Rat Promotes a Systemic Inflammatory Response. Ultrasound Med Biol 45, 137-147, doi:10.1016/j.ultrasmedbio.2018.09.006 (2019).

489 Lechner, M. G. et al. Immunogenicity of murine solid tumor models as a defining feature of in vivo behavior and response to immunotherapy. Journal of immunotherapy (Hagerstown, Md. : 1997) 36, 477-489, doi:10.1097/01.cji.0000436722.46675.4a (2013).

490 Twyman-Saint Victor, C. et al. Radiation and dual checkpoint blockade activate non-redundant immune mechanisms in cancer. Nature 520, 373-377, doi:10.1038/nature14292 (2015).

491 Long, K. B. et al. IFNgamma and CCL2 Cooperate to Redirect Tumor-Infiltrating Monocytes to Degrade Fibrosis and Enhance Chemotherapy Efficacy in Pancreatic Carcinoma. Cancer Discov 6, 400-413, doi:10.1158/2159-8290.Cd-15-1032 (2016).

492 Hunter, T. B., Alsarraj, M., Gladue, R. P., Bedian, V. & Antonia, S. J. An agonist antibody specific for CD40 induces dendritic cell maturation and promotes autologous anti-tumour T-cell responses in an in vitro mixed autologous tumour cell/lymph node cell model. Scandinavian journal of immunology 65, 479-486, doi:10.1111/j.1365-3083.2007.01927.x (2007).

493 Thompson, E. A. et al. Human Anti-CD40 Antibody and Poly IC:LC Adjuvant Combination Induces Potent T Cell Responses in the Lung of Nonhuman Primates. The Journal of Immunology 195, 1015, doi:10.4049/jimmunol.1500078 (2015).

494 Zamarin, D. et al. Localized oncolytic virotherapy overcomes systemic tumor resistance to immune checkpoint blockade immunotherapy. Science translational medicine 6, 226ra232-226ra232, doi:10.1126/scitranslmed.3008095 (2014).

495 Chevillet, J. R. et al. Release of Cell-free MicroRNA Tumor Biomarkers into the Blood Circulation with Pulsed Focused Ultrasound: A Noninvasive, Anatomically Localized, Molecular Liquid Biopsy. Radiology 283, 158-167, doi:10.1148/radiol.2016160024 (2017).

496 Newton, J. M. et al. Immune microenvironment modulation unmasks therapeutic benefit of radiotherapy and checkpoint inhibition. Journal for ImmunoTherapy of Cancer 7, 216, doi:10.1186/s40425-019-0698-6 (2019).

497 Vonderheide, R. H. CD40 Agonist Antibodies in Cancer Immunotherapy. Annual review of medicine 71, 47-58, doi:10.1146/annurev-med-062518-045435 (2020).

498 Bellone, M. et al. Relevance of the Tumor Antigen in the Validation of Three Vaccination Strategies for Melanoma. The Journal of Immunology 165, 2651-2656, doi:10.4049/jimmunol.165.5.2651 (2000).

499 Bloom, M. B. et al. Identification of tyrosinase-related protein 2 as a tumor rejection antigen for the B16 melanoma. J Exp Med 185, 453-459, doi:10.1084/jem.185.3.453 (1997).

500 Sabel, M. S. et al. Intratumoral IL-12 and TNF-α–loaded microspheres lead to regression of breast cancer and systemic antitumor immunity. Annals of surgical oncology 11, 147-156 (2004).

501 Tiberio, L. et al. Chemokine and chemotactic signals in dendritic cell migration. Cellular & molecular immunology 15, 346-352, doi:10.1038/s41423-018-0005-3 (2018).

502 Messina, J. L. et al. 12-Chemokine gene signature identifies lymph node-like structures in melanoma: potential for patient selection for immunotherapy? Sci Rep 2, 765, doi:10.1038/srep00765 (2012).

503 Sokol, C. L. & Luster, A. D. The chemokine system in innate immunity. Cold Spring Harbor perspectives in biology 7, a016303 (2015).

504 Kastenmüller, W. et al. Peripheral Prepositioning and Local CXCL9 Chemokine-Mediated Guidance Orchestrate Rapid Memory CD8+ T Cell Responses in the Lymph Node. Immunity 38, 502-513, doi:https://doi.org/10.1016/j.immuni.2012.11.012 (2013).

505 Böttcher, J. P. & Reis e Sousa, C. The Role of Type 1 Conventional Dendritic Cells in Cancer Immunity. Trends in Cancer 4, 784-792, doi:https://doi.org/10.1016/j.trecan.2018.09.001 (2018).

506 Nakanishi, Y., Lu, B., Gerard, C. & Iwasaki, A. CD8+ T lymphocyte mobilization to virus-infected tissue requires CD4+ T-cell help. Nature 462, 510-513 (2009).

507 Wei, S. C. et al. Combination anti–CTLA-4 plus anti–PD-1 checkpoint blockade utilizes cellular mechanisms partially distinct from monotherapies. Proceedings of the National Academy of Sciences 116, 22699-22709, doi:10.1073/pnas.1821218116 (2019).

508 Vilgelm, A. E. & Richmond, A. Chemokines Modulate Immune Surveillance in Tumorigenesis, Metastasis, and Response to Immunotherapy. Frontiers in immunology 10, doi:10.3389/fimmu.2019.00333 (2019).

509 Woo, S. R. et al. STING-dependent cytosolic DNA sensing mediates innate immune recognition of immunogenic tumors. Immunity 41, 830-842, doi:10.1016/j.immuni.2014.10.017 (2014).

510 Rahman, A. H., Taylor, D. K. & Turka, L. A. The contribution of direct TLR signaling to T cell responses. Immunol Res 45, 25-36, doi:10.1007/s12026-009-8113-x (2009).

511 Bommareddy, P. K., Aspromonte , S., Zloza, A., Rabkin, S. D. & Kaufman, H. L. MEK inhibition enhances oncolytic virus immunotherapy through increased tumor cell killing and T cell activation. Science Translational Medicine 10, eaau0417, doi:10.1126/scitranslmed.aau0417 (2018).

512 Ayers, M. et al. IFN-gamma-related mRNA profile predicts clinical response to PD-1 blockade. J Clin Invest 127, 2930-2940, doi:10.1172/jci91190 (2017).

513 Tumeh, P. C. et al. PD-1 blockade induces responses by inhibiting adaptive immune resistance. Nature 515, 568 (2014).

514 Nakamura, Y. Biomarkers for Immune Checkpoint Inhibitor-Mediated Tumor Response and Adverse Events. Frontiers in Medicine 6, doi:10.3389/fmed.2019.00119 (2019).

515 Izadifar, Z., Izadifar, Z., Chapman, D. & Babyn, P. An Introduction to High Intensity Focused Ultrasound: Systematic Review on Principles, Devices, and Clinical Applications. J Clin Med 9, doi:10.3390/jcm9020460 (2020).

516 Elbasty, A. & Metcalf, J. Safety and Efficacy of Catheter Direct Thrombolysis in Management of Acute Iliofemoral Deep Vein Thrombosis: A Systematic Review. Vasc Specialist Int 33, 121-134, doi:10.5758/vsi.2017.33.4.121 (2017).

517 Gulati, V. & Brazg, J. Central Venous Catheter-directed Tissue Plasminogen Activator in Massive Pulmonary Embolism. Clin Pract Cases Emerg Med 2, 67-70, doi:10.5811/cpcem.2017.11.35845 (2018).

518 Wang, H.-b. et al. Recombinant human TNK tissue-type plasminogen activator (rhTNK-tPA) versus alteplase (rt-PA) as fibrinolytic therapy for acute ST-segment elevation myocardial infarction (China TNK STEMI): protocol for a randomised, controlled, non-inferiority trial. BMJ Open 7, e016838, doi:10.1136/bmjopen-2017-016838 (2017).

519 Gravanis, I. & Tsirka, S. E. Tissue-type plasminogen activator as a therapeutic target in stroke. Expert opinion on therapeutic targets 12, 159-170, doi:10.1517/14728222.12.2.159 (2008).

520 Chester, K. W. et al. Making a case for the right '-ase' in acute ischemic stroke: alteplase, tenecteplase, and reteplase. Expert Opinion on Drug Safety 18, 87-96, doi:10.1080/14740338.2019.1573985 (2019).

521 Uesugi, Y., Kawata, H., Jo, J., Saito, Y. & Tabata, Y. An ultrasound-responsive nano delivery system of tissue-type plasminogen activator for thrombolytic therapy. Journal of controlled release : official journal of the Controlled Release Society 147, 269-277, doi:10.1016/j.jconrel.2010.07.127 (2010).

522 Kim, J.-Y., Kim, J.-K., Park, J.-S., Byun, Y. & Kim, C.-K. The use of PEGylated liposomes to prolong circulation lifetimes of tissue plasminogen activator. Vol. 30 (2009).

523 Yoo, J. W., Chambers, E. & Mitragotri, S. Factors that control the circulation time of nanoparticles in blood: challenges, solutions and future prospects. Current pharmaceutical design 16, 2298-2307, doi:10.2174/138161210791920496 (2010).

524 Liu, S., Feng, X., Jin, R. & Li, G. Tissue plasminogen activator-based nanothrombolysis for ischemic stroke. Expert opinion on drug delivery 15, 173-184, doi:10.1080/17425247.2018.1384464 (2018).

525 Sanhai, W. R., Sakamoto, J. H., Canady, R. & Ferrari, M. Seven challenges for nanomedicine. Nature nanotechnology 3, 242 (2008).

526 Perry, J. L. et al. PEGylated PRINT nanoparticles: the impact of PEG density on protein binding, macrophage association, biodistribution, and pharmacokinetics. Nano letters 12, 5304-5310 (2012).

527 Muzykantov, V. R. Drug delivery by red blood cells: vascular carriers designed by Mother Nature. Expert opinion on drug delivery 7, 403-427, doi:10.1517/17425241003610633 (2010).

528 Shi, J. et al. Engineered red blood cells as carriers for systemic delivery of a wide array of functional probes. Proc Natl Acad Sci U S A 111, 10131-10136, doi:10.1073/pnas.1409861111 (2014).

529 Villa, C. H., Anselmo, A. C., Mitragotri, S. & Muzykantov, V. Red blood cells: Supercarriers for drugs, biologicals, and nanoparticles and inspiration for advanced delivery systems. Adv Drug Deliv Rev 106, 88-103, doi:10.1016/j.addr.2016.02.007 (2016).

530 Chambers, E. & Mitragotri, S. Long circulating nanoparticles via adhesion on red blood cells: mechanism and extended circulation. Experimental biology and medicine (Maywood, N.J.) 232, 958-966 (2007).

531 Murciano, J. C. et al. Prophylactic fibrinolysis through selective dissolution of nascent clots by tPA-carrying erythrocytes. Nature biotechnology 21, 891-896, doi:10.1038/nbt846 (2003).

532 Turan, T. et al. Immune oncology, immune responsiveness and the theory of everything. Journal for immunotherapy of cancer 6, 50, doi:10.1186/s40425-018-0355-5 (2018).

533 de Isla, N. G., Riquelme, B. D., Rasia, R. J., Valverde, J. R. & Stoltz, J. F. Quantification of glycophorin A and glycophorin B on normal human RBCs by flow cytometry. Transfusion 43, 1145-1152 (2003).

534 Spitzer, D., Unsinger, J., Bessler, M. & Atkinson, J. P. ScFv-mediated in vivo targeting of DAF to erythrocytes inhibits lysis by complement. Molecular immunology 40, 911-919 (2004).

535 Zaitsev, S. et al. Sustained thromboprophylaxis mediated by an RBC-targeted pro-urokinase zymogen activated at the site of clot formation. Blood 115, 5241-5248, doi:10.1182/blood-2010-01-261610 (2010).

536 Kontos, S. & Hubbell, J. A. Improving protein pharmacokinetics by engineering erythrocyte affinity. Molecular pharmaceutics 7, 2141-2147 (2010).

537 Sahoo, K. et al. Nanoparticle Attachment to Erythrocyte Via the Glycophorin A Targeted ERY1 Ligand Enhances Binding without Impacting Cellular Function. Pharm Res 33, 1191-1203, doi:10.1007/s11095-016-1864-x (2016).

538 Huang, N.-P., Vörös, J., De Paul, S. M., Textor, M. & Spencer, N. D. Biotin-Derivatized Poly(l-lysine)-g-poly(ethylene glycol): A Novel Polymeric Interface for Bioaffinity Sensing. Langmuir 18, 220-230, doi:10.1021/la010913m (2002).

539 Mahmoud, W. et al. Advanced procedures for labeling of antibodies with quantum dots. Analytical biochemistry 416, 180-185, doi:10.1016/j.ab.2011.05.018 (2011).

540 Sahoo, K. et al. Molecular and Biocompatibility Characterization of Red Blood Cell Membrane Targeted and Cell-Penetrating-Peptide-Modified Polymeric Nanoparticles. 14, 2224-2235, doi:10.1021/acs.molpharmaceut.7b00053 (2017).

541 Azimi, F. et al. Tumor-infiltrating lymphocyte grade is an independent predictor of sentinel lymph node status and survival in patients with cutaneous melanoma. Journal of clinical oncology : official journal of the American Society of Clinical Oncology 30, 2678-2683, doi:10.1200/jco.2011.37.8539 (2012).

542 Danneman, P. J., Suckow, M. A. & Brayton, C. The Laboratory Mouse. (CRC Press, 2012).

543 Zhao, Z., Ukidve, A., Gao, Y., Kim, J. & Mitragotri, S. Erythrocyte leveraged chemotherapy (ELeCt): Nanoparticle assembly on erythrocyte surface to combat lung metastasis. Science Advances 5, eaax9250, doi:10.1126/sciadv.aax9250 (2019).

544 Ferrari, R., Sponchioni, M., Morbidelli, M. & Moscatelli, D. Polymer nanoparticles for the intravenous delivery of anticancer drugs: the checkpoints on the road from the synthesis to clinical translation. Nanoscale 10, 22701-22719, doi:10.1039/C8NR05933K (2018).

545 Moghimi, S. M., Hunter, A. C. & Murray, J. C. Long-circulating and target-specific nanoparticles: theory to practice. Pharmacological reviews 53, 283-318 (2001).

546 Brenner, J. S. et al. Red blood cell-hitchhiking boosts delivery of nanocarriers to chosen organs by orders of magnitude. Nature Communications 9, 2684, doi:10.1038/s41467-018-05079-7 (2018).

547 Gustafson, H. H., Holt-Casper, D., Grainger, D. W. & Ghandehari, H. Nanoparticle Uptake: The Phagocyte Problem. Nano today 10, 487-510, doi:10.1016/j.nantod.2015.06.006 (2015).

548 Blanco, E., Shen, H. & Ferrari, M. Principles of nanoparticle design for overcoming biological barriers to drug delivery. Nature biotechnology 33, 941-951, doi:10.1038/nbt.3330 (2015).

549 Muzykantov, V. R. & Murciano, J. C. Attachment of antibody to biotinylated red blood cells: immuno-red blood cells display high affinity to immobilized antigen and normal biodistribution in rats. Biotechnology and applied biochemistry 24 (Pt 1), 41-45 (1996).

550 Pang, Z. et al. Detoxification of Organophosphate Poisoning Using Nanoparticle Bioscavengers. ACS Nano 9, 6450-6458, doi:10.1021/acsnano.5b02132 (2015).

551 Peura, L. & Huttunen, K. M. Sustained release of metformin via red blood cell accumulated sulfenamide prodrug. Journal of pharmaceutical sciences 103, 2207-2210, doi:10.1002/jps.24040 (2014).

552 Luk, B. T. et al. Safe and Immunocompatible Nanocarriers Cloaked in RBC Membranes for Drug Delivery to Treat Solid Tumors. Theranostics 6, 1004-1011, doi:10.7150/thno.14471 (2016).

553 Anselmo, A. C. et al. Exploiting shape, cellular-hitchhiking and antibodies to target nanoparticles to lung endothelium: Synergy between physical, chemical and biological approaches. Biomaterials 68, 1-8, doi:10.1016/j.biomaterials.2015.07.043 (2015).

554 Sahoo, K. et al. Nanoparticle Attachment to Erythrocyte Via the Glycophorin A Targeted ERY1 Ligand Enhances Binding without Impacting Cellular Function. Pharmaceutical Research 33, 1191-1203, doi:10.1007/s11095-016-1864-x (2016).

555 Anselmo, A. C. & Mitragotri, S. Cell-mediated delivery of nanoparticles: taking advantage of circulatory cells to target nanoparticles. Journal of controlled release : official journal of the Controlled Release Society 190, 531-541, doi:10.1016/j.jconrel.2014.03.050 (2014).

556 El-Sherbiny, I. M., Elkholi, I. E. & Yacoub, M. H. Tissue plasminogen activator-based clot busting: Controlled delivery approaches. Global Cardiology Science & Practice 2014, 336-349, doi:10.5339/gcsp.2014.46 (2014).

557 Kina, T. et al. The monoclonal antibody TER-119 recognizes a molecule associated with glycophorin A and specifically marks the late stages of murine erythroid lineage. British journal of haematology 109, 280-287, doi:10.1046/j.1365-2141.2000.02037.x (2000).

558 Kontos, S., Kourtis, I. C., Dane, K. Y. & Hubbell, J. A. Engineering antigens for in situ erythrocyte binding induces T-cell deletion. Proceedings of the National Academy of Sciences 110, E60-E68 (2013).

559 Hu, C. M. et al. Erythrocyte membrane-camouflaged polymeric nanoparticles as a biomimetic delivery platform. Proc Natl Acad Sci U S A 108, 10980-10985, doi:10.1073/pnas.1106634108 (2011).

560 Nemmar, A. et al. Interaction of amorphous silica nanoparticles with erythrocytes in vitro: role of oxidative stress. Cellular physiology and biochemistry : international journal of experimental cellular physiology, biochemistry, and pharmacology 34, 255-265, doi:10.1159/000362996 (2014).

561 Knowles, D. W., Chasis, J. A., Evans, E. A. & Mohandas, N. Cooperative action between band 3 and glycophorin A in human erythrocytes: immobilization of band 3 induced by antibodies to glycophorin A. Biophys J 66, 1726-1732, doi:10.1016/S0006-3495(94)80965-8 (1994).

562 Mqadmi, A., Abramowitz, S., Zheng, X. & Yazdanbakhsh, K. Reduced red blood cell destruction by antibody fragments. Immunohematology 22, 11-14 (2006).

563 Zhang, Y., Li, N., Suh, H. & Irvine, D. J. Nanoparticle anchoring targets immune agonists to tumors enabling anti-cancer immunity without systemic toxicity. Nature Communications 9, 6, doi:10.1038/s41467-017-02251-3 (2018).

564 Sun, M. M. et al. Reduction-alkylation strategies for the modification of specific monoclonal antibody disulfides. Bioconjugate chemistry 16, 1282-1290, doi:10.1021/bc050201y (2005).

565 Kumar, R. et al. In vivo Biodistribution and Clearance Studies using Multimodal ORMOSIL Nanoparticles. ACS nano 4, 699-708, doi:10.1021/nn901146y (2010).

566 Longmire, M., Choyke, P. L. & Kobayashi, H. Clearance properties of nano-sized particles and molecules as imaging agents: considerations and caveats. Nanomedicine (Lond) 3, 703-717, doi:10.2217/17435889.3.5.703 (2008).

567 Burns, A. A. et al. Fluorescent silica nanoparticles with efficient urinary excretion for nanomedicine. Nano letters 9, 442-448, doi:10.1021/nl803405h (2009).

568 Alexis, F., Pridgen, E., Molnar, L. K. & Farokhzad, O. C. Factors Affecting the Clearance and Biodistribution of Polymeric Nanoparticles. Molecular pharmaceutics 5, 505-515, doi:10.1021/mp800051m (2008).

569 Wibroe, P. P. et al. Bypassing adverse injection reactions to nanoparticles through shape modification and attachment to erythrocytes. Nature Nanotechnology 12, 589-594, doi:10.1038/nnano.2017.47 (2017).

VITA

Mohit Pratap Singh

Candidate for the Degree of

Doctor of Philosophy

Dissertation: ROLE OF FOCUSED ULTRASOUND IN CD40 MEDIATED ANTI-TUMOR IMMUNITY

Major Field: Veterinary Biomedical Sciences

Biographical:

Education:

Completed the requirements for the Doctor of Philosophy in Veterinary Biomedical Sciences at Oklahoma State University, Stillwater, Oklahoma in July, 2020.

Completed the requirements for the Master of Veterinary Surgery and Radiology at G.B.Pant University of Agriculture and Technology, Uttarakhand, India in 2013.

Completed the requirements for the Bachelor of Veterinary Science and Animal Husbandry at Tamil Nadu Veterinary and Animal Sciences University, Chennai, Tamil Nadu, India in 2010.

Experience:

Graduate Teaching Associate for Gross and Developmental Anatomy
(Aug 2015 - May 2020)